U.PORTO
FM UP FACULDADE DE MEDICINA UNIVERSIDADE DO PORTO

3S INSTITUTO DE INVESTIGAÇÃO E INOVAÇÃO EM SAÚDE UNIVERSIDADE DO PORTO

U.PORTO

MESTRADO
MEDICINA E ONCOLOGIA MOLECULAR

Effect of BRAF Inhibition on *TERT* Expression in Thyroid Cancer: Insights from Cell Line Models

Maria Dias Caçador

M

2026

DISSERTAÇÃO DE CANDIDATURA AO GRAU DE MESTRE
EM MEDICINA E ONCOLOGIA MOLECULAR,
APRESENTADA À FACULDADE DE MEDICINA DA UNIVERSIDADE DO PORTO

FACULDADE DE **MEDICINA**

Effect of BRAF Inhibition on *TERT* Expression in Thyroid Cancer: Insights from Cell Line Models

MSc Student

Maria Dias Caçador

Supervisor

Ana Paula Soares Dias Ferreira, PhD

Leader of the Cancer Signalling and Metabolism Group - IPATIMUP/i3S, Porto, Portugal

Associate Professor - FMUP, Porto, Portugal

Co-supervisor

Tito Miguel Boléo Teles de Jesus, PhD

Junior researcher at the Cancer Signalling and Metabolism Group - IPATIMUP/i3S, Porto, Portugal

Acknowledgements

Em primeiro lugar, expresso o meu profundo agradecimento à minha orientadora, a Professora Doutora Paula Soares, por me ter concedido a oportunidade de integrar o grupo *Cancer Signalling and Metabolism* do i3S, no qual encontrei tudo aquilo que procurava: um ambiente que me proporcionou um importante crescimento a nível profissional, através do contacto com inúmeras técnicas laboratoriais, e no qual contei com apoio e orientação científica constantes. A integração neste grupo foi igualmente importante para mim, a nível pessoal, permitindo-me desenvolver uma maior resiliência e capacidade de adaptação perante as adversidades com que, tão frequentemente, nos deparamos nesta área da ciência. Gostaria ainda de agradecer pelo voto de confiança que depositou em mim, ao me permitir estruturar o projeto que tive o prazer de desenvolver e que se tornou a base desta dissertação. Esta oportunidade revelou-se, sem dúvida, um fator que reforçou a minha motivação e aguçou a minha curiosidade.

Ao meu coorientador, o Doutor Tito Jesus, gostaria também de expressar o meu mais sincero agradecimento por todo o apoio e acompanhamento prestados ao longo do desenvolvimento deste projeto. Agradeço profundamente por todas as orientações e sugestões valiosas, pelos conhecimentos que partilhou comigo e, sobretudo, pela sua constante disponibilidade e dedicação. Esteve sempre presente para me ajudar e orientar nos momentos em que mais precisei, principalmente nos Western blots, e não poderia estar mais grata por isso.

Ao Doutor Arnaud Paula, quero agradecer por toda a orientação e apoio prestados na componente de bioinformática deste projeto, que foram fundamentais para o seu desenvolvimento. À Elisa, à Elisângela e à Doutora Helena, agradeço profundamente por todos os conhecimentos que me transmitiram a nível laboratorial, bem como toda a disponibilidade e ajuda que me proporcionaram na superação das dificuldades que foram surgindo ao longo da realização das experiências.

Agradeço também às equipas das plataformas BioSciences Screening e Bioimaging Scientific do i3S, cujo apoio foi crucial para o desenvolvimento deste projeto.

Quero também expressar a minha genuína gratidão aos meus colegas de laboratório por todo o auxílio que me prestaram durante este projeto. Em especial à Bia, à Gabi, à Ana, à Benedita, ao Miguel, ao Reinaldo e ao Nuno, agradeço por terem tornado os meus dias mais

leves e felizes e por todos os momentos engraçados que partilhámos (tanto dentro como fora do laboratório). À Bia, quero agradecer por seres tão boa ouvinte, por estares sempre disposta a ajudar-me e por teres sido, basicamente, o meu braço direito ao longo deste percurso. Obrigada por todos os desabafos, pela paciência e por estares sempre lá quando precisei de ti. E, acima de tudo, obrigada por termos levado esta amizade para além do laboratório e por termos partilhado momentos tão especiais, como a nossa viagem, que guardo com muito carinho. À Gabi, à Ana e à Benedita, agradeço por toda a ajuda que me prestaram, por me ouvirem falar sobre este projeto e por estarem sempre dispostas a dar-me uma palavra de apoio quando precisava. Agradeço também por todos os almoços, conversas e momentos de convívio que partilhámos ao longo deste percurso. Ao Reinaldo, agradeço pelos conhecimentos que partilhou comigo, pela forma como consegue sempre motivar quem está à sua volta e por trazer tanta boa disposição ao laboratório. Ao Miguel, agradeço pelos momentos de convívio e pelo auxílio na parte de bioinformática, mas não posso dizer o mesmo das suas péssimas piadas. Ao Nuno, agradeço também por todos os bons momentos que partilhámos e pela paciência ao me ver ocupar ocasionalmente a sua secretária. A todos vocês, espero que continuemos a fazer muitas mais Escape Rooms e que possamos partilhar muitos mais momentos juntos.

Quero também agradecer à minha família, em especial aos meus pais, ao meu irmão, à minha madrinha e aos meus avós, sem os quais nada disto teria sido possível. Obrigada pelo apoio constante que me deram, por me ouvirem falar com entusiasmo sobre este projeto, mesmo não estando familiarizados com alguns dos conceitos envolvidos, por me transmitirem confiança e por me incentivarem sempre a seguir os meus sonhos. Agradeço também por me proporcionarem as melhores oportunidades e por me acompanharem continuamente nas minhas conquistas, as quais não teriam sido possíveis sem vocês. Expresso ainda a minha profunda gratidão pelo carinho e pelos abraços calorosos com que me recebiam sempre que regressava a casa aos fins de semana, tornando esta jornada mais leve e especial, mesmo estando longe do conforto e do afeto que sempre encontrei junto de vocês.

Por último, quero agradecer a todas as minhas amigas da licenciatura, em especial, à minha colega de casa, Melissa, por estares sempre disponível para me ouvir, por me dares tão bons conselhos e por tornares este percurso certamente mais fácil com a tua companhia; e também à minha amiga Lara, que, mesmo estando longe, foi um enorme apoio para mim, oferecendo sempre palavras reconfortantes nos momentos em que mais precisei. Desejo-vos um futuro com tudo aquilo que ambicionam e espero poder continuar a contar com a vossa amizade ao longo da minha vida.

Resumo

O cancro da tiróide (CT) é a neoplasia endócrina mais comum e representa cerca de 3-4% de todos os cancros. A maioria dos CTs corresponde a pequenos tumores intratiroideus, clinicamente indolentes e associados a um prognóstico favorável. No entanto, aproximadamente 10-15% dos carcinomas diferenciados da tiróide (CDTs) progridem para formas mais agressivas e potencialmente fatais, caracterizadas por doença persistente/recorrente e/ou pelo desenvolvimento de metástases à distância.

No CT, foram identificadas diversas alterações somáticas associadas à iniciação e à progressão tumoral. A mutação *BRAF* V600E está presente em 29-69% dos carcinomas papilares da tiróide (CPTs) e resulta na ativação constitutiva da via de sinalização da proteína quinase ativada por mitógenos (MAPK), que regula processos celulares como a proliferação, a diferenciação e a migração. Por outro lado, as mutações na região promotora do gene *TERT* (mutações *TERTp*) são encontradas, maioritariamente, em formas avançadas de CT. A coocorrência destas mutações com a mutação *BRAF* V600E foi descrita em aproximadamente 10% dos CPTs e está associada a um pior prognóstico em comparação com tumores que apresentam apenas uma destas mutações.

Estudos anteriores realizados pelo nosso grupo demonstraram que os CTs que apresentam simultaneamente a mutação *BRAF* V600E e mutações *TERTp* exibem níveis significativamente mais elevados de mRNA de *TERT*, em comparação com tumores portadores apenas de mutações *TERTp*. Com base nestes resultados, este estudo procurou investigar se a inibição farmacológica da proteína BRAF com Vemurafenib poderia modular a expressão de *TERT*, bem como afetar a viabilidade e a proliferação em células de CT com diferentes contextos genéticos. Adicionalmente, procurou-se caracterizar os efeitos moleculares da inibição da proteína BRAF através da análise da expressão proteica e de dados de sequenciação de RNA.

Para responder a estas questões, foram selecionadas três linhas celulares: uma linha celular normal derivada da tiróide e imortalizada (Nthy-Ori 3-1) e duas linhas celulares derivadas de CPT (B-CPAP e TPC-1). As células B-CPAP apresentam a mutação *BRAF* V600E e uma mutação *TERTp*, enquanto que as células TPC-1 exibem *BRAF* do tipo selvagem (wild-type) e uma mutação *TERTp*. Estas linhas celulares foram tratadas com Vemurafenib durante 48 e 72 horas, após as quais foram avaliadas a viabilidade e a proliferação celular. Adicionalmente, foram recolhidas células para análise da expressão de *TERT* por RT-qPCR e

da expressão proteica por Western blot. Foram ainda analisados dados de sequenciação de RNA de células B-CPAP tratadas com Vemurafenib, disponíveis publicamente.

Os nossos resultados demonstraram que as células B-CPAP apresentaram a maior sensibilidade ao Vemurafenib, evidenciada por uma redução marcada da viabilidade e da proliferação, comparativamente às células TPC-1 e Nthy-Ori 3-1. Na linha celular B-CPAP, também se verificou que 72 horas após o tratamento com Vemurafenib, houve uma diminuição significativa do mRNA de *TERT*, embora não tenham sido observadas alterações significativas nas células Nthy-Ori 3-1 nem nas TPC-1. A análise por Western blot não revelou diferenças significativas na ativação da via de sinalização MAPK nas células Nthy-Ori 3-1 nem nas TPC-1 após o tratamento com Vemurafenib. No entanto, nas células B-CPAP tratadas, observou-se um aparente aumento da ativação da ERK, uma proteína a jusante do BRAF. Por último, a análise dos dados de sequenciação de RNA revelou que, em comparação com as células B-CPAP do grupo de controlo, as células tratadas com Vemurafenib apresentaram uma diminuição da expressão de genes associados à regulação do ciclo celular, à reparação do DNA e aos fatores de transcrição ETS.

Em resumo, os nossos resultados demonstraram que o inibidor de BRAF apresentou um efeito mais marcado nas células B-CPAP, provavelmente devido ao facto de estas células exibirem a mutação *BRAF* V600E. Para além disso, estes resultados sugerem que a inibição de BRAF pode influenciar a expressão de *TERT*, para além de afetar a viabilidade e a proliferação nas células que apresentam simultaneamente as mutações *BRAF* V600E e *TERTp*. Assim, este estudo contribui para uma melhor caracterização da relação entre a sinalização por BRAF e a regulação de *TERT* no CT.

Palavras-chave: Carcinoma Papilar da Tiróide; Mutação *BRAF* V600E; Mutação no promotor de *TERT*; Vemurafenib; Expressão de *TERT*

Abstract

Thyroid cancer (TC) is the most common malignancy of the endocrine system and accounts for 3-4% of all human cancers. Most TCs are small, intrathyroidal neoplasms that are clinically indolent and have a favourable prognosis. Nevertheless, approximately 10-15% of differentiated thyroid carcinomas (DTCs) progress to more aggressive and potentially fatal forms, characterised by persistent/recurrent disease and/or the development of distant metastases.

In TC, specific somatic alterations have been identified as events involved in tumour initiation and progression. The *BRAF* V600E mutation is present in 29-69% of papillary thyroid carcinomas (PTCs) and results in constitutive activation of the mitogen-activated protein kinase (MAPK) signalling pathway, which regulates cell proliferation, differentiation, and migration. Mutations in the promoter region of the *TERT* gene (*TERTp* mutations) are predominantly found in advanced forms of TC. The co-occurrence of *TERTp* mutations with the *BRAF* V600E mutation has been identified in approximately 10% of PTCs and is associated with a poorer prognosis compared with tumours harbouring either alteration alone.

Previous studies conducted by our group demonstrated that TCs harbouring both *BRAF* V600E and *TERTp* mutations exhibit significantly higher levels of *TERT* mRNA compared with tumours carrying *TERTp* mutations alone. Based on these findings, this study aimed to investigate whether pharmacological inhibition of BRAF with Vemurafenib could modulate *TERT* expression and affect cell viability and proliferation in TC cells with different genetic backgrounds. Additionally, this project sought to further characterise the molecular effects of BRAF inhibition through protein expression and RNA-sequencing analyses.

To address these questions, three cell lines were selected: an immortalised normal thyroid-derived cell line (Nthy-Ori 3-1) and two PTC-derived cell lines (B-CPAP and TPC-1). B-CPAP cells harbour the *BRAF* V600E mutation and a *TERTp* mutation, whereas TPC-1 cells are *BRAF* wild-type but also carry a *TERTp* mutation. These cell lines were treated with Vemurafenib for 48 and 72 hours, and cell viability and proliferation were subsequently evaluated. Additionally, cell pellets were collected for *TERT* expression analysis by RT-qPCR and protein expression measurement by Western blot. Publicly available RNA-sequencing data from Vemurafenib-treated B-CPAP cells were also analysed.

Our results showed that B-CPAP cells displayed the highest sensitivity to Vemurafenib, with a marked reduction in cell viability and proliferation compared with TPC-1 and Nthy-Ori 3-1 cells. In the B-CPAP cell line, Vemurafenib treatment also resulted in a significant decrease in *TERT* mRNA expression 72 hours after treatment, whereas no significant changes were observed in Nthy-Ori 3-1 or TPC-1 cells. Western blot analysis showed no significant differences in MAPK pathway activity in Nthy-Ori 3-1 or TPC-1 cells following Vemurafenib treatment. However, an apparent increase in ERK activation, a downstream protein of BRAF, was observed in Vemurafenib-treated B-CPAP cells. Finally, RNA-sequencing analysis demonstrated that, compared with the control group, Vemurafenib-treated B-CPAP cells exhibited reduced expression of genes associated with cell cycle regulation, DNA repair, and ETS transcription factors.

Overall, our results demonstrated that the BRAF inhibitor had a more pronounced effect on B-CPAP cells, likely due to the presence of the *BRAF* V600E mutation. Furthermore, these findings suggest that BRAF inhibition may influence *TERT* expression in addition to affecting cell viability and proliferation in cells harbouring both *BRAF* V600E and *TERTp* mutations. Therefore, this study contributes to a better characterisation of the relationship between BRAF signalling and *TERT* regulation in TC.

Keywords: Papillary Thyroid Carcinoma; *BRAF* V600E mutation; *TERT* promoter mutation; Vemurafenib; *TERT* expression

Table of Contents

Acknowledgements v

Resumo vii

Abstract ix

List of Figures xiv

List of Tables xvi

List of Abbreviations xviii

1. Introduction 1

1.1. Thyroid Gland 1

1.2. Thyroid Cancer 3

1.2.1. Epidemiology 3

1.2.2. Risk Factors 4

1.2.3. Clinical Manifestations and Diagnosis 4

1.2.4. Histological Classification 6

1.2.5. Progression of Thyroid Cancer and Prognostic Risk Stratification 8

1.3. Genetic Alterations in Follicular Cell-derived Thyroid Cancer 11

1.3.1. *BRAF* point mutation 12

1.3.2. RET rearrangements 12

1.3.3. *RAS* mutations 13

1.3.4. *TERTp* mutations 14

1.3.5. *TP53* mutations 15

1.4. Thyroid Cancer Treatment 15

1.4.1. Conventional Treatment 15

1.4.2. Adjuvant Therapy 16

1.4.3. Treatment of Advanced Disease 17

1.5. Vemurafenib and BRAF Inhibitors in Thyroid Cancer 20

1.6. Correlation between *BRAF* V600E and *TERTp* mutations 22

2. Aims 25

3. Materials and Methods 27

3.1. Cell Culture 27

3.2. Treatment with Vemurafenib 27

3.3. Cell Viability Assay and IC_{50} determination 28

3.4. Cell Proliferation Assay 29

3.5. Cell Pellet Collection 30

3.6. RNA Extraction and Quantification 31

3.7. cDNA Synthesis from Extracted RNA 32

3.8. RT-qPCR 33

3.9. Total Protein Extraction and Quantification 34

3.10. Protein Expression Analysis (Western Blot) 36

3.11. Bioinformatics Analysis of RNA-Sequencing Data 38

3.12. Statistical Analysis 39

4. Results 41

4.1. Cell Viability 41

4.1.1. Viability of Nthy-Ori 3-1 Cells 41

4.1.2. Viability of B-CPAP Cells 42

4.1.3. Viability of TPC-1 Cells 43

4.2. Cell Proliferation 44

4.2.1. Proliferation of Nthy-Ori 3-1 Cells 45

4.2.2. Proliferation of B-CPAP Cells 46

4.2.3. Proliferation of TPC-1 Cells 47

4.3. Protein Expression Analysis by Western Blot 49

4.3.1. Protein Expression in Nthy-Ori 3-1 Cells 49

4.3.2. Protein Expression in B-CPAP Cells 50

4.3.3. Protein Expression in TPC-1 Cells 52

4.4. *TERT* Expression Analysis by RT-qPCR 53

4.4.1. *TERT* Expression in Nthy-Ori 3-1 Cells 53

4.4.2. *TERT* Expression in B-CPAP Cells 53

4.4.3. *TERT* Expression in TPC-1 Cells 53

4.5. Bioinformatic Analysis of RNA-sequencing Data 55

4.5.1. Differentially Expressed Genes 55

4.5.2. Enriched Biological Processes 56

5. Discussion 59

5.1. Interpretation of the Experimental Findings 59

5.2. Study Limitations and Future Perspectives 67

6. Conclusions 69

7. References 71

8. Appendix 87

List of Figures

Figure 1: Anatomical and histological illustration of the thyroid gland. 1

Figure 2: Schematic representation of the hypothalamic–pituitary–thyroid axis. 2

Figure 3: Worldwide incidence and mortality of thyroid cancer among all cancers in 2024... 3

Figure 4: The 5th edition of the WHO classification of follicular cell-derived thyroid neoplasms. 7

Figure 5: Schematic representation of the MAPK and PI3K/AKT signalling pathways, highlighting the main molecular components. 11

Figure 6: Cell viability curves of Nthy-Ori 3-1 cells treated with increasing concentrations of Vemurafenib (2.5, 5, 10, 25, and 50 μM) at both timepoints (48 and 72 h). 41

Figure 7: Cell viability curves of B-CPAP cells treated with increasing concentrations of Vemurafenib (2.5, 5, 10, 25, and 50 μM) at both timepoints (48 and 72 h). 42

Figure 8: Cell viability curves of TPC-1 cells treated with increasing concentrations of Vemurafenib (2.5, 5, 10, 25, and 50 μM) at both timepoints (48 and 72 h). 43

Figure 9: EdU proliferation assay to assess the effect of 15 μM Vemurafenib on the proliferation of Nthy-Ori 3-1 cells. 45

Figure 10: EdU proliferation assay to assess the effect of 15 μM Vemurafenib on the proliferation of B-CPAP cells. 46

Figure 11: EdU proliferation assay to assess the effect of 15 μM Vemurafenib on the proliferation of TPC-1 cells. 47

Figure 12: Bar graphs showing the percentage of EdU-positive cells (EdU Pos, %) in the Media control, DMSO control, and 15 μM Vemurafenib-treated groups in the Nthy-Ori 3-1 **(A)**, B-CPAP **(B)**, and TPC-1 **(C)** cell lines at 48 and 72 h post-treatment. 48

Figure 13: Effect of Vemurafenib treatment on MAPK pathway proteins in Nthy-Ori 3-1 cells. 50

Figure 14: Effect of Vemurafenib treatment on MAPK pathway proteins in B-CPAP cells. 51

Figure 15: Effect of Vemurafenib treatment on MAPK pathway proteins in TPC-1 cells. ... 52

Figure 16: Relative *TERT* mRNA expression in Nthy-Ori 3-1 **(A)**, B-CPAP **(B)**, and TPC-1 **(C)** cells following treatment with 15 μM Vemurafenib for 48 and 72 h.....54

Figure 17: Heatmap of the DEGs in B-CPAP cells treated with 20 μM Vemurafenib for 48 h compared with the DMSO-treated control group. 55

Figure 18: Representative GO biological processes significantly enriched among the DEGs identified in B-CPAP cells treated with 20 μM Vemurafenib for 48 h compared with the DMSO-treated control group. 56

List of Tables

Table 1: Summary of the EU-TIRADS thyroid nodule risk stratification system. 5

Table 2: The 8th edition of the AJCC/TNM staging system. 10

Table 3: RTKIs approved by the FDA/EMA, their molecular targets, and their indications in thyroid cancer treatment. 19

Table 4: Volumes of the reagents used to prepare the reaction mixes with reverse transcriptase (RTase) and without reverse transcriptase (no-RTase control). 32

Table 5: Volumes of the reagents used for the preparation of the reaction mixes containing the *TBP* and *TERT* probes. 33

Table 6: Volumes of lysis buffer mixture (µL) used for cell pellet resuspension in each experimental condition: Treatment (15 µM Vemurafenib), DMSO control (cell culture medium with 0.03% DMSO), and Medium-only control at each timepoint (48 h and 72 h) and for each cell line (Nthy-Ori 3-1, B-CPAP and TPC-1). 35

Table 7: Volumes of the reagents used for the preparation of two 10% acrylamide resolving gels. 36

Table 8: Volumes of the reagents used for the preparation of two 4% acrylamide stacking gels. 36

Table 9: References, host species, clonality, and working dilutions of the primary and secondary antibodies used for Western blot analysis of BRAF, phosphorylated-ERK1/2 (pERK1/2), ERK1/2, and α-tubulin. 37

Supplementary Table 1: Cell viability (%), expressed as mean ± SD, of Nthy-Ori 3-1 cells at each Vemurafenib concentration (0, 2.5, 5, 10, 25, and 50 µM) at 48 and 72 h post-treatment. 87

Supplementary Table 2: Cell viability (%), expressed as mean ± SD, of B-CPAP cells at each Vemurafenib concentration (0, 2.5, 5, 10, 25, and 50 µM) at 48 and 72 h post-treatment. 87

Supplementary Table 3: Cell viability (%), expressed as mean ± SD, of TPC-1 cells at each Vemurafenib concentration (0, 2.5, 5, 10, 25, and 50 µM) at 48 and 72 h post-treatment. 87

Supplementary Table 4: Percentage of EdU-positive cells, expressed as mean ± SD, in Nthy-Ori 3-1, B-CPAP, and TPC-1 cells under each experimental condition (Media control, DMSO control, and 15 μM Vemurafenib) at 48 and 72 h post-treatment. 88

List of Abbreviations

A

AJCC	American Joint Committee on Cancer
ANOVA	Analysis of variance
APS	Ammonium persulfate
ATA	American Thyroid Association
ATC	Anaplastic thyroid carcinoma
ATP	Adenosine triphosphate

B

BRAF	B-Raf proto-oncogene, serine/threonine kinase
BSA	Bovine serum albumin

C

cDNA	Complementary DNA
ChIP	Chromatin immunoprecipitation
CI	Confidence interval
CR	Conserved region
CRAF	C-Raf proto-oncogene, serine/threonine kinase
CT	Computed tomography
Ct	Cycle threshold
CTLA-4	Cytotoxic T-lymphocyte–associated protein 4

D

DEG	Differentially expressed gene
DFS	Disease-free survival
dH_2O	Distilled water
DHGTC	Differentiated high-grade thyroid carcinoma
DMSO	Dimethyl sulfoxide
DNA	Deoxyribonucleic acid
DNase	Deoxyribonuclease
dNTP	Deoxyribonucleotide triphosphate
DTC	Differentiated thyroid carcinoma

E

EBRT	External beam radiotherapy
EDTA	Ethylenediaminetetraacetic acid
EdU	5-Ethynyl-2′-deoxyuridine
EGFR	Epidermal growth factor receptor
EHF	ETS homologous factor
ERK	Extracellular signal-regulated kinase
ETA	European Thyroid Association
ETS	E-twenty-six
ETV1	ETS variant transcription factor 1
ETV4	ETS variant transcription factor 4
ETV5	ETS variant transcription factor 5

F

FC	Fold change
FDA	Food and Drug Administration
FDR	False discovery rate
FNA	Fine-needle aspiration
FTC	Follicular thyroid carcinoma
FVPTC	Follicular variant of papillary thyroid carcinoma

G

GABPB	GA-binding protein subunit beta
GEO	Gene Expression Omnibus
GO	Gene Ontology

H

HER2	Human epidermal growth factor receptor 2
HER3	Human epidermal growth factor receptor 3

I

IC_{50}	Half-maximal inhibitory concentration
ICI	Immune checkpoint inhibitor
IgG	Immunoglobulin G

L

logFC	Log fold change

M

MAPK	Mitogen-activated protein kinase
MEK	Mitogen-activated protein kinase kinase
MEN2	Multiple endocrine neoplasia type 2
MET	Mesenchymal–epithelial transition factor receptor
MKI	Multikinase inhibitor
MRI	Magnetic resonance imaging
mRNA	Messenger RNA
MTC	Medullary thyroid carcinoma

N

NCBI	National Center for Biotechnology Information
NHEJ	Non-homologous end joining
NIS	Sodium–iodide symporter
NMTC	Non-medullary thyroid carcinoma
NTRK	Neurotrophic tyrosine receptor kinase

O

ORR	Overall response rate
OS	Overall survival

P

PBS	Phosphate-buffered saline
PCR	Polymerase chain reaction
PD-1	Programmed cell death protein 1
PD-L1	Programmed death-ligand 1
PDTC	Poorly differentiated thyroid carcinoma
PET-CT	Positron emission tomography–computed tomography
PFS	Progression-free survival
PI3K	Phosphatidylinositol 3-kinase
PI3K-AKT	Phosphoinositide 3-kinase/protein kinase B
PTC	Papillary thyroid carcinoma

R

RAF	Rapidly accelerated fibrosarcoma
RAI	Radioactive iodine
RAS	Rat sarcoma
RBD	RAS-binding domain
RET	Rearranged during transfection
RIPA	Radioimmunoprecipitation assay
RNA	Ribonucleic acid
RNase	Ribonuclease
RNA-seq	RNA sequencing
RPMI-1640	Roswell Park Memorial Institute medium 1640
RT	Room temperature
RTase	Reverse transcriptase
RTK	Receptor tyrosine kinase
RTKI	Receptor tyrosine kinase inhibitor
RT-qPCR	Reverse transcription quantitative polymerase chain reaction

S

SD	Standard deviation
SDS	Sodium dodecyl sulfate
SDS-PAGE	Sodium dodecyl sulfate–polyacrylamide gel electrophoresis
SEM	Standard error of the mean
siRNA	Small interfering RNA

T

T3	Triiodothyronine
T4	Thyroxine
TBP	TATA-binding protein
TBS	Tris-buffered saline
TBS-T	Tris-buffered saline with Tween-20
TC	Thyroid cancer
TEMED	Tetramethylethylenediamine
TERC	Telomerase RNA component
TERT	Telomerase reverse transcriptase
TERTp	Telomerase reverse transcriptase promoter

Tg	Thyroglobulin
TgAb	Anti-thyroglobulin antibody
TGS	Tris-glycine-sodium dodecyl sulfate
TMB	Tumour mutational burden
TNM	Tumour–Node–Metastasis
TP53	Tumour protein p53
TRH	Thyrotropin-releasing hormone
TSH	Thyroid-stimulating hormone
TSHR	Thyroid-stimulating hormone receptor

V

VEGFR	Vascular endothelial growth factor receptor

W

WBS	Whole-body radioiodine scintigraphy
WHO	World Health Organization

1. Introduction

1.1. Thyroid Gland

The thyroid gland is located in the anterior region of the neck, below the larynx and anterior to the trachea. It consists of two lobes (the right and left lobes), which are connected by the isthmus. Some individuals also present a structure extending from the superior part of the isthmus, known as the pyramidal lobe, which represents a remnant of the thyroglossal duct (Standring, 2011; Stathatos, 2019).

Histologically, the thyroid gland consists of thousands of thyroid follicles, which are responsible for the synthesis and secretion of the thyroid hormones triiodothyronine (T3) and thyroxine (T4). Thyroid follicles are composed of a single layer of thyroid follicular cells, or thyrocytes, surrounding a central substance called the colloid. Thyrocytes express the sodium–iodide symporter (NIS), a carrier protein that is responsible for iodide uptake, which is essential for thyroid hormone synthesis. The colloid mainly contains thyroglobulin (Tg), the inactive precursor and storage form of the thyroid hormones. In addition, the thyroid gland contains a second major cell type, the parafollicular cells, also known as C cells, which are neuroendocrine cells located between the thyroid follicles. These cells are responsible for the production of the hormone calcitonin (Junqueira & Carneiro, 2013; Standring, 2011; Stathatos, 2019). An anatomical and histologic representation of the thyroid gland is shown in ***Figure 1.***

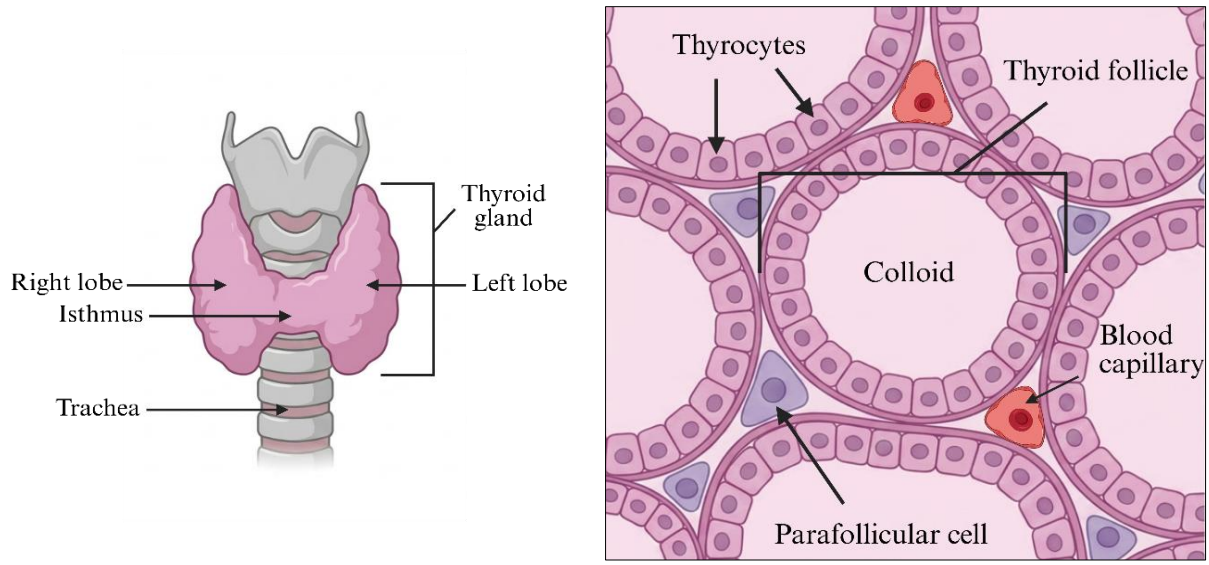


Figure 1: *Anatomical and histological illustration of the thyroid gland.*
Created with Noah AI and subsequently edited and labelled in https://BioRender.com, based on Andreadi et al. (2025), International Journal of Molecular Sciences. DOI: 10.3390/ijms26136522.

The synthesis of the thyroid hormones T3 and T4 is regulated by the hypothalamic–pituitary–thyroid axis. This regulation occurs mainly through the thyroid-stimulating hormone (TSH), which is secreted by the anterior pituitary. In turn, TSH is regulated by the thyrotropin-releasing hormone (TRH) produced by the hypothalamus, as well as by circulating thyroid hormones. Briefly, an increase in circulating thyroid hormone levels inhibits TRH production by the hypothalamus, resulting in reduced TSH secretion by the anterior pituitary and, consequently, decreased thyroid stimulation (Junqueira & Carneiro, 2013; Stathatos, 2019). A schematic overview of this regulatory mechanism is presented in ***Figure 2***.

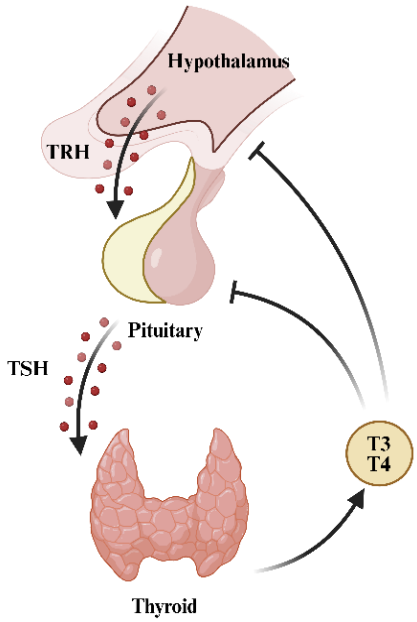


Figure 2: *Schematic representation of the hypothalamic–pituitary–thyroid axis.*
TRH*: Thyrotropin-Releasing Hormone;* ***TSH****: Thyroid-Stimulating Hormone;* ***T3****: Triiodothyronine;* ***T4****: Thyroxine. Created in https://BioRender.com. Adapted from: Cheng et al. (2023), Frontiers in Pharmacology. DOI: 10.3389/fphar.2023.1291856.*

The thyroid hormones T3 and T4 play a crucial role in diverse cellular mechanisms. These hormones affect the cardiovascular system by increasing heart rate and cardiac output through enhanced sensitivity to catecholamines. In terms of metabolism, these hormones increase the basal metabolic rate, oxygen consumption, and heat production. Additionally, they increase carbohydrate metabolism by enhancing glucose absorption, stimulating gluconeogenesis, and promoting glycogen synthesis. Thyroid hormones also regulate lipid metabolism and promote protein anabolism. Furthermore, these hormones are essential for bone growth and neurological development during childhood (Costanzo, 2014; Shahid et al., 2023). Therefore, the thyroid gland is a major endocrine organ that regulates body homeostasis; nevertheless, it can be affected by several clinical conditions, including cancer.

1.2. Thyroid Cancer

1.2.1. Epidemiology

Thyroid cancer (TC) is the most common malignancy of the endocrine system and accounts for approximately 3 to 4% of all human cancers (Romei & Elisei, 2021). In 2024, it was the sixth most common type of cancer worldwide (***Figure 3)***, with Eastern Asia being the region with the highest incidence (Sung et al., 2026). In Portugal in 2022, TC had the eighth-highest incidence among all cancers, excluding breast cancer and sex-specific cancers (Registo Oncológico Nacional, 2025). Among women, it ranked as the fourth most common cancer worldwide in 2024 and fifth in Portugal in 2022, with an incidence approximately three times higher in women than in men (Registo Oncológico Nacional, 2025; Sung et al., 2026). Since the 1980s, an increase in TC incidence has been reported, mainly due to the overdiagnosis of indolent forms, which resulted from the widespread use of neck ultrasonography and fine-needle aspiration (FNA) biopsies (Boucai et al., 2024; Chen & Haymart, 2025). Although the incidence of TC is high, its mortality rate is much lower and has remained stable (Pizzato et al., 2022). In 2024, TC represented the twenty-fifth most lethal cancer worldwide, as shown in ***Figure 3***. Moreover, the incidence of TC is approximately seven times higher in transitioned countries than in transitioning countries; however, mortality rates are not markedly different between these socioeconomic groups (Sung et al., 2026).

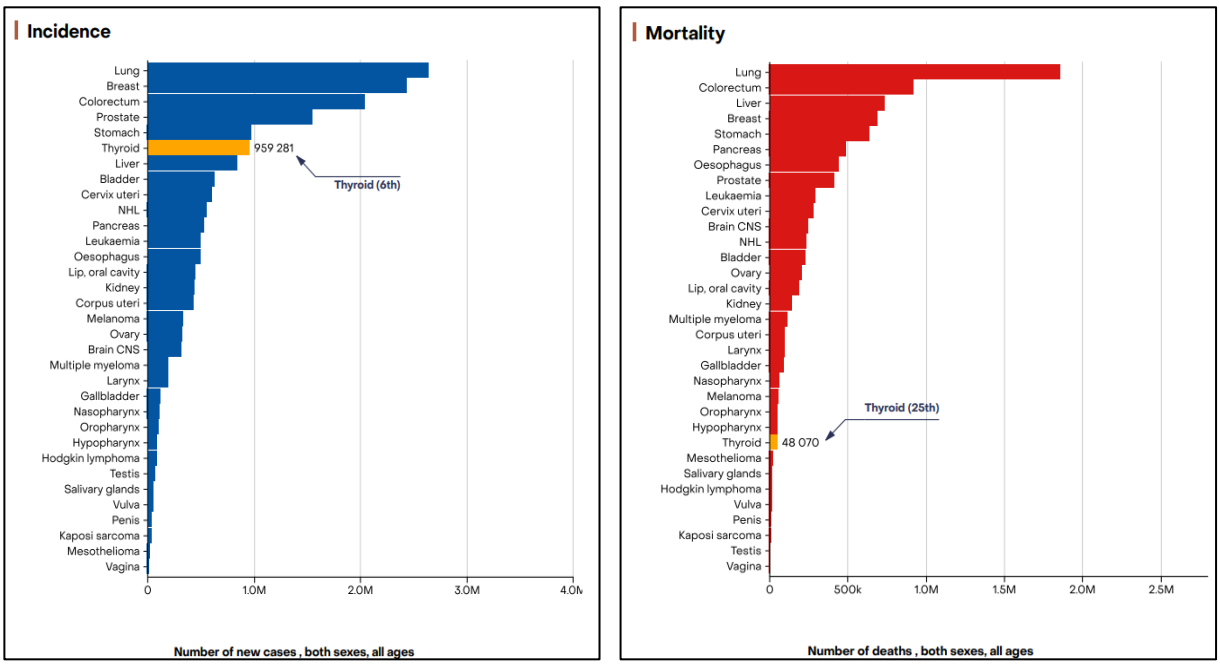


Figure 3: *Worldwide incidence and mortality of thyroid cancer among all cancers in 2024. From Global Cancer Observatory (Ervik et al., 2026), International Agency for Research on Cancer (https://gco.iarc.who.int/today).*

1.2.2. Risk Factors

Exposure to ionizing radiation, particularly in children and adolescents, is the primary environmental risk factor for the development of TC. Nuclear accidents that resulted in the release of large amounts of radioactive material, such as the 1986 Chernobyl disaster in Ukraine, have been associated with a higher incidence of TC in the affected regions, especially among children exposed at the time (Boucai et al., 2024; Kim et al., 2020). Additionally, exposure to radiation for medical reasons during childhood, such as computed tomography (CT) or oncological treatments involving radiotherapy, can also increase the risk of TC (Kim et al., 2020; Lorenz et al., 2018).

Demographic risk factors for the onset of TC include age and sex. As previously mentioned, TC incidence is three times higher in women than in men (Li et al., 2025). On the other hand, although TC can occur at any age, the disease is most commonly diagnosed in the early 50s (Chen et al., 2023).

A family history of a first-degree relative with TC or benign thyroid disease increases the risk of developing TC. Moreover, a proportion of TCs have a hereditary component. TCs arising from the parafollicular cells, the medullary thyroid carcinomas (MTCs), are hereditary in approximately 25% of cases. Genetic syndromes, including multiple endocrine neoplasia type 2 (MEN2), increase the risk of developing TC, specifically the MTC subtype. There are two subtypes of MEN2: MEN2A and MEN2B, both caused by gain-of-function mutations in the rearranged during transfection (*RET*) gene and inherited in an autosomal dominant manner (Boucai et al., 2024; Kim et al., 2020; Li et al., 2025). In contrast, TCs originating from thyroid follicular cells (non-medullary thyroid carcinomas; NMTCs) are hereditary in less than 10% of cases, and the underlying causes remain largely unidentified (Kim et al., 2020).

1.2.3. Clinical Manifestations and Diagnosis

Patients with TC can remain asymptomatic (Boucai et al., 2024; Grani et al., 2024). Nevertheless, some patients may present with symptoms, including a palpable mass in the neck (thyroid nodule or goiter), dysphagia, and hoarseness (Boucai et al., 2024; Cabanillas et al., 2016). Moreover, most thyroid nodules are incidentally detected during imaging exams performed to evaluate adjacent organs or tissues, such as CT, Magnetic Resonance Imaging (MRI), or Positron Emission Tomography–Computed Tomography (PET-CT) (Chen et al.,

2023; Grani et al., 2024). Only 30–40% of diagnoses are made following the detection of a palpable nodule (Chen et al., 2023).

The initial diagnostic assessment of patients with suspected TC includes clinical history (family and personal), physical examination, measurement of serum TSH levels, and neck ultrasound (Durante et al., 2023). Neck ultrasound is the main imaging modality utilised to evaluate thyroid nodules. This approach is performed when a thyroid nodule is suspected or when thyroid nodules are incidentally detected on other imaging examinations (Chen et al., 2023; Durante et al., 2023). It allows the evaluation of the size and number of thyroid nodules, as well as the presence of characteristics suspicious for malignancy. These features include a solid nodule, microcalcifications, irregular margins, a non-parallel orientation, and hypoechogenicity (Chen et al., 2023; Durante et al., 2023; Grani et al., 2024). Neck ultrasound is not recommended as a screening examination for the general asymptomatic population, since it may lead to overdiagnosis. This procedure enables the malignancy risk stratification of the thyroid nodules, which determines whether FNA biopsy is necessary to confirm the nature of the nodules (Chen et al., 2023). There are several international classification systems used for this purpose, including the EU-TIRADS classification system developed by the European Thyroid Association (ETA), which is summarised in ***Table 1*** (Chen et al., 2023; Durante et al., 2023).

Table 1: *Summary of the EU-TIRADS thyroid nodule risk stratification system.*
Adapted from: Durante et al. (2023), European Thyroid Journal. DOI:10.1530/ETJ-23-0067. ***FNA****: fine-needle aspiration.*

Category	Malignancy risk	FNA recommendation
EU-TIRADS 1 Normal	None	No
EU-TIRADS 2 Benign	0%	No
EU-TIRADS 3 Low risk	2-4%	FNA if > 20 mm
EU-TIRADS 4 Intermediate risk	6-17%	FNA if > 15 mm
EU-TIRADS 5 High risk	26-87%	FNA if > 10 mm

Regardless of the EU-TIRADS score, FNA is recommended by the ETA for thyroid nodules when pathological lymph nodes are present or if extrathyroidal extension of the nodule is suspected (Durante et al., 2023). However, most of the risk stratification systems, including those developed by the ETA and the American Thyroid Association (ATA), use a 10 mm size limit for performing FNA (Durante et al., 2023; Ringel et al., 2025). The cytological results obtained from the FNA procedure are evaluated using the Bethesda System for Reporting Thyroid Cytopathology, which classifies thyroid nodules into six diagnostic categories (I–VI), each associated with an estimated risk of malignancy and leading to specific management recommendations (Durante et al., 2023).

For the initial evaluation of thyroid nodules, it is not recommended to use imaging exams such as CT or MRI; nevertheless, these approaches can be useful in advanced forms of the disease, including large tumours with extrathyroidal extension, lymph node metastases, or aggressive histology (Boucai et al., 2024; Durante et al., 2023). Moreover, assessment of serum Tg levels is not indicated in the initial evaluation of thyroid nodules, since this protein is produced by both normal and malignant thyroid cells; however, its measurement can be useful after total thyroidectomy for the follow-up of the disease. In contrast, measuring serum calcitonin levels is recommended in TCs originating from the parafollicular cells (Grani et al., 2024). Additionally, screening for genetic alterations associated with malignancy, including B-Raf proto-oncogene, serine/threonine kinase (*BRAF*) mutations and RET fusions, may be useful in cases of cytologically indeterminate thyroid nodules (Filetti et al., 2019).

1.2.4. Histological Classification

TC can arise from both the thyroid follicular and parafollicular cells. Thyroid tumours originating from the parafollicular cells are the MTCs and represent only 1 to 5% of all cases (Forma et al., 2025; Romei & Elisei, 2021). On the other hand, TCs derived from the thyroid follicular cells account for up to 95% of all TC cases (Forma et al., 2025; Romei & Elisei, 2021). In 2022, the 5th edition of the World Health Organization (WHO) Classification of Endocrine and Neuroendocrine Tumours reorganised follicular cell-derived thyroid neoplasms into three main categories: benign tumours, low-risk neoplasms, and malignant neoplasms, as shown in ***Figure 4*** (Basolo et al., 2023; Juhlin et al., 2022; Jung et al., 2022). This updated

classification is based on the histological features of the tumours, as well as on their morphological and molecular characteristics (Basolo et al., 2023).

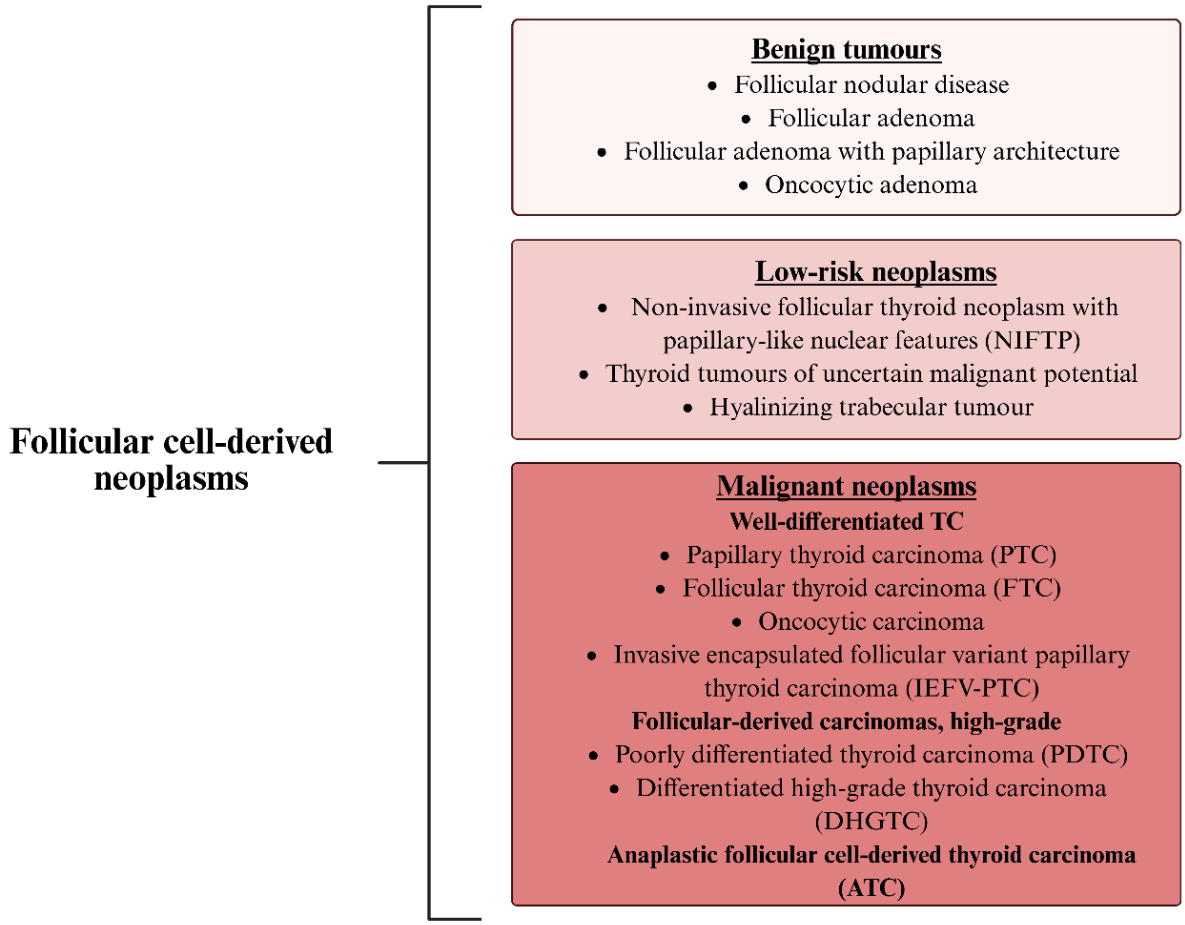


Figure 4: *The 5th edition of the WHO classification of follicular cell-derived thyroid neoplasms. Adapted from: Basolo et al. (2023), Endocrine. DOI:10.1007/s12020-023-03336-4; Jung et al. (2022), Endocrinology and Metabolism. DOI:10.3803/EnM.2022.1553. Created in https://BioRender.com.*

The malignant neoplasms include the papillary thyroid carcinoma (PTC) and the follicular thyroid carcinoma (FTC), which are classified as differentiated thyroid carcinomas (DTCs) (Park et al., 2022). PTC is the most common TC derived from the thyroid follicular cells in both paediatric and adult populations, and accounts for approximately 84% of all cases (Baloch et al., 2022; Boucai et al., 2024). These tumours exhibit a papillary architecture and are characterised by slow tumour growth (Fagin & Mitsiades, 2008; Xing, 2013). They are frequently indolent, and the clinical outcome is generally favourable (Baloch et al., 2022; Fagin & Wells, 2016; Forma et al., 2025). Furthermore, PTCs frequently metastasize to the cervical lymph nodes, particularly to the pretracheal and paratracheal lymph nodes, while distant metastases are a rare event in this type of TC (Forma et al., 2025).

FTC accounts for approximately 4% of all thyroid malignancies and is also associated with a good prognosis (Boucai et al., 2024; Forma et al., 2025). Based on its invasive behaviour, FTC is divided into three subtypes: minimally invasive, encapsulated angioinvasive, and widely invasive (Forma et al., 2025). FTC generally presents as a unifocal tumour, and in contrast to PTC, it rarely metastasizes to the lymph nodes (Fagin & Mitsiades, 2008). Distant metastases are more frequent in this type of TC in comparison to PTC and can occur particularly in the lungs and bones (Fagin & Mitsiades, 2008; Forma et al., 2025).

More aggressive TC subtypes include the differentiated high-grade thyroid carcinoma (DHGTC) and the poorly differentiated thyroid carcinoma (PDTC), which together account for approximately 5% of all TCs (Baloch et al., 2022; Boucai et al., 2024). These tumours represent intermediate forms between DTCs and anaplastic thyroid carcinoma (ATC) and are characterised by specific morphological features, including a solid growth pattern, vascular invasion, a high mitotic rate, infiltrative growth, and tumour necrosis (Fagin & Mitsiades, 2008). Moreover, they can arise from the progression of DTCs due to the accumulation of genetic alterations in the cancer cells (Boucai et al., 2024).

ATC is a very rare form of TC, accounting for approximately 1% of all TCs (Boucai et al., 2024; Forma et al., 2025). It is an undifferentiated tumour that is generally large, highly locally invasive, and can arise from DTCs or PDTCs (Fagin & Mitsiades, 2008; Xing, 2013). These tumours are associated with an extremely poor prognosis, with approximately 50% of TC-related deaths being caused by this type of tumour. Furthermore, distant metastases are frequent in this type of TC, mainly affecting the lungs, bones, and brain (Forma et al., 2025; Jannin et al., 2022).

1.2.5. Progression of Thyroid Cancer and Prognostic Risk Stratification

Most TCs are small, intrathyroidal neoplasms that are clinically indolent, with a favourable prognosis and a low mortality rate (Durante et al., 2023; Soares et al., 2021). Moreover, the life expectancy of patients with TC is similar to that of the general population, with a 10-year survival rate of approximately 90–95% (Dinh et al., 2025). Nevertheless, approximately 10–15% of DTCs progress to more aggressive and potentially fatal forms, characterised by recurrent/persistent disease and/or the development of distant metastases (Agrawal et al., 2014; Mady et al., 2020; Soares et al., 2021). PTCs are more frequently associated with locoregional recurrence, predominantly involving the cervical lymph nodes,

whereas FTCs more commonly progress through the development of distant metastases, mainly in the lungs or bones (Ito & Miyauchi, 2026; Schlumberger & Leboulleux, 2021).

Several prognostic factors have been identified in TC. Age is one of the most important prognostic factors, with advanced age being associated with a worse prognosis. The cut-off age used by the American Joint Committee on Cancer (AJCC) Tumour–Node–Metastasis (TNM) staging system to determine the risk of TC-specific mortality is 55 years. Patients aged 55 years or older are associated with a worse outcome, whereas younger patients are classified as stage I or II, regardless of the presence of metastatic disease (Ibrahimpasic et al., 2019; Ito & Miyauchi, 2026; Zhang & Xu, 2024). Moreover, tumour size also influences prognosis, with tumours larger than 4 cm being associated with poorer disease-free survival (DFS), higher mortality rates, and lower overall survival (OS) (Ito & Miyauchi, 2026). Lymph node metastases measuring 3 cm or more are associated with a higher recurrence risk, and an increasing number of lymph node metastases is correlated with a higher risk of developing distant metastases. In turn, the presence of distant metastases is associated with an overall worse prognosis (Ito & Miyauchi, 2026; Zhang & Xu, 2024). Additionally, although TC is more common in women, male sex has been associated with a worse prognosis, as men more frequently present with aggressive tumour features, including larger tumours, multifocal disease, and lymph node metastases (Ibrahimpasic et al., 2019; Ito & Miyauchi, 2026). However, the prognostic relevance of sex remains controversial (Kim et al., 2024).

As previously mentioned, the AJCC staging system predicts the risk of TC-related mortality. This system is based on the patient's age, the characteristics of the primary tumour (tumour size and macroscopic locoregional disease), and the presence of lymph node or distant metastases (Boucai et al., 2024; Lamartina et al., 2018; Soares et al., 2021; Tuttle & Alzahrani, 2019). ***Table 2*** provides an overview of the 8th edition of the AJCC/TNM staging system.

Table 2: *The 8th edition of the AJCC/TNM staging system.*
Adapted from: Lamartina et al. (2018), Endocrine-Related Cancer. DOI:10.1530/ERC-17-0453.

Patients < 55 years			
Stage I	Any tumour size	Any lymph node status	Without distant metastases
Stage II	Any tumour size	Any lymph node status	With distant metastases
Patients ≥ 55 years			
Stage I	Tumour ≤ 4 cm, limited to the thyroid	Without lymph node metastases	Without distant metastases
Stage II	Tumour of any size with lymph node metastases, or gross extrathyroidal extension invading only the strap muscles, with/without lymph node metastases		Without distant metastases
Stage III	Gross extrathyroidal extension invading the subcutaneous soft tissues, larynx, trachea, oesophagus, or recurrent laryngeal nerve	Any lymph node status	Without distant metastases
Stage IVa	Gross extrathyroidal extension invading the prevertebral fascia or encasing the carotid artery or mediastinal vessels	Any lymph node status	Without distant metastases
Stage IVb	Any tumour size	Any lymph node status	With distant metastases

In addition to the AJCC/TNM staging system, the ATA risk stratification system is used to estimate the risk of disease recurrence based on clinicopathological and molecular tumour features, allowing a dynamic risk assessment. The 2025 version classifies patients into four risk categories: low risk (<10%), low-intermediate risk (10–15%), high-intermediate risk (16–30%), and high risk (>30%) (Ringel et al., 2025; Schlumberger & Leboulleux, 2021; Tuttle & Alzahrani, 2019).

1.3. Genetic Alterations in Follicular Cell-derived Thyroid Cancer

In TC, specific somatic alterations have been identified as key events involved in tumour initiation and progression (Calafato et al., 2025). These genetic alterations predominantly affect the mitogen-activated protein kinase (MAPK) and the phosphoinositide 3-kinase–protein kinase B (PI3K-AKT) pathways, which are illustrated in ***Figure 5*** (Rao & Bernet, 2020; Romei & Elisei, 2021).

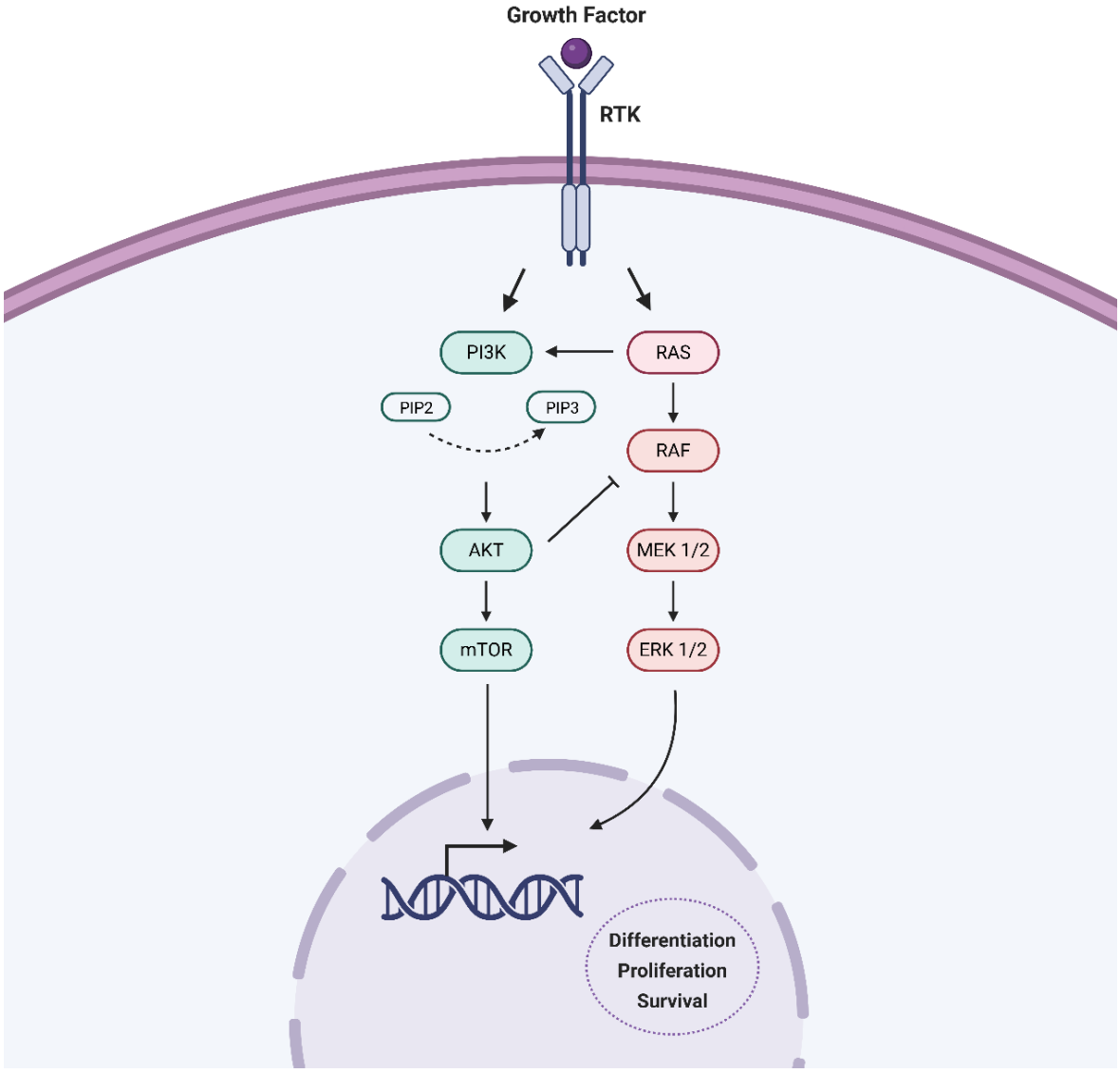


Figure 5: *Schematic representation of the MAPK and PI3K/AKT signalling pathways, highlighting the main molecular components.*
Adapted from: Rao & Bernet (2020), Molecular Genetics & Genomic Medicine. DOI:10.1002/mgg3.1288. Created in https://BioRender.com.

Abbreviations: ***RTK:*** *Receptor Tyrosine Kinase;* ***PI3K:*** *Phosphatidylinositol 3-Kinase;* ***PIP2:*** *Phosphatidylinositol 4,5-Bisphosphate;* ***PIP3:*** *Phosphatidylinositol 3,4,5-Trisphosphate;* ***AKT:*** *Protein Kinase B;* ***mTOR:*** *Mechanistic Target of Rapamycin;* ***RAS:*** *Rat Sarcoma;* ***RAF:*** *Rapidly Accelerated Fibrosarcoma;* ***MEK1/2:*** *Mitogen-Activated Protein Kinase Kinase 1/2;* ***ERK1/2:*** *Extracellular Signal-Regulated Kinase 1/2.*

The MAPK pathway regulates cell differentiation, proliferation, migration, and apoptosis. This signalling pathway is frequently activated in TC cells, mainly through point mutations in the *BRAF* and rat sarcoma (*RAS)* genes, as well as due to RET rearrangements (Liu et al., 2024; Scheffel et al., 2022). These genetic alterations commonly exhibit a mutually exclusive pattern and are present in approximately 70% of PTCs (Prete et al., 2020).

1.3.1. *BRAF* point mutation

The BRAF protein is constitutively active in approximately 7% of all cancers (Prete et al., 2020). The *BRAF* V600E mutation is the most common point mutation affecting the *BRAF* gene in TC, being present in 29–69% of PTCs (Romei & Elisei, 2021; Soares et al., 2021). In this missense mutation, the amino acid valine is replaced by glutamate at codon 600 in exon 15 of the *BRAF* gene (Scheffel et al., 2022; Zhang et al., 2019). As a result, the BRAF protein becomes constitutively active, independently of upstream stimuli, leading to sustained activation of the MAPK pathway and, consequently, promoting cell proliferation and inhibiting apoptosis (Riesco-Eizaguirre, 2025; Tirrò et al., 2019). Furthermore, there is a loss of thyroid cell differentiation, resulting in a decrease in the expression of genes involved in iodine uptake (Riesco-Eizaguirre, 2025). As previously mentioned, this mutation is found in sporadic PTCs; however, it can also be identified in more advanced forms of TC, mainly in ATCs derived from PTCs (19–45%) (Baloch et al., 2022; Zhang et al., 2023). Nevertheless, the *BRAF* V600E mutation is virtually not detected in FTCs nor in benign thyroid lesions (Riesco-Eizaguirre, 2025). Several studies have attempted to describe the impact of this mutation on tumour aggressiveness, recurrence, and mortality; however, its prognostic value remains controversial (Riesco-Eizaguirre, 2025; Scheffel et al., 2022; Soares et al., 2021).

1.3.2. RET rearrangements

RET rearrangements are present in 10-40% of PTCs and are the most common genetic alterations in children and young adults with sporadic PTC (45-60%) (Khonrak et al., 2023). Furthermore, they are particularly frequent in children with PTC following exposure to ionizing radiation after nuclear accidents, such as the Chernobyl disaster (Abdullah et al., 2019; Prete et al., 2020). RET is a receptor tyrosine kinase (RTK) located in the cell membrane (Luzón-Toro et al., 2019). The *RET* gene is located on chromosome 10, and its fusion can occur

with several partner genes, with the *CCDC6* (RET/PTC1) and the *NCOA4* (RET/PTC3) genes being the most common partners (~90% of the cases) (Khonrak et al., 2023; Romei & Elisei, 2021). In RET rearrangements, the 3' region of *RET*, which includes the tyrosine kinase domain, is fused to the 5' portion of the partner gene (Tirrò et al., 2019; Vodopivec & Hu, 2022). This results in the constitutive activation of the RET receptor, independently of ligand binding (Khonrak et al., 2023). Consequently, downstream proteins in the MAPK and PI3K/AKT pathways are continuously activated, leading to sustained stimulation of these pathways and thereby promoting tumorigenesis. Rarely, this genetic alteration is present in more advanced forms of TC, such as ATC (Baloch et al., 2022; Tirrò et al., 2019). However, RET rearrangements have not been consistently associated with prognostic value (Soares et al., 2021).

1.3.3. *RAS* mutations

RAS mutations are primarily found in FTC, with a frequency of 40-50%; however, these alterations are also observed in the follicular variant of papillary thyroid carcinoma (FVPTC) (up to 43%), and in more advanced forms of TC, such as PDTC (5-28%), and ATC (9.5-27%) (Hlozek et al., 2022; Prete et al., 2020). The *RAS* gene family comprises three members: *N-RAS*, *K-RAS*, and *H-RAS*, which encode GTP-binding proteins called p21 RAS proteins, upstream regulators of rapidly accelerated fibrosarcoma (RAF) in the MAPK signalling pathway (Prete et al., 2020; Romei & Elisei, 2021). *N-RAS* is the most frequently mutated in DTCs, followed by *H-RAS* and *K-RAS.* These alterations occur mainly at codons 12, 13, and 61 (Prete et al., 2021; Romei & Elisei, 2021; Tirrò et al., 2019). To be activated, the p21 protein binds to GTP, whereas in its inactive state, it is bound to GDP. Mutations in the *RAS* gene lead to the impairment of p21's ability to hydrolyse GTP to GDP. Consequently, p21 remains constitutively active, resulting in the upregulation of the MAPK pathway (Hernandez-Prera & Wenig, 2024; Romei & Elisei, 2021). Furthermore, these mutations can also promote the activation of the PI3K/AKT pathway through RAS-mediated activation of PI3K (phosphatidylinositol 3-kinase) (Czyzyk et al., 2025; Zhang et al., 2023). Although *RAS* mutations lead to the activation of the MAPK pathway, the level of pathway activation is lower than that observed in BRAF-mutated TCs, as negative feedback loops inhibit RAF proteins in these RAS-mutated tumours. Therefore, they are associated with a better prognosis, as they remain more differentiated (Baloch et al., 2022; Riesco-Eizaguirre, 2025).

1.3.4. *TERTp* mutations

Telomerase is a ribonucleic acid (RNA)-dependent deoxyribonucleic acid (DNA) polymerase that counteracts telomere shortening and, consequently, prevents cells from entering replicative senescence (Schrumpfová & Fajkus, 2020; Smith et al., 2020). This enzyme acts by adding GGTTAG repeats to the 3′ ends of chromosomes. Its structure includes the catalytic subunit, telomerase reverse transcriptase (TERT), which exhibits reverse transcriptase activity, and the telomerase RNA component (TERC), which provides the RNA template for telomeric DNA synthesis. Telomerase activity in human somatic cells is minimal; however, in a large proportion (~80%) of cancers, there is a reactivation of the telomerase enzyme, resulting in replicative immortality, one of the cancer hallmarks (Almansoori et al., 2025; Smith et al., 2020).

In the thyroid gland, cells have limited proliferative activity in adulthood. Nevertheless, approximately 66% of TCs exhibit telomerase reactivation, resulting in an increase in telomerase expression and activity. In TC, telomerase reactivation is primarily driven by mutations in the promoter region of the *TERT* gene (*TERTp* mutations), with −124G>A (C228T) and −146G>A (C250T) being the missense mutations most frequently identified (Matsuse & Mitsutake, 2023; Melo et al., 2014; Soares et al., 2021). These mutations are predominantly found in advanced forms of TC, occurring in approximately 40% of PDTCs and 70% of ATCs. Nevertheless, they can also be identified in PTCs (10%) and FTCs (20%) (Tirrò et al., 2019). Mechanistically, these mutations create novel binding sites for transcription factors, including members of the E-twenty-six (ETS) family, ultimately resulting in increased *TERT* transcription (Almansoori et al., 2025; Melo et al., 2014; Tirrò et al., 2019). Furthermore, *TERTp* mutations have been classified as progression events, being associated with the development of distant metastases, radioactive iodine (RAI) refractoriness, and tumour dedifferentiation, therefore leading to worse clinical outcomes (Baloch et al., 2022; Soares et al., 2021). Moreover, these mutations frequently occur in older patients, with large tumours and extensive local invasion. In PTCs harbouring both the *BRAF* V600E and *TERTp* mutations, a worse prognosis has been described, which suggests that there is a synergistic effect between these genetic alterations (Baloch et al., 2022).

1.3.5. *TP53* mutations

Mutations in the tumour protein p53 (*TP53*) gene, which encodes the tumour suppressor protein p53, can also occur in TC. These alterations are considered tumour progression events, being found in approximately 10-35% of PDTCs and in 40-80% of ATCs (Tirrò et al., 2019). In contrast, these alterations are rare in DTCs (Leandro-García & Landa, 2023). Approximately 80% of *TP53* mutations are missense mutations, predominantly affecting the DNA-binding domain, particularly residues 92–292, and can result in loss of function of the p53 protein (Lacka et al., 2025; Landa & Cabanillas, 2024). p53 is responsible for controlling cell cycle progression and apoptosis, preventing the proliferation and survival of abnormal cells. Therefore, loss of p53 function leads to the impairment of these mechanisms, favouring the proliferation and survival of tumour cells. Consequently, *TP53* mutations can contribute to tumour progression and dedifferentiation, being associated with worse clinical outcomes (Landa & Cabanillas, 2024; Leandro-García & Landa, 2023).

1.4. Thyroid Cancer Treatment

1.4.1. Conventional Treatment

For small thyroid nodules (measuring less than 10 mm or less than 15 mm in the absence of characteristics suspicious for malignancy), patients do not need to undergo biopsy, and their follow-up may consist of periodic ultrasound examinations (Boucai et al., 2024). Additionally, active surveillance with thyroid and cervical lymph node ultrasound is preferred for patients with unifocal PTC measuring up to 1 cm, located away from the recurrent laryngeal nerve and the oesophagus, without evidence of extrathyroidal extension or metastases. These ultrasounds should be performed every 6–12 months (Chen et al., 2023; Filetti et al., 2019). If a significant increase in the tumour size or the development of metastases in the regional lymph nodes is observed, surgery may be required (Chen et al., 2023).

Surgery is the first-line treatment for patients with DTC, and, in approximately 54% of these patients, who have a low risk of recurrence, a cure is achieved. There are two types of surgery that can be performed: lobectomy, in which one of the thyroid lobes is removed, or total thyroidectomy, in which the entire gland is surgically removed. Lobectomy is preferred in cases of small unilateral tumours (1 to 4 cm), without features of high risk, such as

extrathyroidal extension, metastasis, or aggressive cytology. On the other hand, total thyroidectomy is performed in cases of larger tumours (≥ 4 cm) and in bilateral disease. Additionally, removal of the central and lateral cervical lymph node compartments may be considered when lymph node metastases are identified (Boucai et al., 2024; Chen et al., 2023).

1.4.2. Adjuvant Therapy

In DTC treatment, adjuvant therapy includes RAI therapy and TSH suppression (Boucai et al., 2024). RAI therapy utilises iodine-131 (I-131), which leads to selective death of the cells that can capture iodine (Nguyen et al., 2024). RAI administration has three main purposes: (1) elimination of residual normal thyroid tissue to facilitate follow-up by measuring Tg levels; (2) elimination of presumed residual disease; (3) treatment of residual or metastatic disease (Boucai et al., 2024; Chen et al., 2023; Filetti et al., 2019). RAI treatment is recommended in DTCs with high risk of recurrence and is not recommended in patients with low risk. In cases of intermediate risk, it may be used if the tumours present vascular invasion, aggressive histology, or more than five pathological lymph nodes. Additionally, the response to RAI treatment depends on the genetic profile of the tumour: tumours with *RAS* mutations present a greater ability to uptake iodine and therefore have increased sensitivity to RAI treatment, whereas tumours with *BRAF* mutations have been associated with RAI-refractory disease (Boucai et al., 2024).

Levothyroxine therapy has a dual function: on the one hand, it provides thyroid hormone replacement, and on the other hand, it suppresses TSH levels, aiming to decrease the risk of recurrence in patients with DTC (Hannoush & Weiss, 2016). This therapy is based on the assumption that elevated levels of TSH can lead to an increase in tumour cell proliferation as well as an increase in Tg production. Therefore, this approach reduces TSH levels, thereby decreasing tumour cell growth (Boucai et al., 2024; Chen et al., 2023). TSH suppression is recommended in patients with DTC with high risk of recurrence and is not recommended in patients with low or intermediate risk. Moreover, the use of this therapy must be evaluated individually, as it may cause side effects such as osteoporosis and atrial fibrillation (Boucai et al., 2024).

The follow-up of patients with DTC is performed with serum measurement of Tg and anti-thyroglobulin antibodies (TgAb), as well as with cervical ultrasound between 6–18 months after the initial treatment (surgery with or without RAI treatment). In cases of patients with

locoregional and/or distant metastases, or when these are suspected, and in patients with intermediate or high risk of persistent/recurrent disease, other imaging exams may be performed, including PET-CT, MRI, and whole-body radioiodine scintigraphy (WBS) (Boucai et al., 2024; Filetti et al., 2019).

1.4.3. Treatment of Advanced Disease

For the treatment of advanced DTCs, it is important to determine whether the tumours are refractory to RAI, as RAI-refractory disease occurs in approximately 50% of metastatic cases and is associated with a worse prognosis. RAI-refractoriness can be identified by (1) the absence of RAI uptake outside the thyroid bed after the initial treatment; (2) the loss of RAI uptake in lesions that previously concentrated iodine; (3) differences in RAI uptake between tumour lesions, with some lesions showing uptake while others do not; and (4) continued progression of metastatic disease despite RAI uptake, particularly within 6 to 12 months following I-131 treatment.

If the disease is responsive to RAI therapy, this approach remains the main strategy for the treatment of advanced DTCs; however, when RAI-refractory disease progresses, other therapeutic options can be employed. These include external beam radiotherapy (EBRT), immunotherapy, and systemic targeted therapies (Hamidi et al., 2023).

1.4.3.1. Radiotherapy and Chemotherapy

In RAI-refractory DTCs with a high risk of locoregional progression, which are characterised by aggressive histologic subtypes, macroscopic extrathyroidal extension, and invasion of soft tissues or visceral structures, EBRT, with or without chemotherapy, may be used. Additionally, this approach can also be considered in patients with DTC presenting with macroscopic residual disease in the postoperative setting or with locally advanced unresectable disease (Ringel et al., 2025).

In ATCs with localised disease who undergo surgery with complete or near-complete resection, EBRT can also be applied to eliminate microscopic disease and reduce the risk of recurrence. In this case, EBRT can be combined with chemotherapy (mainly doxorubicin and platinum-based agents). Furthermore, it can also be used in advanced unresectable ATC as a palliative treatment (Filetti et al., 2019).

1.4.3.2. Immunotherapy

Immunotherapy, mainly immune checkpoint inhibitors (ICIs), including those targeting programmed cell death protein 1 (PD-1), programmed death-ligand 1 (PD-L1), or cytotoxic T-lymphocyte–associated protein 4 (CTLA-4), is being investigated for use in TC treatment (Cheng & Newbold, 2025). Clinical trials using the immune checkpoint inhibitor pembrolizumab (anti–PD-1) have shown limited efficacy in patients with RAI-refractory DTC. Therefore, it is not a standard treatment for these patients. Nevertheless, this drug is approved by the Food and Drug Administration (FDA) for the treatment of unresectable or metastatic solid tumours with high tumour mutational burden (TMB), regardless of the tumour type. Therefore, it can also be an option in some advanced TCs with high TMB (Ringel et al., 2025). Approximately one-third of ATCs present high expression of PD-L1, tumour lymphocytic infiltration, and high TMB, suggesting a potential response to immunotherapy (Cheng & Newbold, 2025; Filetti et al., 2019). In this type of TC, PD-1/PD-L1 inhibitors, such as spartalizumab (anti–PD-1), have shown promising results (Filetti et al., 2019).

1.4.3.3. Receptor Tyrosine Kinase Inhibitors (RTKIs)

The initiation of systemic therapy in TC is indicated in cases of malignancy progression documented on imaging exams performed within the previous 14 months, symptomatic disease, impairment of organ or limb function, and tumours measuring ≥ 1.5 cm (Boucai et al., 2024).

In locally advanced RAI-refractory DTCs, first-line systemic treatment consists of using the multikinase inhibitors (MKIs), Sorafenib or Lenvatinib. As second-line treatment, Cabozantinib, another MKI, has emerged. Following treatment with the MKIs, targeted therapy can be considered, namely the use of RET inhibitors, such as Selpercatinib and Pralsetinib, in RET fusion-positive tumours (Chen et al., 2023; Karapanou et al., 2022). A detailed description of all RTKIs mentioned in this section is provided in ***Table 2***.

In advanced forms of TC, including ATC, a genetic analysis of the tumour is recommended in order to identify potential molecular targets that can be relevant for targeted therapy. These genetic alterations include the *BRAF* V600E mutation, where tumours harbouring this mutation can be treated with the combination of Dabrafenib and Trametinib, RET fusions, which can be targeted with Selpercatinib or Pralsetinib, and neurotrophic tyrosine

receptor kinase (NTRK) fusions, for which Larotrectinib and Entrectinib are available (Boucai et al., 2024; Chen et al., 2023; Cheng & Newbold, 2025).

***Table 3**: RTKIs approved by the FDA/EMA, their molecular targets, and their indications in thyroid cancer treatment.*
Adapted from: Boucai et al. (2024), JAMA. DOI:10.1001/jama.2023.26348; Chen et al. (2023), The Lancet. DOI:10.1016/S0140-6736(23)00020-X; Cheng & Newbold (2025), Drugs. DOI:10.1007/s40265-025-02233-6; and Karapanou et al. (2022), Endocrine-Related Cancer. DOI:10.1530/ERC-22-0006.

Drugs	Molecular Targets	TC Indications	FDA/EMA Approval
Sorafenib	VEGFR, PDGFR, RET, RAF, c-KIT	1st-line treatment for RAI-refractory DTC	FDA/EMA approved
Lenvatinib	VEGFR, PDGFR, FGFR, RET, c-KIT	1st-line treatment for RAI-refractory DTC	FDA/EMA approved
Cabozantinib	VEGFR, MET, RET	2nd-line treatment for RAI-refractory DTC	FDA/EMA approved
Selpercatinib	RET fusions	RAI-refractory DTC with RET fusion	FDA/EMA approved
Pralsetinib	RET fusions	RAI-refractory DTC with RET fusion	FDA approved
Larotrectinib	NTRK fusions	NTRK-fusion TC	FDA/EMA approved[a]
Entrectinib	NTRK fusions	NTRK-fusion TC	FDA/EMA approved[a]
Dabrafenib + Trametinib	*BRAF* V600E mutation	*BRAF* V600E-mutated TC	FDA/EMA approved[b]

[a]Approved by the FDA and EMA for the treatment of pediatric and adult patients with NTRK fusion-positive solid tumours.
[b]Approved by the FDA for the treatment of patients with *BRAF* V600E-mutant ATC; approved by the EMA for the treatment of patients with locally advanced or metastatic *BRAF* V600E-mutant DTC refractory to or not eligible for RAI.

Abbreviations: **VEGFR:** Vascular Endothelial Growth Factor Receptor; **PDGFR:** Platelet-Derived Growth Factor Receptor; **FGFR:** Fibroblast Growth Factor Receptor; **MET:** Mesenchymal–Epithelial Transition factor receptor; **RAF**: Rapidly Accelerated Fibrosarcoma; **c-KIT:** KIT proto-oncogene receptor tyrosine kinase; **RET:** Rearranged during Transfection proto-oncogene**; NTRK:** Neurotrophic Tyrosine Receptor Kinase; **BRAF:** B-Raf proto-oncogene, serine/threonine kinase; **RAI-refractory DTC:** Radioactive Iodine-Refractory Differentiated Thyroid Cancer; **ATC:** Anaplastic Thyroid Carcinoma; **FDA:** Food and Drug Administration; **EMA:** European Medicines Agency.

1.5. Vemurafenib and BRAF Inhibitors in Thyroid Cancer

The RAF family of serine/threonine kinases includes three isoforms: A-RAF, B-RAF and C-RAF, which can function as monomers or dimers. These isoforms present three conserved regions (CRs): CR1, CR2, and CR3. The CR1 region has the RAS-binding domain (RBD), which mediates the interaction between RAS and RAF proteins. The CR2 region contains binding sites for regulatory proteins. The CR3 region represents the kinase domain, where the adenosine triphosphate (ATP)-binding pocket is located, and contains the binding site for mitogen-activated protein kinase kinase 1/2 (MEK1/2) proteins. This domain also includes the activation segment, which regulates the conformation and activity of the BRAF protein (Roskoski, 2010). The *BRAF* V600E mutation occurs within the activation segment and results in the substitution of the amino acid valine by glutamate, introducing a negative charge that mimics the negative charge of a phosphate group. Consequently, the BRAF protein remains in a constitutively active conformation, allowing the ATP molecule to bind to the catalytic site, thereby leading to a sustained phosphorylation of the MEK1 and MEK2 downstream proteins (Bollag et al., 2012; Harris, 2014; Roskoski, 2010).

Vemurafenib is an ATP-competitive inhibitor that was first synthesised in 2005. This drug binds to the ATP-binding pocket of the BRAF protein, thereby preventing ATP binding. Dabrafenib is another ATP-competitive BRAF inhibitor with a similar mechanism of action (Bollag et al., 2012; Harris, 2014). Moreover, both Vemurafenib and Dabrafenib bind preferentially to the mutated form of the BRAF protein (Holderfield et al., 2014).

In TC cells harbouring the *BRAF* V600E mutation, Vemurafenib has been shown to decrease cell viability and proliferation. Additionally, it blocks the cell cycle (with accumulation of cells in the G0/G1 phase) and inhibits the MAPK pathway by decreasing extracellular signal-regulated kinase (ERK) phosphorylation levels (Notarangelo et al., 2017); nevertheless, a rebound in ERK phosphorylation levels has also been described following prolonged treatment with this drug (Montero-Conde et al., 2013; Notarangelo et al., 2017).

In 2016, a phase II clinical trial conducted by Brose et al. evaluated Vemurafenib and included 51 patients with metastatic or unresectable RAI-refractory PTC harbouring the *BRAF* V600E mutation. The individuals were separated into two cohorts: cohort 1 included 26 patients who had never been treated with a vascular endothelial growth factor receptor (VEGFR)-targeted MKI, whereas cohort 2 comprised 25 patients who had undergone therapy with a VEGFR-targeted MKI. This clinical trial showed promising results, since Vemurafenib

exhibited an antitumour effect in patients from both cohorts. In cohort 1, 38.5% of the patients achieved a partial response, compared with 27.3% in cohort 2. Therefore, Vemurafenib showed efficacy in RAI-refractory PTC presenting the *BRAF* V600E mutation, with better responses in patients without previous MKI therapy (Brose et al., 2016).

In a subsequent pilot study that included 10 patients with RAI-refractory TC harbouring the *BRAF* V600E mutation, Vemurafenib also exhibited promising results. The patients underwent treatment with Vemurafenib for 4 weeks, after which a PET-CT scan was performed to evaluate whether the ability to uptake iodine was restored. They observed that 4 of the 10 patients were iodine-124 responders and were subsequently treated with I-131. In these patients, tumour regression was observed, indicating that Vemurafenib can restore RAI uptake and the sensitivity of the tumour to RAI therapy (Dunn et al., 2019).

Although Vemurafenib showed promising results in TC treatment, some studies have also reported molecular mechanisms leading to the development of resistance to this drug. In 2013, Montero-Conde et al. described that in TC cells with the *BRAF* V600E mutation, in contrast to melanoma cell lines, there is a reactivation of the MAPK pathway upon treatment with Vemurafenib. This reactivation was explained by an increase in the expression and activation of upstream RTKs, namely human epidermal growth factor receptor 2 (HER2) and human epidermal growth factor receptor 3 (HER3), which can activate the MAPK pathway (Montero-Conde et al., 2013). Moreover, an additional study has demonstrated that in TC cells with the *BRAF* V600E mutation, treatment with Vemurafenib leads to a rapid feedback mechanism involving epidermal growth factor receptor (EGFR) activation. Therefore, blocking EGFR and BRAF simultaneously resulted in a prolonged inhibition of the MAPK pathway, ultimately leading to a decrease in the survival of the cells and potentiating the effects of Vemurafenib (Notarangelo et al., 2017). Therefore, combination strategies were investigated to overcome the resistance mechanisms associated with Vemurafenib. Montero-Conde et al. demonstrated that the MEK inhibitor AZD6244 blocked the ERK rebound induced by the BRAF inhibitor Vemurafenib in *BRAF* V600E-mutant TC cell lines, providing a rationale for combined BRAF and MEK inhibition (Montero-Conde et al., 2013).

The phase II clinical trial conducted by Subbiah et al. evaluated the efficacy of the combination therapy with the BRAF inhibitor Dabrafenib and the MEK inhibitor Trametinib in patients with ATC harbouring the *BRAF* V600E mutation. The study demonstrated clinically meaningful results, with an overall response rate (ORR) of 56%, a median progression-free

survival (PFS) of 6.7 months, and a median OS of 14.5 months. These findings represented a major advance in the treatment of ATC, a highly aggressive malignancy that has historically been associated with a median OS of less than 6 months (Subbiah et al., 2022).

1.6. Correlation between *BRAF* V600E and *TERTp* mutations

The co-occurrence of *TERTp* mutations with the *BRAF* V600E mutation has been reported in approximately 10% of PTCs (Song & Park, 2020). Several studies have shown that PTCs harbouring both the *BRAF* V600E and *TERTp* mutations are associated with a poorer prognosis than tumours carrying either alteration alone. These tumours have been associated with a higher risk of recurrence, advanced disease stage, presence of metastases, loss of thyroid differentiation, and increased mortality (Landa, 2023; Xing et al., 2014). In vivo, Landa et al. further demonstrated that *TERTp* mutations can promote tumour progression in the context of oncogenic *BRAF* V600E, showing that the introduction of a *TERTp* mutation into mice already harbouring the *BRAF* V600E mutation led to the progression of PTC to more aggressive forms, such as PDTC and ATC (Landa et al., 2023).

Additionally, our group has demonstrated that TCs harbouring both the *BRAF* V600E and *TERTp* mutations display significantly higher levels of *TERT* messenger RNA (mRNA) expression than tumours carrying only *TERTp* mutations (Vinagre et al., 2013). This finding may be explained by the ability of the *BRAF* V600E mutation to upregulate the expression of transcription factors, particularly members of the ETS family, which are capable of binding to the mutant *TERTp* in TC cells, thereby enhancing *TERT* transcription (Liu et al., 2014; Song & Park, 2020). Several ETS transcription factors have been reported to be upregulated downstream of *BRAF* V600E and to promote *TERT* expression, including GA-binding protein subunit beta (GABPB), ETS variant transcription factor 1 (ETV1), ETS variant transcription factor 4 (ETV4), ETS variant transcription factor 5 (ETV5), and ETS homologous factor (EHF) (Bullock et al., 2019; Liu et al., 2018; Song et al., 2019; Y. Xu et al., 2025).

Moreover, a study conducted in 2025 by Xu et al. showed that, in a PTC cell line with concurrent *BRAF* V600E and *TERTp* mutations, *TERT* mRNA expression significantly decreased following *BRAF* V600E knockdown using a small interfering RNA (siRNA). In contrast, *TERT* expression was not significantly reduced in a PTC cell line harbouring the *BRAF* V600E mutation but carrying a wild-type *TERT* promoter. These findings suggest that

BRAF activity is required to maintain *TERT* expression, particularly in the presence of a *TERT* promoter mutation (Y. Xu et al., 2025).

An additional study demonstrated that treatment with the BRAF inhibitor PLX4032 (Vemurafenib) reduced both *TERT* mRNA and protein expression in TC cell lines harbouring both the *BRAF* V600E and *TERTp* mutations. This highlighted that *TERT* expression depends on MAPK pathway activation. However, this study evaluated the effects of BRAF inhibition under limited timepoint and concentration conditions (24 h and 0.5 μM, respectively) (Liu et al., 2018). Therefore, it remains unclear whether this reduction is maintained during prolonged treatment, particularly considering the adaptive MAPK pathway reactivation reported in TC following BRAF inhibition (Montero-Conde et al., 2013; Notarangelo et al., 2017).

2. Aims

Over recent years, several strategies have been investigated to target telomerase reactivation, which leads to replicative immortality, one of the hallmarks of cancer. These approaches include immunotherapies, such as cancer vaccines, and direct telomerase inhibitors, such as the oligonucleotide Imetelstat (Shou et al., 2025). Nevertheless, targeted therapies for TCs harbouring *TERTp* mutations remain unavailable, and these mutations are used only as prognostic biomarkers (Yang et al., 2026).

Based on the previously described association between the presence of the *BRAF* V600E mutation and increased *TERT* expression reported in TCs, there is a rationale to investigate whether pharmacological BRAF inhibition can decrease *TERT* expression in TCs harbouring both the *BRAF* V600E and *TERTp* mutations. This effect can be further investigated at 48 and 72 h after treatment to assess if the reduction in *TERT* expression is sustained over prolonged treatment and reflected in changes in cellular biological parameters.

Therefore, the present study aims to:

- Determine whether Vemurafenib, a BRAF inhibitor, can modulate *TERT* expression in TC cells harbouring both the *BRAF* V600E and *TERTp* mutations.
- Functionally characterise the effects of Vemurafenib on the viability and proliferation of immortalised thyroid-derived cells as well as on TC-derived cell lines.
- Molecularly characterise the effects of Vemurafenib on the expression of key proteins involved in the MAPK signalling pathway in cell lines with different genetic backgrounds.
- Analyse publicly available RNA sequencing (RNA-seq) data from TC cells carrying both the *BRAF* V600E and *TERTp* mutations and treated with Vemurafenib, to identify differentially expressed genes (DEGs) and the biological processes affected by BRAF inhibition.

3. Materials and Methods

3.1. Cell Culture

For the assays conducted in this project, three cell lines were selected: an immortalised normal thyroid-derived cell line (Nthy-Ori 3-1) and two PTC-derived cell lines (B-CPAP and TPC-1). B-CPAP harbours the *BRAF* V600E, *TP53* D259Y, and *TERTp* (-124 G>A) mutations, whereas TPC-1 carries the RET/PTC1 rearrangement and the *TERTp* mutation (-124 G>A) (Caria et al., 2018; Cellosaurus, 2025a, 2025b). These cell lines were cultured in Roswell Park Memorial Institute medium 1640 (RPMI 1640) with stable glutamine (Capricorn Scientific) supplemented with 10% fetal bovine serum (heat inactivated, Gibco™, Thermo Fisher Scientific), 1% Penicillin–Streptomycin Solution (100×, Biowest), and 0.5% Amphotericin B solution (250 µg/mL, Corning). These adherent cells were maintained at 37°C in a humidified atmosphere with 5% CO_2.

3.2. Treatment with Vemurafenib

Vemurafenib (Genentech, Roche Group; molecular weight 489.92 g/mol) was completely dissolved in dimethyl sulfoxide (DMSO), resulting in a 50 mM stock solution. For the half-maximal inhibitory concentration (IC_{50}) determination, the 50 mM stock solution was serially diluted in complete culture medium to obtain the following Vemurafenib concentrations: 2.5, 5, 10, 25, and 50 µM. For the subsequent experiments, the three cell lines were treated with cell culture medium supplemented with 15 µM Vemurafenib, which corresponds to the IC_{50} concentration determined for the B-CPAP cell line after 48 h of exposure. The negative control consisted of cell culture medium containing 0.03% (v/V) DMSO, corresponding to the final DMSO concentration used in cells treated with 15 µM Vemurafenib. The effects of the drug were then evaluated using different assays.

3.3. Cell Viability Assay and IC_{50} determination

The cell viability assay was based on the PrestoBlue™ test (Invitrogen™, Thermo Fisher Scientific), which assesses cellular metabolic activity. Resazurin, the active component of the PrestoBlue™ reagent, is blue and virtually non-fluorescent. Upon entering viable cells, resazurin is reduced by the intracellular reducing environment to resorufin, which is red and highly fluorescent. Therefore, fluorescence intensity correlates with the percentage of viable cells (Thermo Fisher Scientific, 2019).

In this assay, the Nthy-Ori 3-1, B-CPAP, and TPC-1 cell lines were seeded in 96-well solid black flat-bottom plates (Corning). B-CPAP cells were seeded at 3 000 cells per well, whereas TPC-1 and Nthy-Ori 3-1 cells were seeded at 1 500 cells per well, with each well containing a final volume of 100 µL of cell suspension. To determine the IC_{50}, 24 h after seeding, the cells were treated with cell culture medium supplemented with increasing concentrations of Vemurafenib (2.5, 5, 10, 25, and 50 µM). Additionally, control wells containing the same DMSO percentage as in each Vemurafenib-treated condition were included, as well as control wells receiving fresh culture medium only. After the treatment, the cells were incubated for 48 and 72 h at 37 °C in a 5% CO_2 atmosphere.

Following the incubation periods, the cell culture medium in each well was replaced with fresh cell culture medium containing 11% (v/V) of the PrestoBlue™ reagent, and the cells were incubated for 1 h at 37 °C in a 5% CO_2 atmosphere. Cell viability was then evaluated using a microplate reader – CLARIOstar (BMG Labtech) by measuring fluorescence (excitation/emission: 560/590 nm). The IC_{50} values of Vemurafenib for each cell line were determined using GraphPad Prism 11 (GraphPad Software) by nonlinear regression analysis of inhibitor concentration versus normalised response.

This experiment was done in three biological replicates, each including three technical replicates per condition.

3.4. Cell Proliferation Assay

Cell proliferation was assessed in the Nthy-Ori 3-1, B-CPAP, and TPC-1 cell lines using the Click-iT™ Plus EdU Cell Proliferation Kit for Imaging, Alexa Fluor™ 647 dye (Thermo Fisher Scientific). This assay is based on the incorporation of 5-ethynyl-2′-deoxyuridine (EdU), a thymidine nucleoside analogue, into newly synthesised DNA strands during the S-phase of the cell cycle. The incorporated EdU is subsequently detected through a copper-catalysed click reaction between an alkyne group present in the EdU and an azide present in the Alexa Fluor™ 647 dye, resulting in the formation of a covalent bond that enables the red fluorescent labelling of the nuclei of the proliferating cells. In addition, staining with the blue fluorescent nuclear dye Hoechst® 33342 enables visualization and quantification of total cells (Thermo Fisher Scientific, 2014).

For this assay, the cells were seeded in 96-well black, optically clear flat-bottom PhenoPlates (Revvity). Nthy-Ori 3-1, B-CPAP, and TPC-1 cells were seeded at 1 500, 2 000, and 750 cells per well, respectively, using 100 µL of cell suspension per well, followed by incubation at 37 ºC in a 5% CO_2 atmosphere. After 24 h, the cell culture medium was replaced with 100 µL per well of fresh medium corresponding to the three experimental conditions: cell culture medium supplemented with 15 µM Vemurafenib (treatment), cell culture medium with 0.03% (v/V) DMSO (negative control), or fresh cell culture medium. For each cell line, three biological replicates were used, each including three technical replicates per condition: 15 µM Vemurafenib, 0.03% DMSO, and cell culture medium.

At 46 h and 70 h post-treatment, 50 µL of the cell culture medium was removed from each well and replaced with fresh culture medium under the same three experimental conditions (medium with 15 µM of Vemurafenib, medium with 0.03% DMSO, or complete medium) supplemented with 10 µM of EdU. The cells were then incubated for 2 h at 37 ºC in a 5% CO_2 atmosphere, completing 48 h and 72 h of exposure to the respective conditions (treatment, negative control, and cell culture medium).

After incubation, the cells were washed once with 1× phosphate-buffered saline (PBS) and then fixed with 4% (w/V) paraformaldehyde in 1× PBS for 20 minutes at room temperature (RT). Afterward, the cells were washed twice with 3% (w/V) bovine serum albumin (BSA) in 1× PBS, and 100 µL of the permeabilization solution (0.5% Triton X-100 in 1× PBS) was added, followed by incubation at RT for 20 minutes. Subsequently, the cells were washed twice with 3% BSA in 1× PBS, and 50 µL of the Click-iT™ reaction cocktail was added to each well,

followed by incubation for 30 minutes at RT. Thereafter, the cells were washed once with 3% BSA in 1× PBS and once with 1× PBS. Finally, 50 µL of the nuclear dye (Hoechst 33342; 1:10 000, diluted in 1× PBS) was applied for 30 minutes, after which the cells were washed three times with 1× PBS, and 100 µL of 1× PBS was added to each well. Cell proliferation was then evaluated using the Operetta CLS imaging system (Revvity).

Data analysis was performed using Harmony™ High-Content Imaging and Analysis Software (Revvity), and the percentage of proliferating cells was calculated using the following formula:

$$Percentage\ of\ Proliferating\ Cells = \frac{Number\ of\ EdU\ positive\ nuclei}{Total\ number\ of\ nuclei} \times 100$$

3.5. Cell Pellet Collection

Cell pellets were collected for subsequent RNA and protein extraction. For this purpose, Nthy-Ori 3-1, B-CPAP, and TPC-1 cells were seeded at 150 000, 175 000, and 25 000 cells per T-25 flask, respectively, in 5 mL of cell suspension per flask, and kept at 37 °C in a 5% CO_2 atmosphere, to reach approximately 70–80% confluence 96 h after seeding.

At 24 h post-seeding, the cell culture medium was replaced according to each experimental condition: cell culture medium supplemented with 15 µM Vemurafenib for the treatment condition, cell culture medium containing 0.03% DMSO for the negative control, or fresh cell culture medium only for the control condition.

At 48 h and 72 h post-treatment, the cell culture medium was collected and transferred to a 15 mL Falcon tube (one per T-25 flask). Subsequently, cells were washed with 2 mL of 1× PBS, which was combined with the respective collected medium. The adherent cells were detached using TrypLE Express (1 mL) at 37 ºC, and enzymatic activity was neutralised by the addition of cell culture medium (4 mL). The resulting cell suspension was then pooled with the corresponding fraction in the same Falcon tube and centrifuged at 300 × g for 5 minutes at 4 °C. The supernatant was discarded, and the pellet was resuspended in 1 mL of 1× PBS (4 °C) and transferred to an Eppendorf tube. Subsequently, the resuspended cells were centrifuged again at 300 × g for 5 minutes at 4 °C. The supernatant was discarded, and the pellets were stored at −80 °C until further use.

This procedure involved three biological replicates for each cell line, three experimental conditions (treatment, medium with DMSO, and medium only), two technical replicates per condition, and two time points (48 h and 72 h). Cells from a whole T-25 flask were used for either protein or RNA extraction, without fractionation.

3.6. RNA Extraction and Quantification

RNA extraction was performed using the GRS Total RNA Kit – Blood & Cultured Cells (GK08.0100; GRiSP), following the manufacturer's instructions. First, cell pellets were resuspended in 100 µL of Red Blood Lysis Buffer. Subsequently, 400 µL of Buffer R1 were added, followed by the addition of 4 µL of β-mercaptoethanol. The mixture was vigorously mixed and incubated for 5 minutes at RT. Afterwards, 500 µL of 70% ethanol were added. The RNA mini spin column was then placed in a 2 mL collection tube, and 500 µL of the sample mixture were transferred to the column, followed by centrifugation at 16 000 × g for 1 minute at RT. Unless indicated otherwise, the flow-through was discarded after each centrifugation step. The remaining sample mixture was then loaded onto the column and centrifuged at 16 000 × g for 1 minute at RT.

Next, 400 µL of Wash Buffer 2 were added, followed by centrifugation at 16 000 × g for 1 minute at RT. A mixture of 45 µL of deoxyribonuclease (DNase) I reaction buffer with 5 µL of DNase I solution was then dispensed into each column, and the columns were incubated for 15 minutes at RT. Subsequently, 400 µL of Wash Buffer 1 were added, followed by centrifugation at 16 000 × g for 1 minute at RT. Then, 600 µL of Wash Buffer 2 were loaded onto each column and centrifuged at 16 000 × g for 1 minute at RT; this step was repeated once. The columns were then dried by centrifugation for 3 minutes at 16 000 × g at RT.

For elution, each column was transferred to a new ribonuclease (RNase)-free 1.5 mL microcentrifuge tube. DNase/RNase-free water (Invitrogen™, Thermo Fisher Scientific) was added to each column (20 µL for Nthy-Ori 3-1, 15 µL for B-CPAP, and 30 µL for TPC-1 samples), followed by incubation at RT for 2 minutes. RNA was eluted by centrifugation at 16 000 × g for 1 minute at RT. The column was discarded, and the eluted RNA was stored at −80 °C.

RNA quantification was performed using 1.5 µL of each RNA sample on a NanoDrop™ One spectrophotometer (Thermo Scientific).

3.7. cDNA Synthesis from Extracted RNA

For complementary DNA (cDNA) synthesis, 1 µg of total RNA from each sample was used. The volume of each RNA sample was adjusted with nuclease-free water to a final volume of 8 µL. Subsequently, DNase I treatment was performed to remove potential genomic DNA contamination. For this purpose, 1 µL of DNase I, RNase-free (1 U/µL) (Thermo Fisher Scientific), and 1 µL of 10× Reaction Buffer with $MgCl_2$ for DNase I (Thermo Fisher Scientific) were added to each RNA sample. The samples were then incubated for 30 minutes at 37 °C in a thermal cycler. Afterwards, 1 µL of the chelating agent ethylenediaminetetraacetic acid (EDTA) (50 mM; Thermo Fisher Scientific) was added to each sample, and the samples were incubated for 10 minutes at 65 °C in a thermal cycler. Next, 1 µL of Random Hexamer Primer (0.2 µg/µL; Thermo Fisher Scientific) was added to each sample, and the samples were incubated for 5 minutes at 65 °C in a thermal cycler. Subsequently, two master mixes were prepared using the volumes shown in the following table (***Table 4***), with all reagents obtained from Thermo Fisher Scientific.

Table 4: *Volumes of the reagents used to prepare the reaction mixes with reverse transcriptase (RTase) and without reverse transcriptase (no-RTase control).*

Component	RTase reaction mix	no-RTase control mix
Nuclease-free water	0.5 µL	1.5 µL
5× Reaction Buffer for Reverse Transcriptase	4 µL	4 µL
RiboLock RNase Inhibitor (40 U/µL)	0.5 µL	0.5 µL
Deoxyribonucleotide triphosphate (dNTP) Mix (10 mM)	2 µL	2 µL
RevertAid Reverse Transcriptase (200 U/µL)	1 µL	-
Total volume	8 µL	8 µL

Note. Volumes correspond to a single reaction. Master mixes were prepared by scaling the volumes according to the number of sample reactions.

From the reverse transcriptase (RTase) reaction mix, 8 µL were added to each RNA sample, as well as to a no-template control without RNA. In addition, 8 µL of the no-RTase control mix was dispensed into a control reaction containing RNA but lacking the RTase enzyme.

The samples, together with the negative controls (no-RTase and no-template controls), were then incubated for 10 minutes at 25 °C, 60 minutes at 42 °C, and 10 minutes at 70 °C in a thermal cycler, enabling first-strand cDNA synthesis from RNA templates through reverse transcription. Finally, the cDNA samples and the negative controls were stored at −20 °C for further use.

3.8. RT-qPCR

Reverse transcription products were amplified for the *TERT* gene by reverse transcription quantitative polymerase chain reaction (RT-qPCR) (IDT; no. Hs.PT.58.21382682), using the TATA-binding protein gene (*TBP*) as an endogenous control (IDT; no. Hs.PT.39a.22214825).

For each target gene, an independent master mix was prepared using the volumes shown in the following table (***Table 5***).

Table 5: *Volumes of the reagents used for the preparation of the reaction mixes containing the TBP and TERT probes.*

Components	*TBP* reaction mix	*TERT* reaction mix
Nuclease-free water	3.5 µL	3.5 µL
TaqMan™ Universal PCR Master Mix, No AmpErase™ UNG (Applied Biosystems™, Thermo Fisher Scientific)	5 µL	5 µL
TaqMan *TBP* probe	0.5 µL	-
TaqMan *TERT* probe	-	0.5 µL
Total volume	9 µL	9 µL

Note. Volumes correspond to a single reaction. Master mixes were prepared by scaling the volumes according to the number of sample reactions.

From each master mix, 9 µL were dispensed into the wells of a MicroAmp™ Optical 96-Well Reaction Plate (Applied Biosystems™, Thermo Fisher Scientific). Subsequently, 1 µL of each cDNA sample was added in triplicate, generating three technical replicates per reaction (final volume of 10 µL per well), for both the *TBP* and *TERT* assays. In addition, wells containing only the reaction mixes without cDNA template were included as non-template controls for each assay. The negative controls (no-template and no-RTase controls) generated during cDNA synthesis were also included and analysed for both the *TERT* and *TBP* genes.

RT-qPCR was performed on a QuantStudio™ 5 Real-Time polymerase chain reaction (PCR) System (Applied Biosystems™, Thermo Fisher Scientific), using the following cycling conditions: initial denaturation at 95 °C for 10 minutes, followed by 50 cycles of 95 °C for 15 seconds and 60 °C for 1 minute, with a ramp rate of 1.6 °C/s. Relative gene expression was determined using the $2^{-\Delta\Delta Ct}$ method, where Ct represents the cycle threshold.

3.9. Total Protein Extraction and Quantification

Protein extraction was performed from cell pellets of Nthy-Ori 3-1, B-CPAP, and TPC-1 cells. A lysis buffer mixture was prepared by supplementing radioimmunoprecipitation assay (RIPA) buffer (50 mM Tris-HCl pH = 7.4, 1% (v/V) NP-40, 150 mM NaCl, 0.1% (w/V) SDS, and 2 mM EDTA) with phosphatase and protease inhibitors at final concentrations of 1% (v/V) and 4% (v/V), respectively. The volume of lysis buffer mixture used to resuspend the cell pellets from each experimental condition (treatment with 15 µM Vemurafenib, 0.03% DMSO control, and medium-only control), at each timepoint and for each cell line, is summarised in ***Table 6***.

Table 6: *Volumes of lysis buffer mixture (µL) used for cell pellet resuspension in each experimental condition: Treatment (15 µM Vemurafenib), DMSO control (cell culture medium with 0.03% DMSO), and Medium-only control at each timepoint (48 h and 72 h) and for each cell line (Nthy-Ori 3-1, B-CPAP and TPC-1).*

Cell lines	Conditions					
	48 h			72 h		
	Treatment	DMSO control	Medium-only control	Treatment	DMSO control	Medium-only control
Nthy-Ori 3-1	75 µL	75 µL	75 µL	100 µL	100 µL	100 µL
B-CPAP	50 µL	50 µL	50 µL	50 µL	100 µL	100 µL
TPC-1	100 µL	100 µL	100 µL	100 µL	100 µL	100 µL

Following the resuspension of the cell pellets in the lysis buffer mixture, samples were incubated on ice for 15 minutes and subsequently centrifuged at 14 000 rpm for 10 minutes at 4 °C. The supernatant was collected and stored at −80 °C, while the pellet was discarded. Additionally, 3 µL of each protein lysate was aliquoted and stored separately for subsequent protein quantification.

The protein lysates obtained were quantified using the Bio-Rad DC Protein Assay (Bio-Rad Laboratories), following the manufacturer's instructions. For this purpose, 3 µL of each protein lysate was diluted 1:5 in nuclease-free water before quantification. A standard curve was generated in a 96-well flat-bottom plate (TPP) by adding 5 µL of nuclease-free water as a blank and 5 µL of BSA standards at known concentrations (0.25, 0.5, 0.75, 1.0, 1.25, 1.5, and 3.0 mg/mL), all prepared in duplicate. Subsequently, samples were loaded in duplicate (5 µL per well).

After that, a mixture was prepared with reagent A (an alkaline copper tartrate solution) and reagent S (a surfactant solution) by adding 20 µL of reagent S to each mL of reagent A. Then, 25 µL of this mixture was added to each well, followed by 200 µL of reagent B (a Folin reagent). Subsequently, the plate was incubated for 10 minutes at RT, protected from light, to allow colour development.

After the incubation period, absorbance was measured at 650 nm using the CLARIOstar (BMG Labtech) microplate reader. Protein concentrations were calculated by interpolation from the BSA standard curve.

3.10. Protein Expression Analysis (Western Blot)

Protein expression analysis was performed using the Western blot technique. The compositions of the resolving and stacking gels, prepared for sodium dodecyl sulfate–polyacrylamide gel electrophoresis (SDS-PAGE), are summarised in ***Tables 7*** and ***8***, respectively. The reagents are listed in the order in which they were added.

Table 7: *Volumes of the reagents used for the preparation of two 10% acrylamide resolving gels.*

Resolving gel (10% acrylamide)	
Acrylamide 30%	6.66 mL
1.5 M Tris buffer (pH = 8.8)	5 mL
Distilled water (dH_2O)	8 mL
Sodium dodecyl sulfate (SDS) 10%	200 µL
Ammonium persulfate (APS) 10%	200 µL
Tetramethylethylenediamine (TEMED)	20 µL

Table 8: *Volumes of the reagents used for the preparation of two 4% acrylamide stacking gels.*

Stacking gel (4% acrylamide)	
Distilled water (dH2O)	4.78 mL
0.5 M Tris buffer (pH = 6.8)	2 mL
Acrylamide 30%	1060 µL
Sodium dodecyl sulfate (SDS) 10%	80 µL
Ammonium persulfate (APS) 10%	80 µL
Tetramethylethylenediamine (TEMED)	8 µL

Protein samples were prepared by diluting lysates from the three cell lines (Nthy-Ori 3-1, B-CPAP, and TPC-1) in nuclease-free water to obtain 30 µg of total protein per sample. Laemmli loading buffer (4×) was added to the lysates to achieve a final 1× concentration. Samples were then vortexed and denatured at 95 °C for 5 minutes at 800 rpm in a thermomixer. The protein samples, together with the Precision Plus Protein Standard Dual Color marker (Bio-Rad Laboratories), were loaded onto the gels. SDS-PAGE was performed at 80 V for 30 minutes, or until the samples entered the resolving gel, followed by 100 V for 90 minutes, to enable the separation of the proteins by molecular weight. The running buffer was prepared by diluting 10× Tris–glycine–SDS (TGS) buffer (GRiSP) 1:10 in distilled water (dH_2O).

Following electrophoresis, proteins were transferred onto a nitrocellulose membrane (Amersham™, Cytiva) using a wet transfer system for 2 h at 4 °C and 500 mA. The transfer buffer consisted of 1× TGS with 20% (v/V) of methanol. Membranes were stained with Ponceau S to confirm successful protein transfer and subsequently blocked for 1 h at RT in 5% (w/V) BSA in 1× Tris-buffered saline (TBS).

To analyse the effects of Vemurafenib on MAPK signalling proteins, the nitrocellulose membranes were incubated with primary antibodies against BRAF, phosphorylated-ERK1/2 (pERK1/2) Thr202/Tyr204, and ERK1/2, all obtained from Cell Signaling Technology. An anti-α-tubulin antibody (Sigma-Aldrich) was used to detect α-tubulin, which served as a loading control. BRAF, pERK1/2, and ERK1/2 primary antibodies were diluted in 5% (w/V) BSA in 1× TBS containing 0.1% (v/V) Tween-20 (0.1% TBS-T), whereas the anti-α-tubulin antibody was diluted in 5% (w/V) non-fat dry milk in 0.1% TBS-T. A detailed description of the primary and secondary antibodies used is provided in ***Table 9***. Primary antibody incubation was performed overnight at 4 °C under agitation.

On the following day, membranes were washed four times for 5 minutes with 0.1% TBS-T and incubated for 1 h at RT under agitation with the following fluorescent secondary antibodies: IRDye® 800CW Donkey anti-Rabbit Immunoglobulin G (IgG) for BRAF and pERK1/2, IRDye® 680RD Donkey anti-Rabbit IgG for ERK1/2, and IRDye® 680RD Donkey anti-Mouse IgG for α-tubulin. All secondary antibodies were obtained from LI-COR Biosciences.

Table 9: *References, host species, clonality, and working dilutions of the primary and secondary antibodies used for Western blot analysis of BRAF, phosphorylated-ERK1/2 (pERK1/2), ERK1/2, and α-tubulin.*

Protein	Primary antibody	Secondary antibody
BRAF	#9433; 1:1 000; rabbit monoclonal	IRDye® 800CW Donkey anti-Rabbit IgG (926-32213); 1:20 000
pERK1/2	#4370; 1:2 000; rabbit monoclonal	IRDye® 800CW Donkey anti-Rabbit IgG (926-32213); 1:20 000
ERK1/2	#9102; 1:1 000; rabbit polyclonal	IRDye® 680RD Donkey anti-Rabbit IgG (926-68073); 1:20 000
α-tubulin	T6074; 1:5 000; mouse monoclonal	IRDye® 680RD Donkey anti-Mouse IgG (926-68072); 1:10 000

After incubation with the secondary antibodies, membranes were washed four times for 5 minutes with 0.1% TBS-T and imaged using the Odyssey CLx Infrared Imaging System (LI-COR Biosciences) at 800 nm and 680 nm channels. Protein quantification was performed using Image Studio™ Lite software (version 5.2.5; LI-COR Biosciences).

For antibody stripping, membranes were incubated at RT in a mild stripping buffer containing 25 mM glycine and 1% SDS (w/V) (pH = 2.5) for 45 minutes. Thereafter, membranes were washed five times for 5 minutes with 0.1% TBS-T, blocked again for 1 h at RT in 5% BSA (w/V) prepared in 1× TBS, and re-incubated with the appropriate secondary antibody. Finally, membranes were washed five times for 5 minutes with 0.1% TBS-T and re-imaged to confirm successful stripping before proceeding to the incubation with a different primary antibody.

3.11. Bioinformatics Analysis of RNA-Sequencing Data

RNA-seq data were obtained from the Gene Expression Omnibus (GEO) database of the National Center for Biotechnology Information (NCBI), under accession number GSE171483. This dataset contains gene expression profiles of B-CPAP cells treated with the BRAF inhibitor Vemurafenib (20 μM) and control cells treated with DMSO for 48 h, with three technical replicates per experimental condition. Differential gene expression analysis was performed using the GEO2R web tool, an online tool provided by NCBI that enables comparisons between experimental groups within GEO datasets using the limma package. This allowed the comparison of gene expression profiles between the two conditions: Vemurafenib-treated and negative control samples. The DEGs were ranked according to statistical significance. These genes were then filtered using a significance threshold of $p \leq 0.0001$ and a log fold change (logFC) ≥ 1 or ≤ -1. In order to focus on cancer-relevant genes, the resulting DEGs list was cross-referenced with a list of cancer-related genes, leading to a final set of 50 genes. Subsequently, these DEGs were used to generate a heatmap using RStudio v4.3.1.

Gene Ontology (GO) Biological Process enrichment analysis was performed using the PANTHER Classification System, and only the genes with stronger expression changes (logFC ≥ 1.5 or logFC ≤ -2) were selected. Significantly enriched biological processes were filtered using a false discovery rate (FDR)-adjusted $p\text{-}value \leq 0.01$ as the threshold. Although an initial

set of enriched processes was identified, only representative processes were retained for further interpretation due to substantial redundancy and overlap among GO terms.

3.12. Statistical Analysis

Statistical analysis was performed using GraphPad Prism software (version 11; GraphPad Software). Data were analysed using two-way analysis of variance (two-way ANOVA), with treatment condition and timepoints as the two factors. When appropriate, multiple comparisons were performed using either Sidak's or Dunnett's post hoc test. A $p\text{-}value \leq 0.05$ was considered statistically significant.

4. Results

4.1. Cell Viability

In the cell viability assay, the three cell lines (Nthy-Ori 3-1, B-CPAP, and TPC-1) were treated with increasing concentrations of Vemurafenib (2.5, 5, 10, 25, and 50 µM), and cell viability was evaluated at 48 and 72 h after treatment, using the PrestoBlue assay.

4.1.1. Viability of Nthy-Ori 3-1 Cells

In Nthy-Ori 3-1 cells (***Figure 6***), the IC_{50} value of Vemurafenib was not reached at either 48 or 72 h of treatment within the tested concentration range (2.5 to 50 µM). Nevertheless, compared with the DMSO control group, a significant reduction in cell viability was observed at the two highest Vemurafenib concentrations (25 and 50 µM) at both 48 and 72 h post-treatment (Dunnett's multiple comparisons test; 25 µM: $p = 0.0414$ at 48 h and $p = 0.0056$ at 72 h; 50 µM: $p = 0.0022$ at 48 h and $p < 0.0001$ at 72 h). Sidak's multiple comparisons test did not reveal any significant differences between the 48 and 72 h timepoints at any of the Vemurafenib concentrations tested. ***Supplementary Table 1*** presents the percentage of viable cells (mean ± standard deviation (SD)) at each drug concentration and at each timepoint in the Nthy-Ori 3-1 cell line.

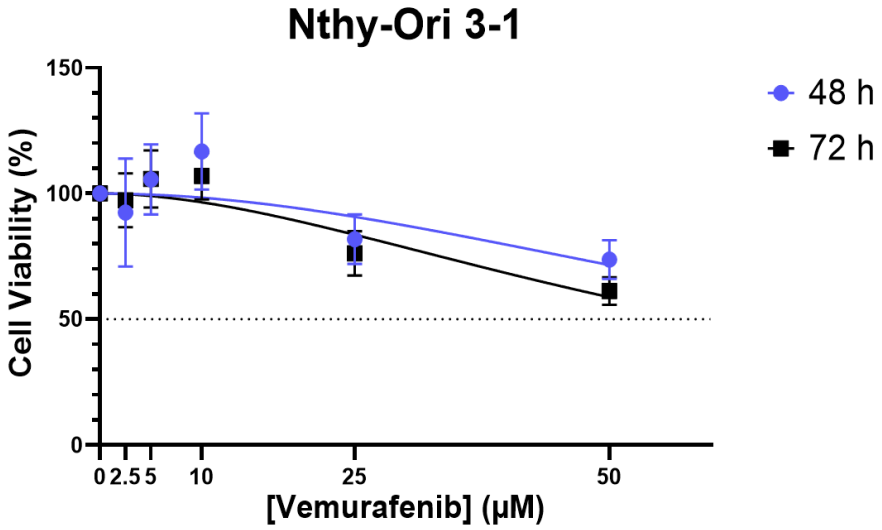


Figure 6: *Cell viability curves of Nthy-Ori 3-1 cells treated with increasing concentrations of Vemurafenib (2.5, 5, 10, 25, and 50 µM) at both timepoints (48 and 72 h).*
Data points represent the mean percentage of viable cells, and error bars indicate the standard deviation (SD). Values from each treatment group were normalised to their respective negative control, consisting of cells treated with DMSO at the same concentration as in each Vemurafenib-treated condition.

4.1.2. Viability of B-CPAP Cells

In the B-CPAP cell line (***Figure 7***), the IC_{50} of Vemurafenib was determined, being 14.90 µM (95% confidence interval (CI): 12.43–18.05 µM) after 48 h of treatment and 4.45 µM (95% CI: 3.63–5.29 µM) after 72 h. At both timepoints, increasing Vemurafenib concentration resulted in a concentration-dependent decrease in cell viability. Furthermore, compared with the DMSO control group, treatment with Vemurafenib significantly reduced cell viability across all tested concentrations at both 48 and 72 h post-treatment (Dunnett's multiple comparisons test, $p < 0.0001$). Overall, the dose–response curves showed that mean cell viability was consistently lower after 72 h of treatment across all Vemurafenib concentrations. However, when comparing the two timepoints, significant differences in the percentage of viable cells were only identified at 2.5, 5, and 10 µM Vemurafenib concentrations (Sidak's multiple comparisons test; $p = 0.0015$, $p = 0.0055$, and $p = 0.0004$, respectively). ***Supplementary Table 2*** presents the percentage of viable cells (mean ± SD) at each drug concentration and at each timepoint in the B-CPAP cell line.

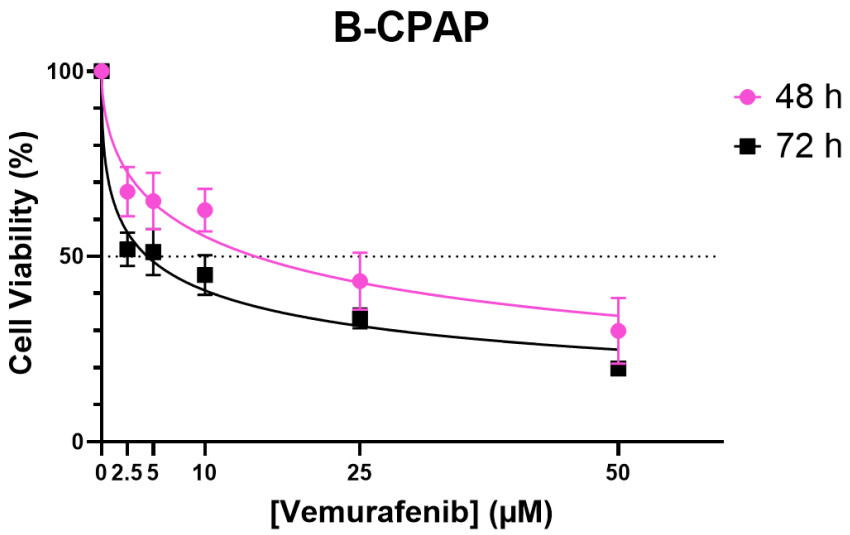


Figure 7: *Cell viability curves of B-CPAP cells treated with increasing concentrations of Vemurafenib (2.5, 5, 10, 25, and 50 µM) at both timepoints (48 and 72 h).*
Data points represent the mean percentage of viable cells, and error bars indicate the SD. Values from each treatment group were normalised to their respective negative control, consisting of cells treated with DMSO at the same concentration as in each Vemurafenib-treated condition.

4.1.3. Viability of TPC-1 Cells

In TPC-1 cells (***Figure 8***), similarly to the Nthy-Ori 3-1 cell line, the IC_{50} of Vemurafenib was not reached at either 48 h or 72 h of treatment within the tested concentration range (2.5 to 50 µM). Compared with the DMSO control group, a significant decrease in cell viability was only observed at the highest Vemurafenib concentration (50 µM) at both 48 and 72 h (Dunnett's multiple comparisons test; $p = 0.0381$ and $p = 0.0011$, respectively). Overall, mean cell viability was lower at the 72 h timepoint than at the 48 h timepoint across all drug concentrations; however, significant differences between the two timepoints were only identified at the 2.5 µM Vemurafenib concentration ($p = 0.0485$). ***Supplementary Table 3*** presents the percentage of viable cells (mean ± SD) at each drug concentration and at each timepoint in the TPC-1 cell line

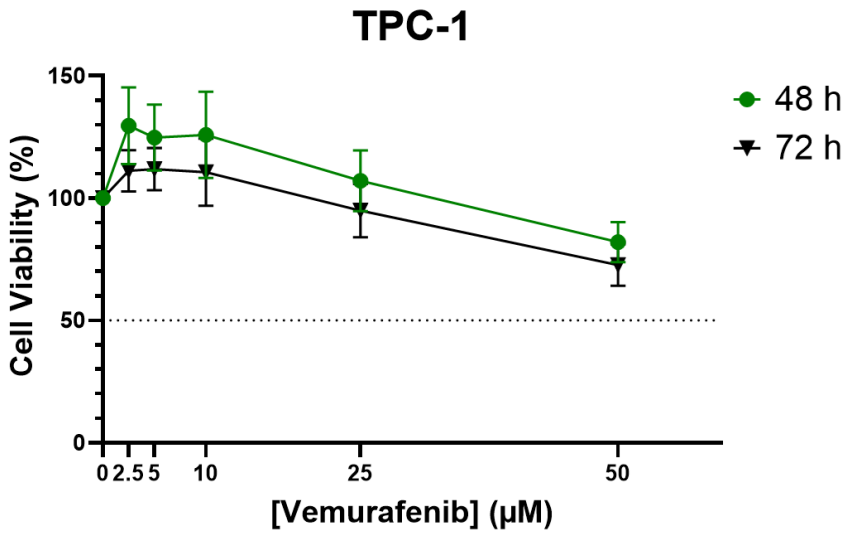


Figure 8: *Cell viability curves of TPC-1 cells treated with increasing concentrations of Vemurafenib (2.5, 5, 10, 25, and 50 µM) at both timepoints (48 and 72 h).*
Data points represent the mean percentage of viable cells, and error bars indicate the SD. Values from each treatment group were normalised to their respective negative control, consisting of cells treated with DMSO at the same concentration as in each Vemurafenib-treated condition.

In the subsequent assays, cells were treated with 15 µM Vemurafenib, which corresponded to the IC_{50} value determined for the B-CPAP cell line after 48 h of treatment. This concentration was selected because, in the most sensitive cell line (B-CPAP), it induced a significant biological effect while maintaining a sufficient number of viable cells, thereby enabling subsequent assessment of cell proliferation, protein expression, and gene transcription.

4.2. Cell Proliferation

Cell proliferation was assessed using the Click-iT™ Plus EdU Cell Proliferation Kit for Imaging (Thermo Fisher Scientific). All three cell lines (Nthy-Ori 3-1, B-CPAP, and TPC-1) were treated with 15 μM Vemurafenib. Control groups consisting of cells treated with 0.03% DMSO and untreated cells cultured in medium only were also included. Cell proliferation was evaluated at 48 h and 72 h following treatment, based on the EdU incorporation by the cells in the S-phase of the cell cycle. Statistical significance was assessed using Sidak's multiple comparisons test.

4.2.1. Proliferation of Nthy-Ori 3-1 Cells

In Nthy-Ori 3-1 cells, Vemurafenib treatment significantly reduced cell proliferation compared with the DMSO control group after 72 h (*p = 0.0182);* nevertheless, this effect was not significant at 48 h post-treatment (*p = 0.1397*), as shown in ***Figures 9*** and ***12(A)***. Moreover, there was a significant difference in the percentage of EdU-positive cells within the treatment group between 48 and 72 h, with a significantly lower mean percentage at 72 h (*p = 0.0491*). Furthermore, no significant differences were observed between the media and DMSO control groups at either 48 or 72 h (*p > 0.9999* and *p = 0.7887*, respectively).

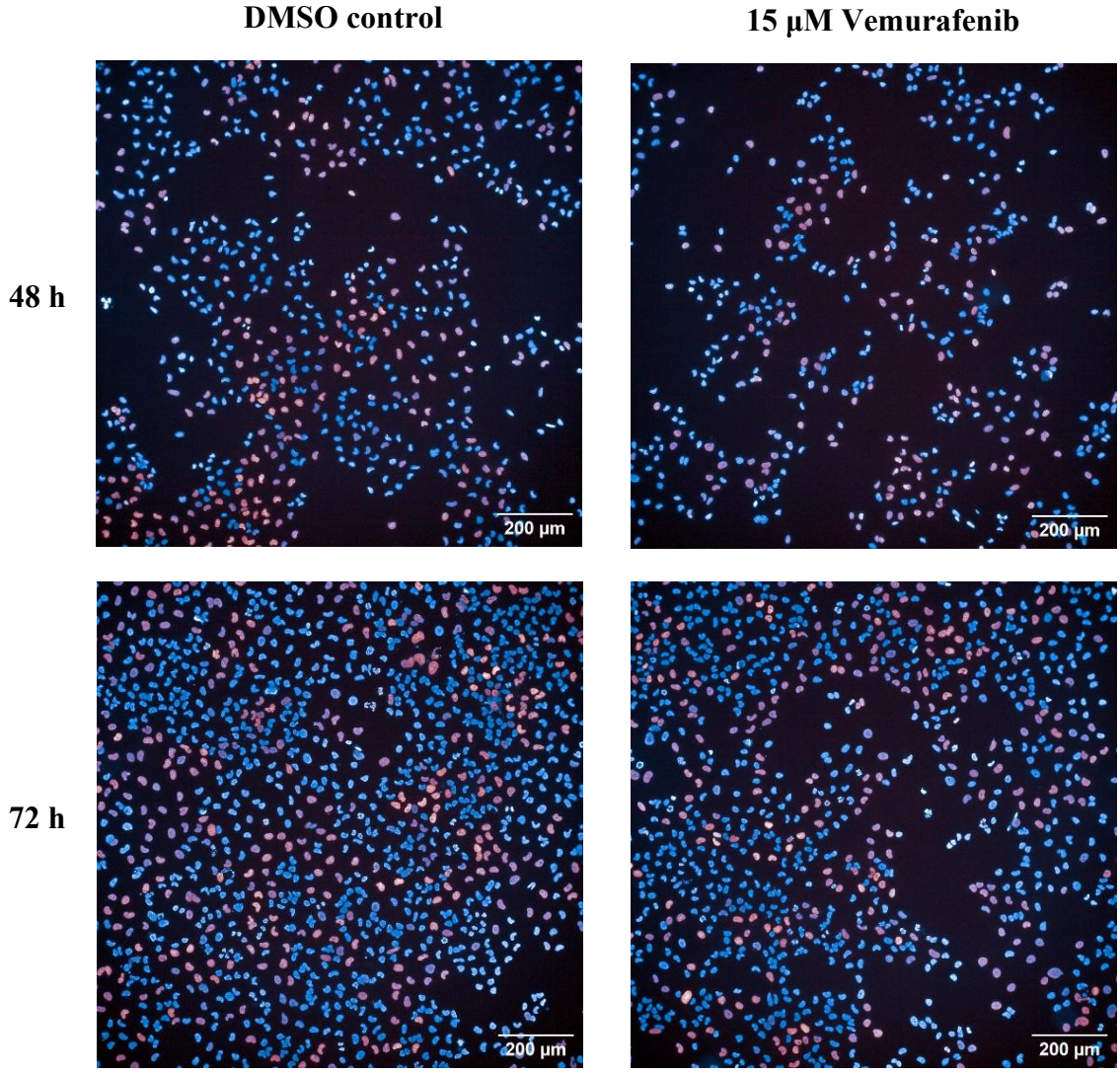


Figure 9: *EdU proliferation assay to assess the effect of 15 µM Vemurafenib on the proliferation of Nthy-Ori 3-1 cells.*
Nuclei of proliferating cells are stained red, whereas all cell nuclei are stained blue with Hoechst 33342. Representative images of the DMSO control group and cells treated with 15 µM Vemurafenib at 48 and 72 h post-treatment are shown. Scale bar = 200 µm.

4.2.2. Proliferation of B-CPAP Cells

In the B-CPAP cell line, cell proliferation was markedly affected by treatment with 15 µM Vemurafenib, as shown in ***Figures 10*** and ***12(B)***. In the treatment group, the percentage of EdU-positive cells was significantly lower at both 48 h and 72 h compared with the DMSO control group ($p < 0.0001$). At 48 h post-treatment, this corresponded to an approximate 50% reduction in the percentage of EdU-positive cells relative to the DMSO control. Nevertheless, no significant difference in the percentage of proliferating cells was observed between 48 h and 72 h within the treatment group ($p = 0.6002$). Furthermore, no significant changes were identified between the media and DMSO control groups at either 48 or 72 h ($p = 0.8685$ and $p = 0.9344$, respectively).

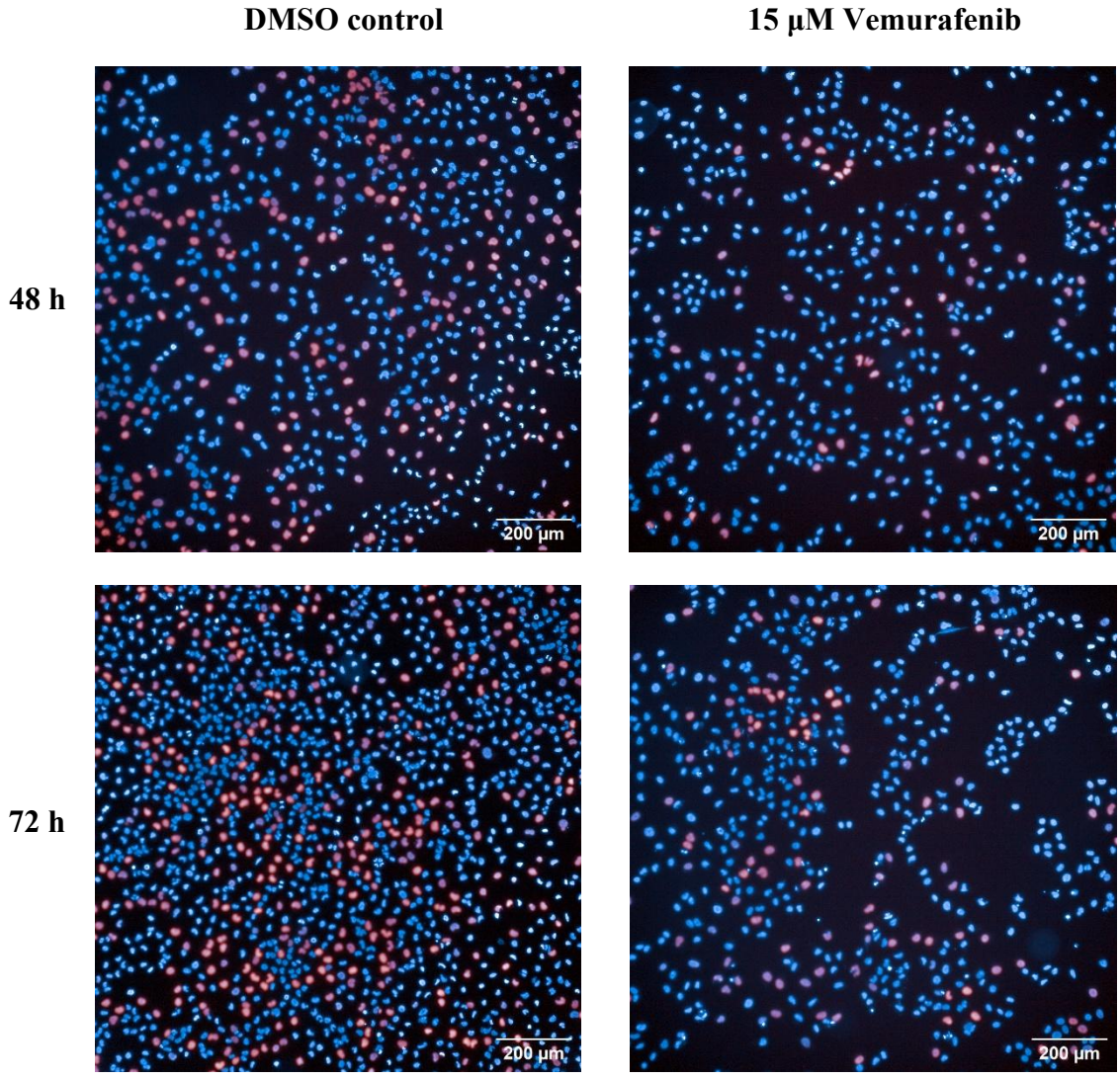


Figure 10: *EdU proliferation assay to assess the effect of 15 µM Vemurafenib on the proliferation of B-CPAP cells.*
Nuclei of proliferating cells are stained red, whereas all cell nuclei are stained blue with Hoechst 33342. Representative images of the DMSO control group and cells treated with 15 µM Vemurafenib at 48 and 72 h post-treatment are shown. Scale bar = 200 µm.

4.2.3. Proliferation of TPC-1 Cells

In the TPC-1 cell line, Vemurafenib significantly reduced cell proliferation at 48 h post-treatment compared with the DMSO control group ($p = 0.0134$), as shown in ***Figures 11*** and ***12(C)***. Nevertheless, no significant difference was observed between these groups at 72 h post-treatment ($p = 0.1360$). Moreover, the percentage of EdU-positive cells did not change significantly between 48 and 72 h within the treatment group ($p = 0.4297$). No significant differences were observed between the media and DMSO control groups at either 48 or 72 h post-treatment ($p = 0.9426$ and $p = 0.9752$, respectively).

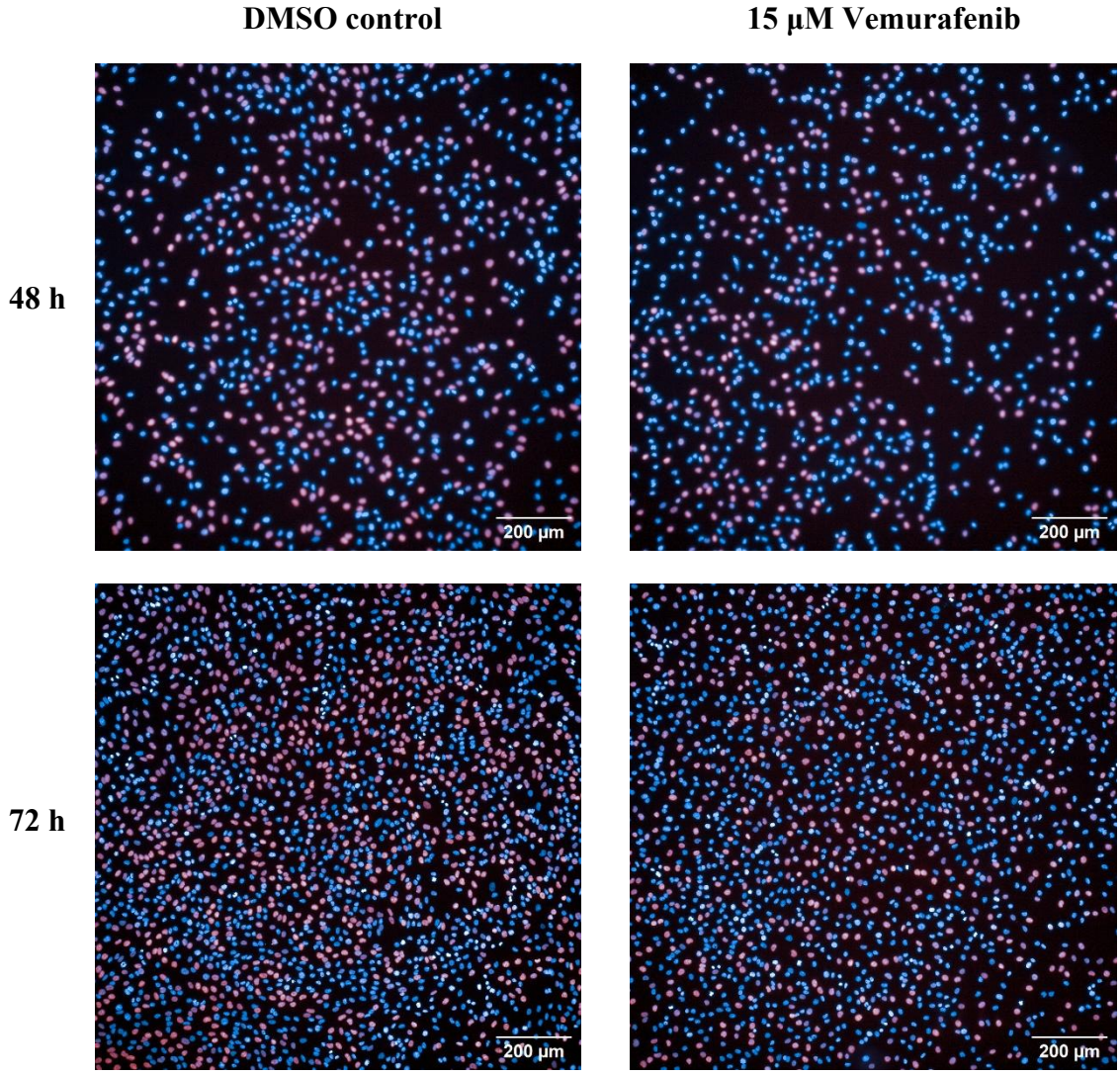


Figure 11: *EdU proliferation assay to assess the effect of 15 µM Vemurafenib on the proliferation of TPC-1 cells.*
Nuclei of proliferating cells are stained red, whereas all cell nuclei are stained blue with Hoechst 33342. Representative images of the DMSO control group and cells treated with 15 µM Vemurafenib at 48 and 72 h post-treatment are shown. Scale bar = 200 µm.

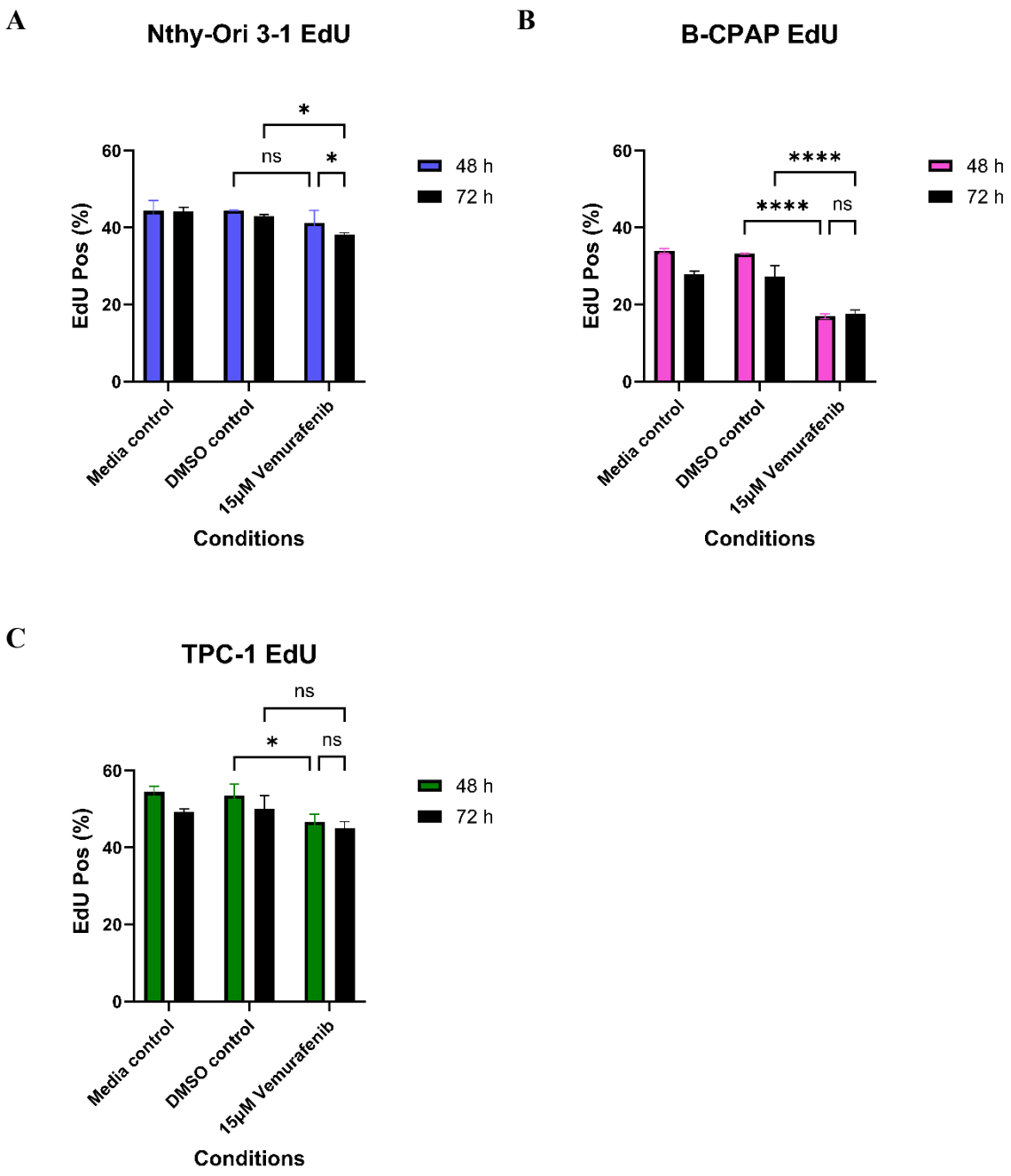


Figure 12: *Bar graphs showing the percentage of EdU-positive cells (EdU Pos, %) in the Media control, DMSO control, and 15 μM Vemurafenib-treated groups in the Nthy-Ori 3-1* ***(A)****, B-CPAP* ***(B)****, and TPC-1* ***(C)*** *cell lines at 48 and 72 h post-treatment.*
Bars represent the mean percentage of EdU-positive cells ± SD. Statistical analysis was performed using two-way ANOVA followed by Sidak's multiple comparisons test. The corresponding mean percentage of EdU-positive cells ± SD for each experimental group and at each timepoint in all three cell lines is provided in ***Supplementary Table 4****. ns, not significant; * $p < 0.05$; ** $p < 0.01$; *** $p < 0.001$; **** $p < 0.0001$.*

4.3. Protein Expression Analysis by Western Blot

The effect of Vemurafenib treatment on MAPK signalling proteins was assessed by Western blot. The three cell lines (Nthy-Ori 3-1, B-CPAP, and TPC-1) were treated with 15 μM Vemurafenib for 48 and 72 h, followed by protein extraction, quantification, and evaluation of protein expression by Western blot. This experiment also included control groups consisting of cells treated with medium containing 0.03% DMSO (DMSO control) and cells cultured in medium only (media control). Statistical significance was assessed using two-way ANOVA followed by Sidak's multiple comparisons test.

4.3.1. Protein Expression in Nthy-Ori 3-1 Cells

In Nthy-Ori 3-1 cells (***Figure 13***), treatment with 15 μM Vemurafenib did not significantly alter total BRAF protein expression compared with the DMSO control group after either 48 or 72 h of treatment (Sidak's multiple comparisons test: 48 h, $p = 0.6540$; 72 h, $p = 0.2880$). Furthermore, the pERK/ERK ratio also remained unchanged following treatment at both timepoints (Sidak's multiple comparisons test: 48 h, $p = 0.4199$; 72 h, $p = 0.3753$).

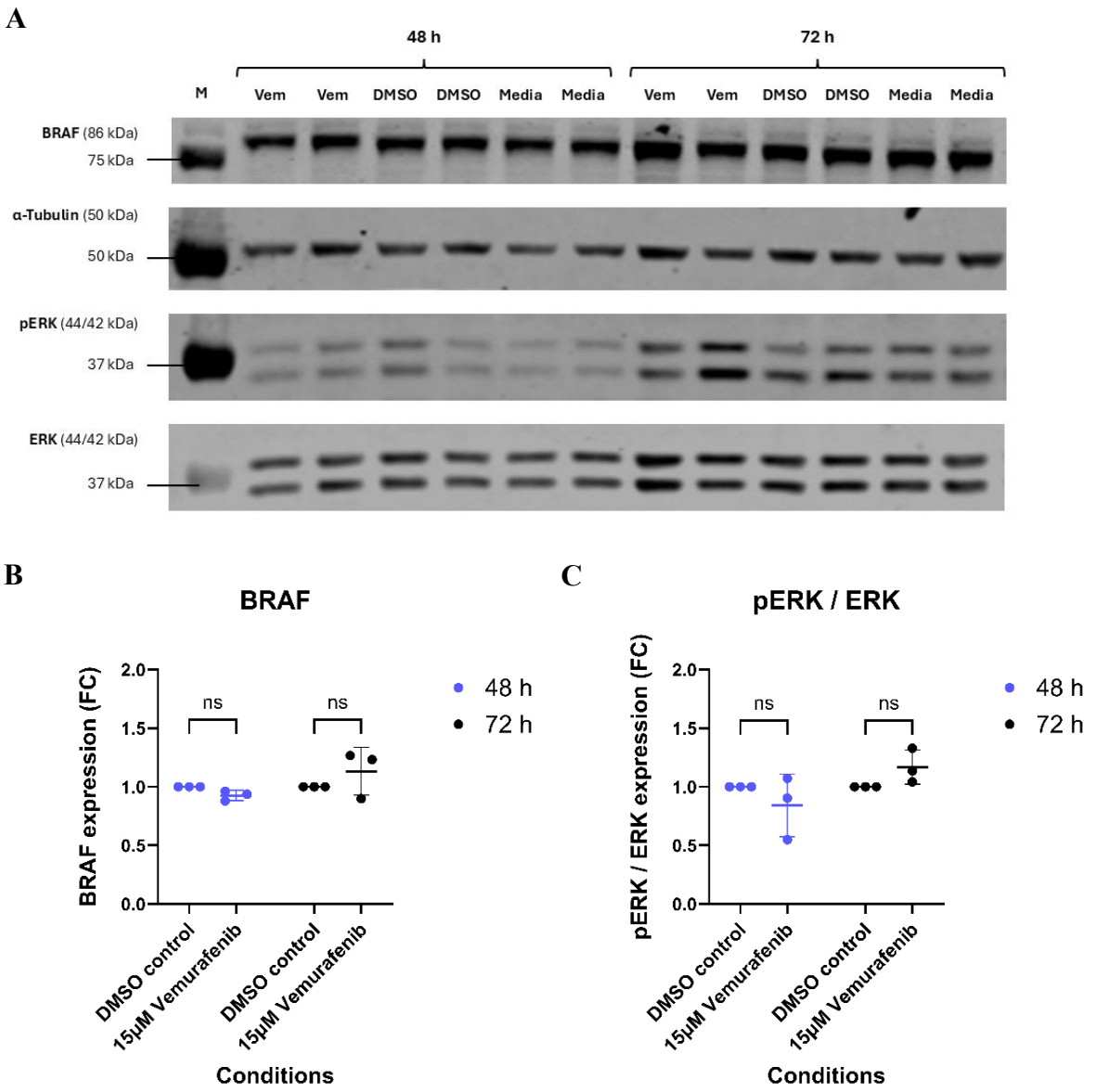


Figure 13: *Effect of Vemurafenib treatment on MAPK pathway proteins in Nthy-Ori 3-1 cells.*
(A) *Representative Western blot showing BRAF, α-tubulin, pERK, and ERK expression in cells treated with 15 μM Vemurafenib (Vem), DMSO vehicle control (DMSO), or medium control (Media) at 48 and 72 h. M, molecular weight marker. α-tubulin was used as a loading control.* ***(B)*** *Relative BRAF expression (fold change, FC) in Vemurafenib-treated cells compared with the DMSO control group.* ***(C)*** *Relative pERK/ERK ratio (FC) in Vemurafenib-treated cells compared with the DMSO control group. Data in panels* ***B*** *and* ***C*** *are presented as mean ± SD. Statistical analysis was performed using two-way ANOVA followed by Sidak's multiple comparisons test. ns, not significant; * $p < 0.05$; ** $p < 0.01$; *** $p < 0.001$; **** $p < 0.0001$.*

4.3.2. Protein Expression in B-CPAP Cells

In the B-CPAP cell line (***Figure 14***), treatment with 15 μM Vemurafenib resulted in a significant increase in total BRAF protein expression compared with the DMSO control group at 48 h post-treatment, but not at 72 h ($p = 0.0056$ and $p = 0.9981$, respectively). Furthermore, pERK signals were detected only in the Vemurafenib-treated group, whereas no pERK signals

were observed in the media or DMSO control groups. This pattern was consistently observed across all three biological replicates and at both timepoints. In addition, total ERK protein levels were significantly higher in the treatment group compared with the DMSO control group at both 48 and 72 h post-treatment ($p = 0.0012$ and $p = 0.0185$, respectively).

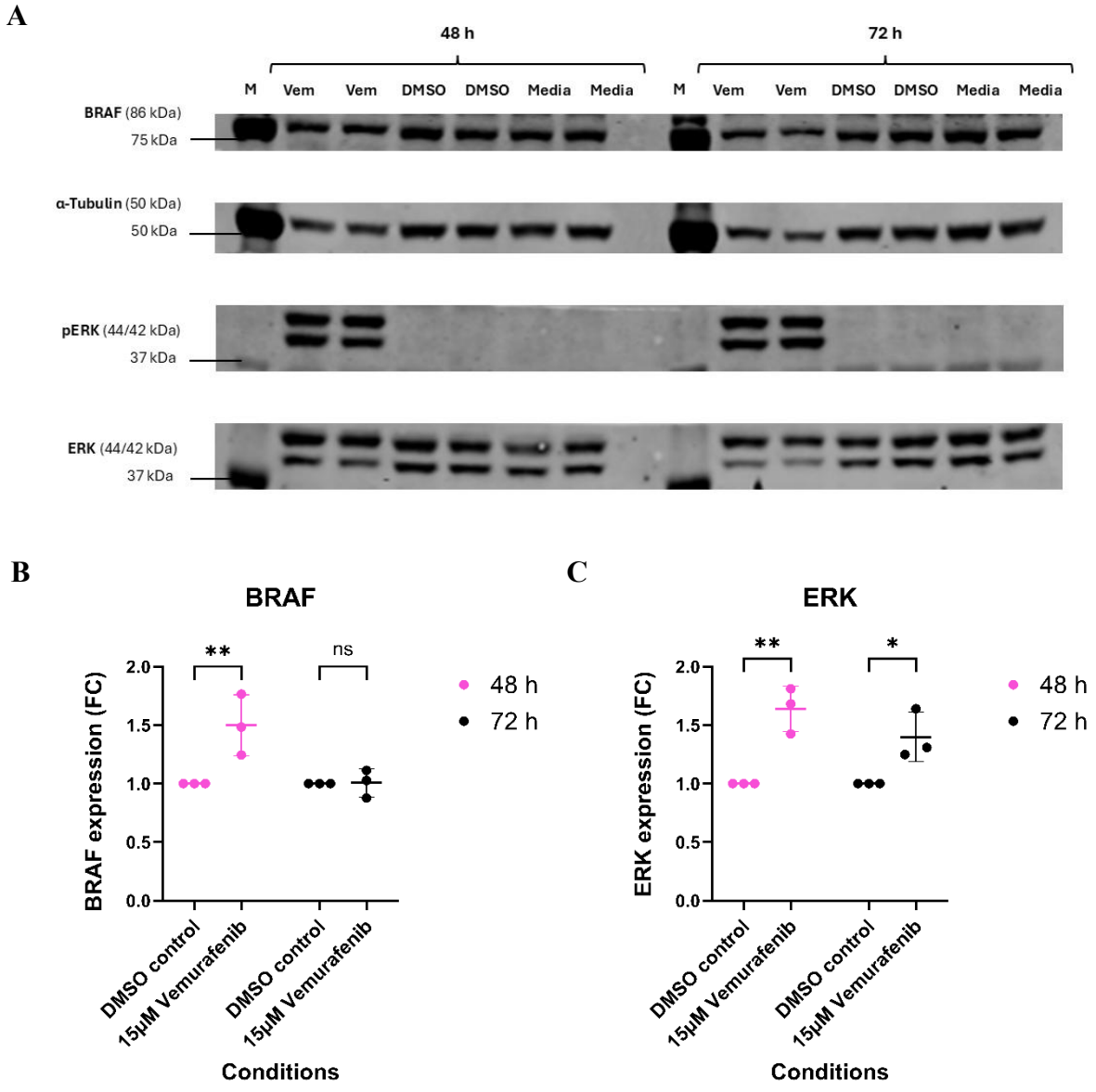


Figure 14: *Effect of Vemurafenib treatment on MAPK pathway proteins in B-CPAP cells.*
(A) *Representative Western blot showing BRAF, α-tubulin, pERK, and ERK expression in cells treated with 15 μM Vemurafenib (Vem), DMSO vehicle control (DMSO), or medium control (Media) at 48 and 72 h. M, molecular weight marker. α-tubulin was used as a loading control.* ***(B)*** *Relative BRAF expression (FC) in Vemurafenib-treated cells compared with the DMSO control group.* ***(C)*** *Relative ERK expression (FC) in Vemurafenib-treated cells compared with the DMSO control group. Data in panels* ***B*** *and* ***C*** *are presented as mean ± SD. Statistical analysis was performed using two-way ANOVA followed by Sidak's multiple comparisons test. ns, not significant; * $p < 0.05$; ** $p < 0.01$; *** $p < 0.001$; **** $p < 0.0001$.*

4.3.3. Protein Expression in TPC-1 Cells

In TPC-1 cells, as observed in the Nthy-Ori 3-1 cell line, no significant differences were detected in total BRAF protein expression or in the pERK/ERK ratio between Vemurafenib-treated cells and the DMSO control group at either 48 or 72 h after treatment, as shown in ***Figure 15*** (Sidak's multiple comparisons test; BRAF: 48 h, $p = 0.1680$; 72 h, $p = 0.9902$; pERK/ERK ratio: 48 h, $p = 0.4450$; 72 h, $p = 0.7311$).

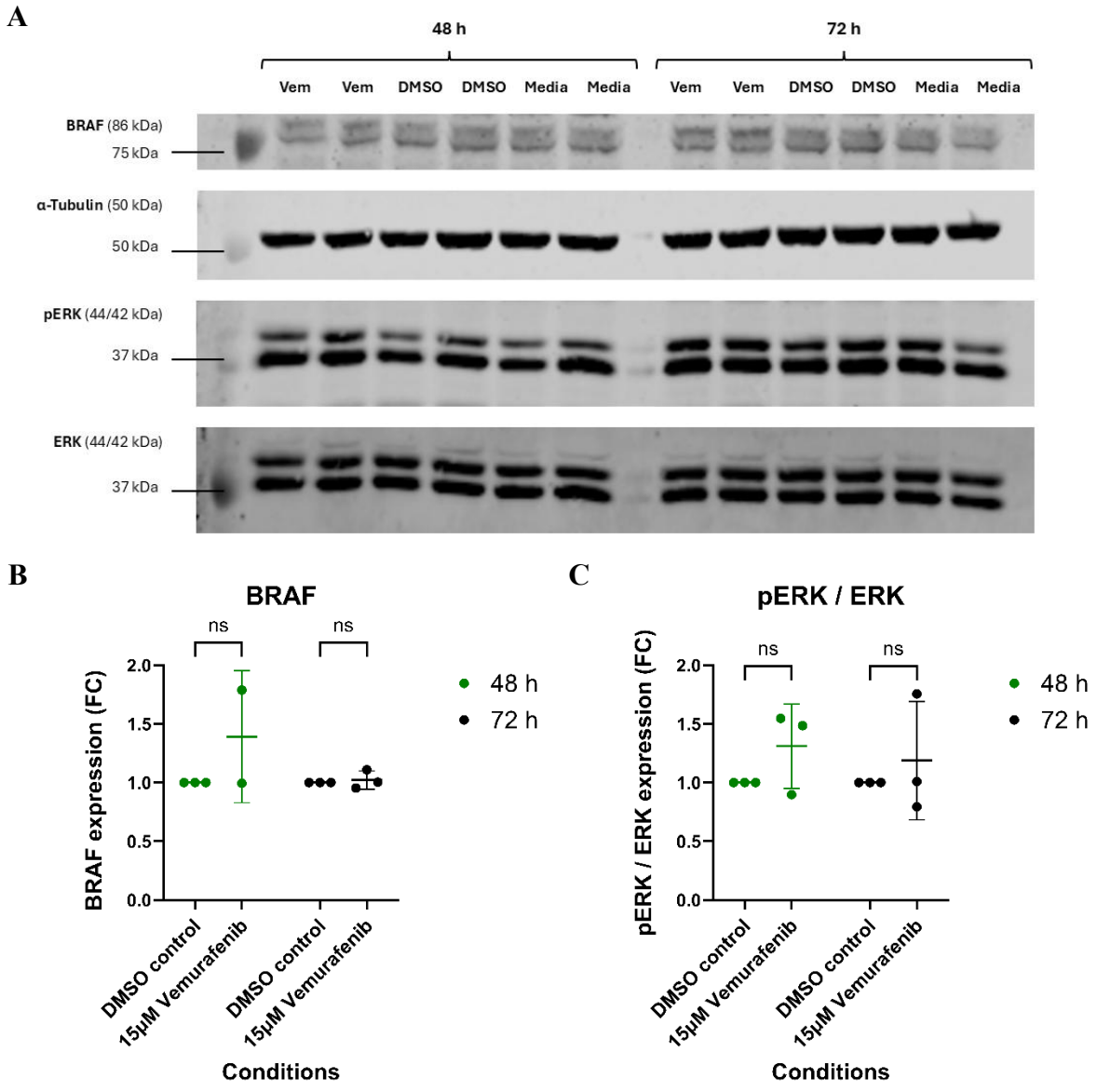


Figure 15: *Effect of Vemurafenib treatment on MAPK pathway proteins in TPC-1 cells.*
(A) *Representative Western blot showing BRAF, α-tubulin, pERK, and ERK expression in cells treated with 15 μM Vemurafenib (Vem), DMSO vehicle control (DMSO), or medium control (Media) at 48 and 72 h. M, molecular weight marker. α-tubulin was used as a loading control.* ***(B)*** *Relative BRAF expression (FC) in Vemurafenib-treated cells compared with the DMSO control group.* ***(C)*** *Relative pERK/ERK ratio (FC) in Vemurafenib-treated cells compared with the DMSO control group. Data in panels* ***B*** *and* ***C*** *are presented as mean ± SD. Statistical analysis was performed using two-way ANOVA followed by Sidak's multiple comparisons test. ns, not significant; * $p < 0.05$; ** $p < 0.01$; *** $p < 0.001$; **** $p < 0.0001$.*

4.4. *TERT* Expression Analysis by RT-qPCR

TERT expression was evaluated in the three cell lines (Nthy-Ori 3-1, B-CPAP, and TPC-1) by RT-qPCR using *TBP* as the endogenous control. The cells were treated with 15 µM Vemurafenib for 48 and 72 h, and subsequently RNA extraction, cDNA synthesis, and RT-qPCR were performed. This experiment also included control groups consisting of cells treated with medium containing 0.03% DMSO (DMSO control) and cells cultured in medium only (media control). Statistical significance was assessed using two-way ANOVA followed by Sidak's multiple comparisons test.

4.4.1. *TERT* Expression in Nthy-Ori 3-1 Cells

In Nthy-Ori 3-1 cells, treatment with 15 µM Vemurafenib did not significantly affect *TERT* expression at either 48 or 72 h ($p = 0.1969$ and $p = 0.7865$, respectively), as shown in ***Figure 16(A)***. However, a significant difference in ΔCt values was observed within the Vemurafenib-treated group between the two timepoints ($p = 0.0398$), with a higher mean ΔCt at 72 h. Moreover, no significant differences were observed between the DMSO and media control groups at either 48 or 72 h post-treatment ($p = 0.9293$ and $p = 0.4541$, respectively).

4.4.2. *TERT* Expression in B-CPAP Cells

In the B-CPAP cell line, treatment with 15 µM Vemurafenib significantly reduced *TERT* mRNA expression at 72 h post-treatment ($p = 0.0386$), as presented in ***Figure 16(B)***. Although no significant difference was observed at 48 h ($p = 0.0646$), a trend towards reduced *TERT* expression was already evident. Moreover, *TERT* expression did not differ within the Vemurafenib-treated group between 48 and 72 h of treatment ($p = 0.9620$). Furthermore, no significant changes were observed between the DMSO and media control groups at either 48 h ($p > 0.9999$) or 72 h ($p = 0.9318$).

4.4.3. *TERT* Expression in TPC-1 Cells

In TPC-1 cells, no significant differences in *TERT* expression were observed between the Vemurafenib-treated and the DMSO control groups at either 48 or 72 h post-treatment ($p = 0.8469$ and $p = 0.9320$, respectively), as shown in ***Figure 16(C)***. Additionally, no significant changes in *TERT* expression were detected within the Vemurafenib-treated group between the two timepoints ($p = 0.1259$). Moreover, *TERT* expression did not differ significantly between the DMSO and media control groups at either 48 h ($p = 0.5122$) or 72 h ($p = 0.9728$).

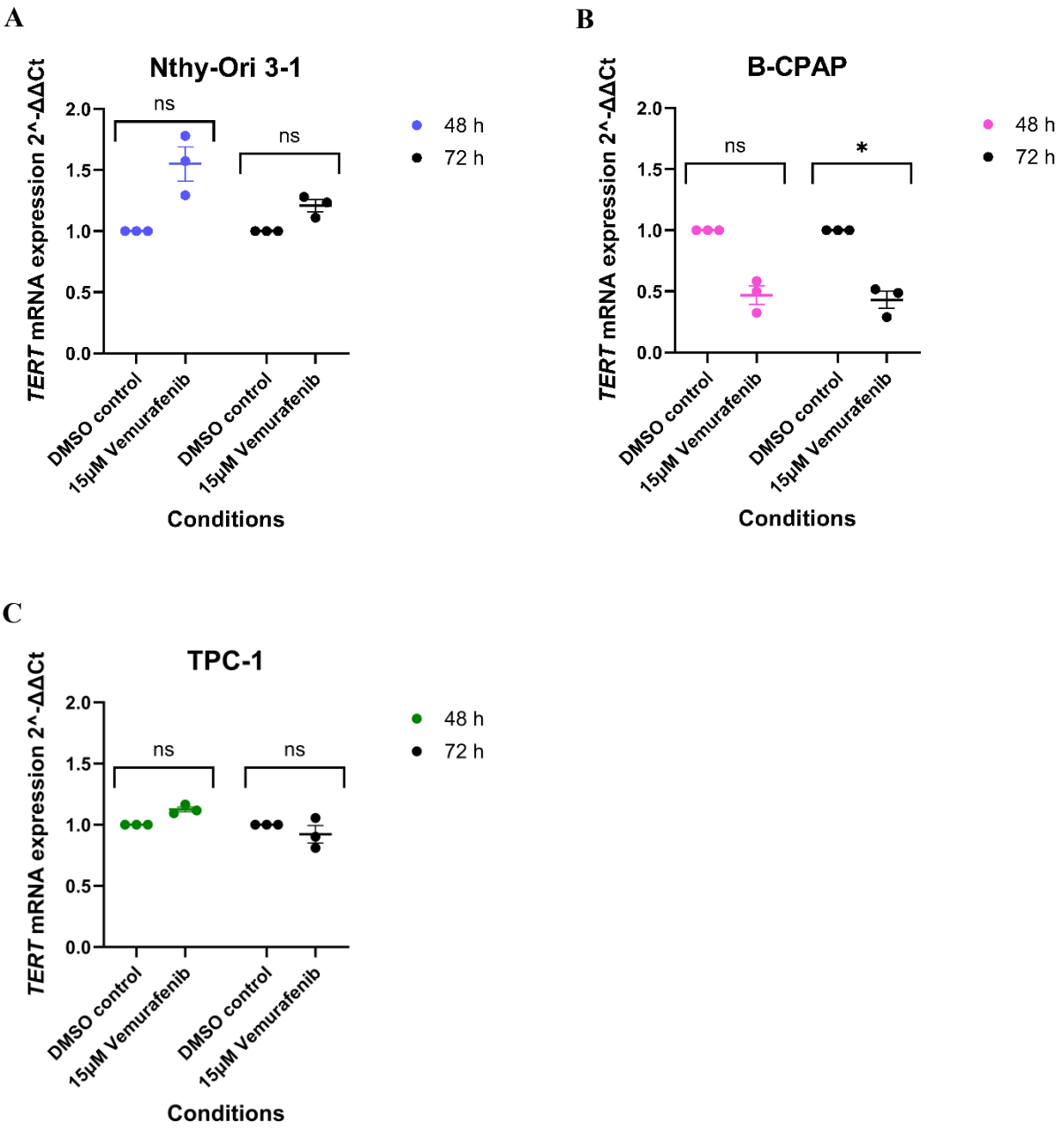


Figure 16: *Relative TERT mRNA expression in Nthy-Ori 3-1* ***(A)****, B-CPAP* ***(B)****, and TPC-1* ***(C)*** *cells following treatment with 15 μM Vemurafenib for 48 and 72 h.*
*Dot plots represent relative TERT mRNA expression levels calculated using the 2^-ΔΔCt method and normalised to the DMSO-treated control group. Data are presented as mean ± standard error of the mean (SEM) from three independent experiments. Statistical analysis was performed on ΔCt values using two-way ANOVA followed by Sidak's multiple comparisons test. ns, not significant; * $p < 0.05$; ** $p < 0.01$; *** $p < 0.001$; **** $p < 0.0001$.*

4.5. Bioinformatic Analysis of RNA-sequencing Data

To further identify possible molecules or pathways involved in the effects of Vemurafenib in B-CPAP cells, publicly available RNA-seq data containing gene expression profiles of B-CPAP cells treated with 20 µM Vemurafenib or DMSO for 48 h were analysed. DEGs and enriched biological processes were evaluated in response to BRAF inhibition.

4.5.1. Differentially Expressed Genes

Based on the RNA-seq data, 50 cancer-associated DEGs were identified in B-CPAP cells treated with 20 µM Vemurafenib, after applying the filtering criteria described in the Materials and Methods section ($p \leq 0.0001$ and an absolute logFC ≥ 1) and matching the DEG list with a predefined cancer-associated gene list. The DEGs are shown in ***Figure 17***.

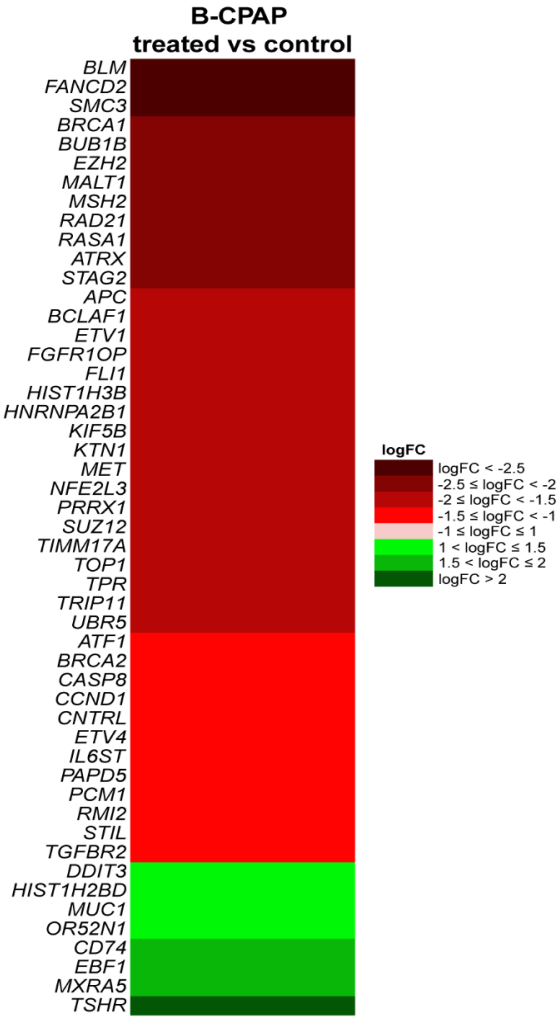


Figure 17: *Heatmap of the DEGs in B-CPAP cells treated with 20 µM Vemurafenib for 48 h compared with the DMSO-treated control group.*
Red and green indicate lower and higher relative gene expression levels, respectively, according to the logFC scale.

4.5.2. Enriched Biological Processes

Figure 18 summarises the enriched biological processes associated with the DEGs exhibiting the strongest expression changes (logFC ≥ 1.5 or ≤ −2) from the final set of 50 cancer-associated DEGs.

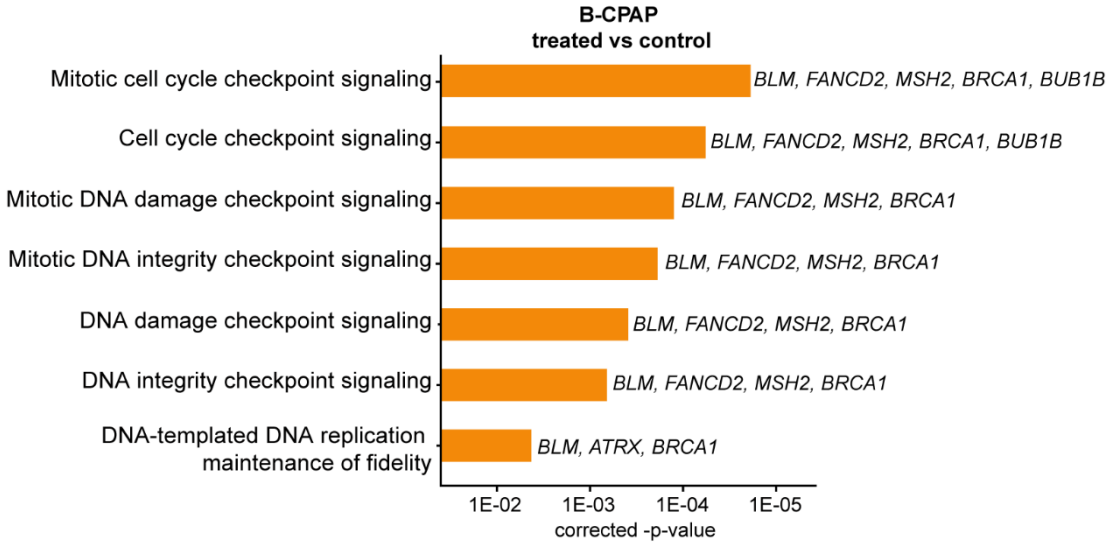


Figure 18: *Representative GO biological processes significantly enriched among the DEGs identified in B-CPAP cells treated with 20 µM Vemurafenib for 48 h compared with the DMSO-treated control group.*
Only representative biological processes are shown due to redundancy among GO terms. The DEGs contributing to each enriched biological process are indicated. The x-axis represents the FDR-corrected p-value.

5. Discussion

5.1. Interpretation of the Experimental Findings

DTCs have a high incidence, but most of them are associated with a favourable prognosis. Nevertheless, approximately 10 to 15% progress to more advanced and aggressive forms of TC, characterised by persistent/recurrent or metastatic disease, which is frequently RAI-refractory (Agrawal et al., 2014; Mady et al., 2020; Soares et al., 2021). Furthermore, it is well established that the coexistence of the *BRAF* V600E mutation with *TERTp* mutations is associated with a worse overall outcome, defined by increased recurrence risk, greater incidence of metastases, and higher mortality rates compared with either alteration alone (Baloch et al., 2022; Landa, 2023; Xing et al., 2014). For patients with tumours harbouring both mutations that are RAI-refractory, therapeutic options remain limited (Gild et al., 2018). Nevertheless, kinase inhibitors have emerged as a promising therapeutic approach (Cheng & Newbold, 2025; Gild et al., 2018). These compounds include BRAF inhibitors, such as Vemurafenib and Dabrafenib, which selectively target the *BRAF* V600E mutation (Harris, 2014; Holderfield et al., 2014). It has been reported that these inhibitors have demonstrated efficacy in TCs harbouring the *BRAF* V600E mutation, mainly by blocking the MAPK pathway; however, their effects beyond MAPK pathway inhibition, including downstream transcriptional regulation, remain poorly characterised (Brose et al., 2016; Dunn et al., 2019; Notarangelo et al., 2017). Since a synergistic effect between the *BRAF* V600E and *TERTp* mutations has been identified, there is a rationale to further explore how BRAF inhibition using BRAF inhibitors, such as Vemurafenib, can modulate *TERT* expression (Landa et al., 2023; Liu et al., 2018; Y. Xu et al., 2025).

To address this question, three cell lines with distinct genetic backgrounds were selected. These included an immortalized normal human thyroid-derived cell line (Nthy-Ori 3-1), which was utilised to evaluate the effects of BRAF inhibition in human thyroid cells, and two PTC-derived cell lines: B-CPAP, which harbours both the *BRAF* V600E and a *TERTp* mutation (-124 G>A), thereby enabling the study of the synergistic effect of these mutations; and TPC-1, which carries a RET/PTC rearrangement, a *TERTp* mutation (-124 G>A) but is wild-type for the *BRAF* gene. Furthermore, the impact of BRAF inhibition in the thyroid cell models was assessed at 48 and 72 h post-treatment, since the effect of Vemurafenib on *TERT* expression has already been described at 24 h in TC cells, whereas information regarding later timepoints remains limited (Liu et al., 2018). In addition, Montero-Conde et al. demonstrated

that MAPK pathway reactivation occurs following BRAF inhibition, raising the possibility that this reactivation at later timepoints may influence *TERT* expression (Montero-Conde et al., 2013). Therefore, 48 and 72 h timepoints were selected to investigate whether prolonged BRAF inhibition, together with potential MAPK pathway reactivation, could influence *TERT* expression.

The cell viability assay revealed distinct dose–response profiles among the three cell lines, following treatment with increasing Vemurafenib concentrations. Based on the dose–response curves, B-CPAP cells appeared to be the most sensitive to the BRAF inhibitor, as a more pronounced reduction in cell viability was consistently observed across the range of concentrations tested. Additionally, B-CPAP was the only cell line in which IC_{50} values could be determined at both 48 and 72 h post-treatment. The IC_{50} value was 14.90 μM at 48 h and decreased to 4.45 μM at 72 h, indicating increased sensitivity to the BRAF inhibitor following prolonged exposure. Previous studies have reported similar IC_{50} values to those obtained in the present study. Hanly et al. reported an IC_{50} value of 10 μM for Vemurafenib in B-CPAP cells after 48 h of exposure (Hanly et al., 2014). Additionally, Park et al. determined an IC_{50} value of 5 μM after 72 h of treatment in the 8505C cell line, an ATC cell line that also harbours the *BRAF* V600E mutation, suggesting a similar sensitivity to BRAF inhibition in *BRAF* V600E-mutated TC cells (Park et al., 2021). Nevertheless, among the studies analysed that used Vemurafenib in B-CPAP cells, IC_{50} values showed some variability, with studies reporting IC_{50} values ranging from approximately 2.7 μM to values exceeding 15 μM at 48 h (Bonaldi et al., 2021; Run et al., 2021). A similar variability was observed at 72 h, with reported IC_{50} values ranging from approximately 900 nM to 6.92 μM (Jiang et al., 2023; Wang et al., 2017). This variation may be explained by differences in cell viability assessment methods, cell seeding density, and cell culture conditions.

Additionally, in the B-CPAP cell line, significant differences were observed at 2.5, 5, and 10 μM between the 48 and 72 h timepoints, with a lower percentage of viable cells detected at 72 h at these Vemurafenib concentrations. This indicates that prolonged treatment has a more pronounced effect on cell viability. At 25 and 50 μM, no significant differences were detected between the two timepoints, suggesting that these higher concentrations may already exert a maximal effect at 48 h, resulting in no further significant reduction in cell viability after prolonged exposure.

Several studies have consistently shown that TC cells harbouring the *BRAF* V600E mutation generally exhibit greater sensitivity to Vemurafenib than *BRAF* wild-type TC cell lines or immortalized normal human thyroid-derived cell lines, such as Nthy-Ori 3-1 (Hanly et al., 2014; Ma et al., 2023). These findings suggest that Vemurafenib is selective for the mutant BRAF protein and that cells harbouring the *BRAF* V600E mutation are highly dependent on the MAPK pathway for survival. Consistent with these observations, the dose–response curves obtained in the present study showed that TPC-1 and Nthy-Ori 3-1 cells were more resistant to Vemurafenib exposure than B-CPAP cells. Both TPC-1 and Nthy-Ori 3-1 cells are wild-type for the *BRAF* gene, which may explain their greater resistance to the BRAF inhibitor. A possible explanation for this is that signalling driven by the BRAF V600E mutant protein occurs predominantly through monomeric BRAF, whereas signalling in *BRAF* wild-type cells frequently involves RAF dimer formation. As Vemurafenib is more effective at inhibiting activated monomeric BRAF, *BRAF* wild-type cells may exhibit reduced sensitivity to this inhibitor (Adamopoulos et al., 2021). Additionally, TPC-1 cells harbour the RET/PTC1 rearrangement, which also constitutively activates the MAPK pathway; however, it has been demonstrated that TC cells presenting RET rearrangements can also activate the PI3K/AKT signalling pathway, which, similarly to the MAPK pathway, is involved in the regulation of cell survival, proliferation, and growth (Roy, 2024; Xing, 2010). Therefore, the limited response of this cell line to BRAF inhibition suggests that signalling through the PI3K/AKT pathway may also contribute to the reduced sensitivity of TPC-1 cells to BRAF inhibition. Consistent with these findings, the cell proliferation assay revealed a similar pattern, with a less pronounced decrease in cell proliferation in these cell lines than in B-CPAP cells following treatment with Vemurafenib. In Nthy-Ori 3-1 cells, a significant reduction in cell proliferation was identified in the treated group compared with the DMSO control group at 72 h post-treatment, but not at 48 h. In contrast, the TPC-1 cell line showed a significant reduction in the percentage of EdU-positive cells in the treatment group at 48 h post-treatment; however, this effect was not maintained at 72 h, which may partly reflect the lower statistical power at 72 h, since only two biological replicates were available for analysis at this timepoint. Overall, the less pronounced effects on cell viability and proliferation observed in TPC-1 and Nthy-Ori 3-1 cells compared with the B-CPAP cell line further reinforce their greater resistance to Vemurafenib and suggest a lower dependence of these cell lines on BRAF-mediated signalling.

In contrast, in B-CPAP cells, a marked reduction in cell proliferation was observed at both timepoints in the treated group compared with the DMSO control group. Nevertheless, no

significant difference in the percentage of proliferative cells was observed between the two timepoints in the treated group, indicating that the antiproliferative response to BRAF inhibition is not dependent on the duration of exposure. This may suggest that the antiproliferative effect of Vemurafenib had already reached a plateau by 48 h, meaning that most susceptible cells had already undergone cell cycle arrest at this timepoint. Therefore, prolonged exposure did not result in a further significant reduction in cell proliferation. Furthermore, it should be noted that a significant difference in the percentage of EdU-positive cells was identified between the 48 and 72 h timepoints within the control groups of the B-CPAP cell line. The initial seeding density was optimised to ensure enough viable cells in the treatment condition while simultaneously avoiding excessive confluence in the control groups at 72 h post-treatment. Nevertheless, the reduction in cell proliferation observed in the control groups from 48 h to 72 h may reflect the cells reaching high confluence and the occurrence of contact inhibition. In the treatment group, no significant difference was observed between 48 and 72 h; therefore, cell confluence is unlikely to have influenced the treatment response. Furthermore, the substantial decrease in cell proliferation observed in B-CPAP cells following Vemurafenib treatment is consistent with previous studies. Hu et al. demonstrated that treatment with 10 μM Vemurafenib significantly reduced the percentage of B-CPAP cells in the S-phase of the cell cycle, a finding that was also reported by Notarangelo et al. using the same Vemurafenib concentration (Hu et al., 2022; Notarangelo et al., 2017). Overall, our findings are consistent with the cell viability results, as the presence of the *BRAF* V600E mutation makes B-CPAP cells highly dependent on MAPK signalling, resulting in a marked reduction in both cell viability and proliferation following BRAF inhibition. Together, these findings further support the efficacy of Vemurafenib in this cell line.

To evaluate the impact of Vemurafenib on the MAPK signalling pathway, the levels of total BRAF, pERK, and ERK were measured by Western blot. Total BRAF protein levels were analysed to determine whether Vemurafenib treatment could alter BRAF expression, whereas pERK indicates the activation state of the MAPK signalling pathway. Total ERK was measured to normalise pERK expression.

In Nthy-Ori 3-1 and TPC-1 cells, treatment with Vemurafenib did not significantly alter total BRAF expression or the pERK/ERK ratio. This indicates that Vemurafenib treatment did not significantly affect MAPK pathway activity in either cell line, which is consistent with the modest effects observed on cell viability and proliferation in these cell lines.

In the B-CPAP cell line, pERK signal was only observed in the Vemurafenib-treated group, suggesting an apparent increase in pERK levels at both 48 and 72 h. This represents a qualitative observation, since statistical analysis could not be performed due to the absence of detectable signals in the control groups. This qualitative increase is puzzling and contrasts with what would be expected. Since Vemurafenib inhibits mutant BRAF, reduced activation of downstream MAPK signalling proteins, reflected by lower pERK levels, would be expected following treatment. However, similar increases in pERK following prolonged exposure to BRAF inhibitors, referred to as ERK rebound, have been described in several studies using BRAF-mutant TC cell lines. One of the mechanisms proposed to explain this phenomenon is the reactivation of upstream signalling through the overexpression and activation of RTKs (Dahmani et al., 2022). Montero-Conde et al. observed the reactivation of the MAPK pathway following BRAF inhibition in BRAF-mutant TC cells, characterised by increased active RAS levels and ERK rebound, and proposed that this was associated with increased phosphorylation of the RTKs HER2 and HER3 (Montero-Conde et al., 2013). Furthermore, other RTKs have also been implicated, including EGFR and mesenchymal–epithelial transition factor receptor (MET) (Byeon et al., 2016; Dahmani et al., 2022; Notarangelo et al., 2017). In BRAF-mutant TC cell lines, BRAF inhibition was shown to increase phosphorylated MET levels, thereby leading to ERK rebound together with activation of the PI3K/AKT pathway (Byeon et al., 2016). An additional adaptive mechanism following BRAF inhibition is the formation of dimers involving the C-Raf proto-oncogene, serine/threonine kinase (CRAF) isoform. The formation of CRAF dimers has been shown to reactivate downstream ERK signalling, thereby promoting the reactivation of the MAPK pathway (Hanly et al., 2016; Maji et al., 2024). Furthermore, *RAS* mutations, including *KRAS* G12D and *NRAS* Q61K, may also emerge after BRAF inhibition as an adaptive mechanism, resulting in constitutive activation of RAS (Dahmani et al., 2022; Danysh et al., 2016). Since RAS is a common upstream signalling molecule for both the MAPK and PI3K/AKT pathways (Roy, 2024), these mutations may promote ERK rebound together with activation of the PI3K/AKT pathway (Crispo et al., 2019; Dahmani et al., 2022; Danysh et al., 2016). Although an apparent increase in pERK levels was observed following Vemurafenib treatment in B-CPAP cells, the mechanisms proposed to explain ERK rebound were not investigated in the present study. Additionally, the absence of a detectable pERK signal in the control groups may be explained by the lower basal levels of phosphorylated proteins, together with the limited amount of total protein that could be loaded for Western blot analysis. Furthermore, in B-CPAP cells, total BRAF expression was significantly higher in the Vemurafenib-treated group than in the DMSO control group at 48

h, but not at 72 h. This suggests that a response leading to increased BRAF expression may occur following Vemurafenib treatment, although this hypothesis requires further confirmation. In melanoma, BRAF copy number gain has been described as a mechanism of resistance to BRAF inhibitors (Cosci et al., 2025); however, evidence supporting this mechanism in TC is limited. Moreover, total ERK expression was also significantly increased in the Vemurafenib-treated group compared with the DMSO control group at both timepoints. Additionally, it should be noted that slight variability in α-tubulin signal intensity was observed between the Vemurafenib-treated and the control groups. Nevertheless, total protein staining with Ponceau S indicated comparable protein loading between the two conditions. Therefore, this variability may have influenced the normalised BRAF and ERK expression values and should be considered when interpreting these results.

The evaluation of *TERT* expression in the three cell lines revealed different responses to the BRAF inhibitor. In Nthy-Ori 3-1 cells, treatment with Vemurafenib did not significantly alter *TERT* expression at either timepoint. This indicates that, in this immortalised normal thyroid-derived cell line, which is *BRAF* and *TERTp* wild-type, Vemurafenib does not significantly influence *TERT* expression. This is consistent with the Western blot results, which revealed no significant differences in the pERK/ERK ratio following Vemurafenib treatment at either timepoint, suggesting that MAPK pathway activity and its downstream signalling were not significantly affected by treatment. Moreover, Nthy-Ori 3-1 cells lack both the *BRAF* V600E and *TERTp* mutations characteristic of the molecular context in which an interaction between MAPK signalling and *TERT* expression has been described in TC.

In TPC-1 cells, similarly to the Nthy-Ori 3-1 cell line, no significant differences in *TERT* expression were observed between the Vemurafenib-treated and DMSO control groups at either 48 or 72 h of treatment. Although this cell line harbours a *TERTp* mutation, it is *BRAF* wild-type. Therefore, since *TERT* expression was not affected by BRAF inhibition, this observation suggests that the coexistence of both mutations may be required for BRAF inhibition to alter *TERT* expression. These findings are consistent with the Western blot results, which also showed no significant differences in the pERK/ERK ratio following Vemurafenib treatment at either timepoint, suggesting that MAPK pathway activity and its downstream signalling were not significantly affected by treatment.

On the other hand, the results obtained in the B-CPAP cell line indicate that BRAF inhibition can influence *TERT* expression in TC cells harbouring both the *BRAF* V600E

mutation and a *TERTp* mutation, since a significant decrease in *TERT* mRNA expression was observed after 72 h of Vemurafenib treatment. Although a significant decrease in *TERT* mRNA expression was not identified at 48 h of treatment, a trend towards reduced *TERT* expression was already evident at this timepoint. These results are consistent with those reported by Liu et al., who observed a significant decrease in *TERT* expression in B-CPAP cells following 24 h of Vemurafenib treatment (Liu et al., 2018). Here, we observed that this effect was also maintained after longer treatment periods. This effect may be explained by the previously described association between the *BRAF* V600E mutation and *TERT* expression. The *BRAF* V600E mutation has been reported to lead to the upregulation of transcription factors capable of binding to the mutant *TERTp*, thereby increasing *TERT* expression in TC cells carrying both the *BRAF* V600E mutation and a mutant *TERTp*. Therefore, it is reasonable to hypothesise that, in these cells, inhibition of the MAPK pathway through inhibition of the mutant BRAF protein may culminate in a decrease in *TERT* expression. This may explain the reduction in *TERT* expression observed in the B-CPAP cell line, which harbours both the *BRAF* V600E mutation and a mutant *TERTp*. Moreover, the reduction in cell viability and proliferation following Vemurafenib treatment supports the greater sensitivity of B-CPAP cells to BRAF inhibition. These findings, together with the observed decrease in *TERT* expression, suggest that Vemurafenib treatment may also affect downstream processes of the MAPK pathway, including *TERT* regulation. Although Western blot analysis showed an apparent increase in pERK levels following Vemurafenib treatment, a significant reduction in *TERT* expression was still observed after 72 h of treatment.

The analysis of the RNA-seq data comparing B-CPAP cells treated with 20 µM Vemurafenib for 48 h with the DMSO control group revealed a list of DEGs, which were subsequently filtered and cross-referenced with a list of cancer-related genes. This resulted in a total of 50 cancer-associated DEGs. Among these genes, several are involved in biological processes that correlate with the findings of the present study.

The *CCND1* gene, which encodes cyclin D1, a key regulator of the transition from the G1 to the S-phase of the cell cycle (Montalto & De Amicis, 2020), was downregulated following Vemurafenib treatment. This finding is consistent with the cell proliferation results observed in B-CPAP cells, since Vemurafenib treatment led to a marked decrease in the percentage of cells in the S-phase of the cell cycle. Furthermore, other genes involved in mitotic progression, chromosome segregation, and spindle assembly, including *SMC3*, *RAD21*,

STAG2, and *BUB1B*, were also downregulated in the treatment group, further supporting the antiproliferative effect of Vemurafenib (Di Nardo et al., 2022; Jia et al., 2016).

Moreover, several genes involved in DNA repair and maintenance of genomic stability were also downregulated in the Vemurafenib-treated group, including *BLM*, *FANCD2*, *BRCA1*, *BRCA2*, *MLH1*, and *MSH2* (Chae et al., 2016). This finding is consistent with the results obtained by Robb et al., who showed that BRAF inhibition in BRAF-mutant TC cell lines impairs non-homologous end joining (NHEJ)-mediated DNA repair accompanied by reduced expression of XLF, a key component of this pathway (Robb et al., 2019). Taken together, these observations suggest that Vemurafenib may affect DNA repair capacity in BRAF-mutant TC cell lines.

Interestingly, the *TSHR* gene, which encodes the thyroid-stimulating hormone receptor (S. Xu et al., 2025), appeared to be upregulated in the treatment group. Previous studies have reported that Vemurafenib treatment promotes redifferentiation of TC cells harbouring the *BRAF* V600E mutation by increasing NIS expression (Bonaldi et al., 2021; Cheng et al., 2016). Therefore, the upregulation of *TSHR* may further support the hypothesis of redifferentiation following BRAF inhibition.

Furthermore, *ETV1*, *ETV4*, and *FLI1*, which encode transcription factors of the ETS family, were downregulated following Vemurafenib treatment (Qian et al., 2022). This finding is relevant considering the well-established association between the *BRAF* V600E mutation and *TERT* expression. Mutant BRAF signalling has been reported to promote the expression of ETS transcription factors, which bind to the mutant *TERTp* (Liu et al., 2014; Song & Park, 2020). Therefore, inhibition of BRAF may reduce the expression of these transcription factors, potentially leading to a decrease in *TERT* expression. These results fit with our findings as well as those reported by Liu et al., with both studies showing a decrease in *TERT* mRNA expression following Vemurafenib treatment in B-CPAP cells (Liu et al., 2018). However, analysis of the RNA-seq dataset showed no significant changes in *TERT* expression (*adjusted p-value = 0.9710*).

Finally, GO enrichment analysis demonstrated that the main enriched biological processes were predominantly associated with cell cycle regulation, particularly mitotic and DNA damage checkpoints. The genes associated with these processes were predominantly downregulated in the Vemurafenib-treated group. Overall, these results support the overall effect of Vemurafenib on biological processes involved in the regulation of cell proliferation.

5.2. Study Limitations and Future Perspectives

A limitation of the present study is that only one TC cell line with the relevant genetic background was used to evaluate the association between BRAF inhibition and *TERT* expression, since B-CPAP was the only model harbouring both the *BRAF* V600E mutation and a mutant T*ERTp*. Therefore, as a future perspective, this study could be expanded to include other TC cell lines with the same molecular context, in order to assess whether the effect of BRAF inhibition is maintained across different cell lines, including cell lines derived from different TC subtypes.

Additionally, the present study did not investigate the molecular mechanisms that may underlie the limited response observed in the *BRAF* wild-type cell models or the adaptive mechanisms that may be occurring in B-CPAP cells. Therefore, future studies should evaluate the activation of RTKs, the formation of CRAF dimers, the acquisition of RAS mutations, and the activation of the PI3K/AKT pathway in order to better characterise these mechanisms.

The involvement of ETS family transcription factors in the regulation of *TERT* expression following BRAF inhibition should also be further investigated. In particular, chromatin immunoprecipitation (ChIP) assays could be performed to determine whether the binding of these transcription factors to the mutant *TERTp* is modulated following BRAF inhibition in *BRAF*-mutant TC cells.

Moreover, since the combination of a BRAF inhibitor with a MEK inhibitor has been reported to reduce ERK rebound in TC cells harbouring both the *BRAF* V600E mutation and a mutant *TERTp* (Montero-Conde et al., 2013), and considering that combined BRAF and MEK inhibition (Dabrafenib + Trametinib), rather than BRAF inhibitor monotherapy, is the strategy approved by the FDA and EMA for *BRAF* V600E-mutant TCs, it would be of interest to compare the effects of Vemurafenib monotherapy with combined BRAF and MEK inhibition.

Finally, in vivo studies should be performed to verify whether the effects observed in vitro are maintained in vivo.

6. Conclusions

Regarding the main aim of this project, which was to evaluate whether BRAF inhibition could modulate *TERT* expression in a TC cell line harbouring both the *BRAF* V600E mutation and a mutant *TERTp*, this hypothesis was confirmed. A significant reduction in *TERT* expression was observed after 72 h of treatment, while a trend towards reduced *TERT* was already evident after 48 h.

Additionally, Vemurafenib treatment markedly reduced cell viability and proliferation in the B-CPAP cell line. However, the apparent increase in pERK expression suggests that an adaptive response may be activated following prolonged drug exposure.

Furthermore, this study reinforced that BRAF inhibitors have a greater effect on TC cell lines harbouring the *BRAF* V600E mutation, whereas *BRAF* wild-type TC cell lines showed only a limited response to the treatment.

Overall, this study provides further insight into the regulatory relationship between MAPK signalling and *TERT* expression, which is particularly relevant given the limited therapeutic strategies targeting *TERTp* mutations. Nevertheless, further studies are needed to consolidate these findings and to elucidate the molecular mechanisms involved in the response to BRAF inhibition.

7. References

Abdullah, M. I., Junit, S. M., Ng, K. L., Jayapalan, J. J., Karikalan, B., & Hashim, O. H. (2019). Papillary Thyroid Cancer: Genetic Alterations and Molecular Biomarker Investigations. *International Journal of Medical Sciences*, *16*(3), 450-460. https://doi.org/10.7150/ijms.29935

Adamopoulos, C., Ahmed, T. A., Tucker, M. R., Ung, P. M. U., Xiao, M., Karoulia, Z., Amabile, A., Wu, X., Aaronson, S. A., Ang, C., Rebecca, V. W., Brown, B. D., Schlessinger, A., Herlyn, M., Wang, Q., Shaw, D. E., & Poulikakos, P. I. (2021). Exploiting Allosteric Properties of RAF and MEK Inhibitors to Target Therapy-Resistant Tumors Driven by Oncogenic BRAF Signaling. *Cancer Discovery*, *11*(7), 1716-1735. https://doi.org/10.1158/2159-8290.CD-20-1351

Agrawal, N., Akbani, R., Aksoy, B. A., Ally, A., Arachchi, H., Asa, S. L., Auman, J. T., Balasundaram, M., Balu, S., Baylin, S. B., Behera, M., Bernard, B., Beroukhim, R., Bishop, J. A., Black, A. D., Bodenheimer, T., Boice, L., Bootwalla, M. S., Bowen, J.,…Zou, L. (2014). Integrated Genomic Characterization of Papillary Thyroid Carcinoma. *Cell*, *159*(3), 676-690. https://doi.org/10.1016/j.cell.2014.09.050

Almansoori, M. E., Awad, A., Dhaiban, S., Alduhoori, M. T., Sharif, H., & Sajini, A. (2025). Recent progress in human telomerase structure and its therapeutic targeting. *Frontiers in Molecular Biosciences*, *12*, 1681988. https://doi.org/10.3389/fmolb.2025.1681988

Baloch, Z. W., Asa, S. L., Barletta, J. A., Ghossein, R. A., Juhlin, C. C., Jung, C. K., LiVolsi, V. A., Papotti, M. G., Sobrinho-Simões, M., Tallini, G., & Mete, O. (2022). Overview of the 2022 WHO Classification of Thyroid Neoplasms. *Endocrine Pathology*, *33*(1), 27-63. https://doi.org/10.1007/s12022-022-09707-3

Basolo, F., Macerola, E., Poma, A. M., & Torregrossa, L. (2023). The 5th edition of WHO classification of tumors of endocrine organs: changes in the diagnosis of follicular-derived thyroid carcinoma. *Endocrine*, *80*(3), 470-476. https://doi.org/10.1007/s12020-023-03336-4

Bollag, G., Tsai, J., Zhang, J., Zhang, C., Ibrahim, P., Nolop, K., & Hirth, P. (2012). Vemurafenib: the first drug approved for *BRAF*-mutant cancer. *Nature Reviews Drug Discovery*, *11*, 873-886. https://doi.org/10.1038/nrd3847

Bonaldi, E., Gargiuli, C., De Cecco, L., Micali, A., Rizzetti, M. G., Greco, A., Borrello, M. G., & Minna, E. (2021). BRAF Inhibitors Induce Feedback Activation of RAS

Pathway in Thyroid Cancer Cells. *International Journal of Molecular Sciences*, *22*(11), 5744. https://doi.org/10.3390/ijms22115744

Boucai, L., Zafereo, M., & Cabanillas, M. E. (2024). Thyroid Cancer: A Review. *JAMA*, *331*(5), 425-435. https://doi.org/10.1001/jama.2023.26348

Brose, M. S., Cabanillas, M. E., Cohen, E. E., Wirth, L. J., Riehl, T., Yue, H., Sherman, S. I., & Sherman, E. J. (2016). Vemurafenib in patients with $BRAF^{V600E}$-positive metastatic or unresectable papillary thyroid cancer refractory to radioactive iodine: a non-randomised, multicentre, open-label, phase 2 trial. *The Lancet Oncology*, *17*(9), 1272-1282. https://doi.org/10.1016/S1470-2045(16)30166-8

Bullock, M., Lim, G., Zhu, Y., Åberg, H., Kurdyukov, S., & Clifton-Bligh, R. (2019). ETS Factor ETV5 Activates the Mutant Telomerase Reverse Transcriptase Promoter in Thyroid Cancer. *Thyroid®*, *29*(11), 1623-1633. https://doi.org/10.1089/thy.2018.0314

Byeon, H. K., Na, H. J., Yang, Y. J., Kwon, H. J., Chang, J. W., Ban, M. J., Kim, W. S., Shin, D. Y., Lee, E. J., Koh, Y. W., Yoon, J.-H., & Choi, E. C. (2016). c-Met-mediated reactivation of PI3K/AKT signaling contributes to insensitivity of BRAF(V600E) mutant thyroid cancer to BRAF inhibition. *Molecular Carcinogenesis*, *55*(11), 1678-1687. https://doi.org/10.1002/mc.22418

Cabanillas, M. E., McFadden, D. G., & Durante, C. (2016). Thyroid cancer. *The Lancet*, *388*(10061), 2783-2795. https://doi.org/10.1016/S0140-6736(16)30172-6

Calafato, G., Di Paola, F. J., De Leo, A., Maloberti, T., Coluccelli, S., Poppi, L., Repaci, A., Solaroli, E., Damiani, S., Chillotti, S., Chiarucci, F., Rhoden, K. J., de Biase, D., & Tallini, G. (2025). Somatic genetic alterations in the development and progression in thyroid tumors of follicular cells. *European Thyroid Journal*, *14*(5), e250104. https://doi.org/10.1530/ETJ-25-0104

Caria, P., Tronci, L., Dettori, T., Murgia, F., Santoru, M., Griffin, J., Vanni, R., & Atzori, L. (2018). Metabolomic Alterations in Thyrospheres and Adherent Parental Cells in Papillary Thyroid Carcinoma Cell Lines: A Pilot Study. *International Journal of Molecular Sciences*, *19*(10), 2948. https://doi.org/10.3390/ijms19102948

Cellosaurus. (2025a, April 10). *B-CPAP (RRID:CVCL_0153)*. Retrieved June 5, 2026, from https://www.cellosaurus.org/CVCL_0153

Cellosaurus. (2025b, April 10). *TPC-1 (RRID:CVCL_6298)*. Retrieved June 5, 2026, from https://www.cellosaurus.org/CVCL_6298

Chae, Y. K., Anker, J. F., Carneiro, B. A., Chandra, S., Kaplan, J., Kalyan, A., Santa-Maria, C. A., Platanias, L. C., & Giles, F. J. (2016). Genomic landscape of DNA repair genes in cancer. *Oncotarget*, *7*(17), 23312-23321. https://doi.org/10.18632/oncotarget.8196

Chen, D. W., & Haymart, M. R. (2025). Unravelling the rise in thyroid cancer incidence and addressing overdiagnosis. *Nature Reviews Endocrinology*, *22*(1), 10-20. https://doi.org/10.1038/s41574-025-01168-y

Chen, D. W., Lang, B. H. H., McLeod, D. S. A., Newbold, K., & Haymart, M. R. (2023). Thyroid cancer. *The Lancet*, *401*(10387), 1531-1544. https://doi.org/10.1016/S0140-6736(23)00020-X

Cheng, L., & Newbold, K. (2025). Systemic Therapy for Advanced Thyroid Cancer—New Personalized Options. *Drugs*, *85*(11), 1381-1390. https://doi.org/10.1007/s40265-025-02233-6

Cheng, W., Liu, R., Zhu, G., Wang, H., & Xing, M. (2016). Robust Thyroid Gene Expression and Radioiodine Uptake Induced by Simultaneous Suppression of BRAF V600E and Histone Deacetylase in Thyroid Cancer Cells. *The Journal of Clinical Endocrinology & Metabolism*, *101*(3), 962-971. https://doi.org/10.1210/jc.2015-3433

Cosci, I., Salizzato, V., Del Fiore, P., Pigozzo, J., Guarneri, V., Mocellin, S., Ferlin, A., Mathlouthi, S., Piccin, L., & Garofalo, M. (2025). Molecular Basis of BRAF Inhibitor Resistance in Melanoma: A Systematic Review. *Pharmaceuticals*, *18*(8), 1235. https://doi.org/10.3390/ph18081235

Costanzo, L. S. (2014). *Fisiologia* (5th ed.). Elsevier Editora Ltda.

Crispo, F., Notarangelo, T., Pietrafesa, M., Lettini, G., Storto, G., Sgambato, A., Maddalena, F., & Landriscina, M. (2019). BRAF Inhibitors in Thyroid Cancer: Clinical Impact, Mechanisms of Resistance and Future Perspectives. *Cancers*, *11*(9), 1388. https://doi.org/10.3390/cancers11091388

Czyzyk, D., Yan, W., Messing, S., Gillette, W., Tsuji, T., Yamaguchi, M., Furuzono, S., Turner, D. M., Esposito, D., Nissley, D. V., McCormick, F., & Simanshu, D. K. (2025). Structural insights into isoform-specific RAS-PI3Kα interactions and the role of RAS in PI3Kα activation. *Nature Communications*, *16*(1), 525. https://doi.org/10.1038/s41467-024-55766-x

Dahmani, C., Corre, E., Dandou, S., Mangé, A., Radulescu, O., Coopman, P. J., Cuq, P., & Larive, R. M. (2022). La résistance aux inhibiteurs de BRAF - Les leçons de la clinique. *médecine/sciences*, *38*(6-7), 570-578. https://doi.org/10.1051/medsci/2022083

Danysh, B. P., Rieger, E. Y., Sinha, D. K., Evers, C. V., Cote, G. J., Cabanillas, M. E., & Hofmann, M. C. (2016). Long-term vemurafenib treatment drives inhibitor resistance through a spontaneous KRAS G12D mutation in a BRAF V600E papillary thyroid carcinoma model. *Oncotarget*, *7*(21), 30907-30923. https://doi.org/10.18632/oncotarget.9023

Di Nardo, M., Pallotta, M. M., & Musio, A. (2022). The multifaceted roles of cohesin in cancer. *Journal of Experimental & Clinical Cancer Research*, *41*(1), 96. https://doi.org/10.1186/s13046-022-02321-5

Dinh, T. H., Nguyen, H.-B., Nguyen, T. B.-S., Pham, H. T.-N., Doan-Van, L., Luu-Nguyen, T.-T., Nguyen, T. H., Pham, H.-Q., Le, T. X.-T., & Nguyen, K.-H. (2025). A comprehensive analysis of health-related quality of life in thyroid cancer patients using the THYCA-24 questionnaire. *Scientific Reports*, *15*(1), 29626. https://doi.org/10.1038/s41598-025-15084-8

Dunn, L. A., Sherman, E. J., Baxi, S. S., Tchekmedyian, V., Grewal, R. K., Larson, S. M., Pentlow, K. S., Haque, S., Tuttle, R. M., Sabra, M. M., Fish, S., Boucai, L., Walters, J., Ghossein, R. A., Seshan, V. E., Ni, A., Li, D., Knauf, J. A., Pfister, D. G.,…Ho, A. L. (2019). Vemurafenib Redifferentiation of *BRAF* Mutant, RAI-Refractory Thyroid Cancers. *The Journal of Clinical Endocrinology & Metabolism*, *104*(5), 1417-1428. https://doi.org/10.1210/jc.2018-01478

Durante, C., Hegedüs, L., Czarniecka, A., Paschke, R., Russ, G., Schmitt, F., Soares, P., Solymosi, T., & Papini, E. (2023). 2023 European Thyroid Association Clinical Practice Guidelines for thyroid nodule management. *European Thyroid Journal*, *12*(5), e230067. https://doi.org/10.1530/ETJ-23-0067

Fagin, J. A., & Mitsiades, N. (2008). Molecular pathology of thyroid cancer: diagnostic and clinical implications. *Best Practice & Research Clinical Endocrinology & Metabolism*, *22*(6), 955-969. https://doi.org/10.1016/j.beem.2008.09.017

Fagin, J. A., & Wells, S. A., Jr. (2016). Biologic and Clinical Perspectives on Thyroid Cancer. *The New England Journal of Medicine*, *375*(11), 1054-1067. https://doi.org/10.1056/NEJMra1501993

Filetti, S., Durante, C., Hartl, D., Leboulleux, S., Locati, L. D., Newbold, K., Papotti, M. G., & Berruti, A. (2019). Thyroid cancer: ESMO Clinical Practice Guidelines for diagnosis, treatment and follow-up. *Annals of Oncology*, *30*(12), 1856-1883. https://doi.org/10.1093/annonc/mdz400

Forma, A., Kłodnicka, K., Pająk, W., Flieger, J., Teresińska, B., Januszewski, J., & Baj, J. (2025). Thyroid Cancer: Epidemiology, Classification, Risk Factors, Diagnostic and Prognostic Markers, and Current Treatment Strategies. *International Journal of Molecular Sciences*, *26*(11), 5173. https://doi.org/10.3390/ijms26115173

Gild, M. L., Topliss, D. J., Learoyd, D., Parnis, F., Tie, J., Hughes, B., Walsh, J. P., McLeod, D. S. A., Clifton-Bligh, R. J., & Robinson, B. G. (2018). Clinical guidance for radioiodine refractory differentiated thyroid cancer. *Clinical Endocrinology*, *88*(4), 529-537. https://doi.org/10.1111/cen.13508

Grani, G., Sponziello, M., Filetti, S., & Durante, C. (2024). Thyroid nodules: diagnosis and management. *Nature Reviews Endocrinology*, *20*(12), 715-728. https://doi.org/10.1038/s41574-024-01025-4

Hamidi, S., Hofmann, M.-C., Iyer, P. C., Cabanillas, M. E., Hu, M. I., Busaidy, N. L., & Dadu, R. (2023). Review article: new treatments for advanced differentiated thyroid cancers and potential mechanisms of drug resistance. *Frontiers in Endocrinology*, *14:1176731*. https://doi.org/10.3389/fendo.2023.1176731

Hanly, E. K., Rajoria, S., Darzynkiewicz, Z., Zhao, H., Suriano, R., Tuli, N., George, A. L., Bednarczyk, R., Shin, E. J., Geliebter, J., & Tiwari, R. K. (2014). Disruption of mutated BRAF signaling modulates thyroid cancer phenotype. *BMC Research Notes*, *7*(1), 187. https://doi.org/10.1186/1756-0500-7-187

Hanly, E. K., Tuli, N. Y., Bednarczyk, R. B., Suriano, R., Geliebter, J., Moscatello, A. L., Darzynkiewicz, Z., & Tiwari, R. K. (2016). Hyperactive ERK and persistent mTOR signaling characterize vemurafenib resistance in papillary thyroid cancer cells. *Oncotarget*, *7*(8), 8676-8687. https://doi.org/10.18632/oncotarget.6779

Hannoush, Z. C., & Weiss, R. E. (2016). Thyroid Hormone Replacement in Patients Following Thyroidectomy for Thyroid Cancer. *Rambam Maimonides Medical Journal*, *7*(1), e0002. https://doi.org/10.5041/rmmj.10229

Harris, P. A. (2014). Chapter 18 - Targeting B-RAF: The Discovery and Development of B-RAF Inhibitors. In *Cancer Drug Design and Discovery* (pp. 529-563). Academic Press. https://doi.org/10.1016/B978-0-12-396521-9.00018-8

Hernandez-Prera, J. C., & Wenig, B. M. (2024). *RAS*-Mutant Follicular Thyroid Tumors: A Continuous Challenge for Pathologists. *Endocrine Pathology*, *35*(3), 167-184. https://doi.org/10.1007/s12022-024-09812-5

Hlozek, J., Pekova, B., Rotnágl, J., Holý, R., & Astl, J. (2022). Genetic Changes in Thyroid Cancers and the Importance of Their Preoperative Detection in Relation to the

General Treatment and Determination of the Extent of Surgical Intervention-A Review. *Biomedicines*, *10*(7), 1515. https://doi.org/10.3390/biomedicines10071515

Holderfield, M., Deuker, M. M., McCormick, F., & McMahon, M. (2014). Targeting RAF kinases for cancer therapy: BRAF-mutated melanoma and beyond. *Nature Reviews Cancer*, *14*(7), 455-467. https://doi.org/10.1038/nrc3760

Hu, L., Zhang, J., Tian, M., Kang, N., Xu, G., Zhi, J., Ruan, X., Hou, X., Zhang, W., Yi, J., Ma, W., Chang, L., Tang, T., Zheng, X., Wei, X., & Gao, M. (2022). Pharmacological inhibition of Ref-1 enhances the therapeutic sensitivity of papillary thyroid carcinoma to vemurafenib. *Cell Death & Disease*, *13*(2), 124. https://doi.org/10.1038/s41419-022-04550-0

Ibrahimpasic, T., Ghossein, R., Shah, J. P., & Ganly, I. (2019). Poorly Differentiated Carcinoma of the Thyroid Gland: Current Status and Future Prospects. *Thyroid*®, *29*(3), 311-321. https://doi.org/10.1089/thy.2018.0509

Ito, Y., & Miyauchi, A. (2026). Prognostic factors evaluated in differentiated thyroid carcinomas. *Endocrine Connections*, *15*(1), e250751. https://doi.org/10.1530/EC-25-0751

Jannin, A., Escande, A., Al Ghuzlan, A., Blanchard, P., Hartl, D., Chevalier, B., Deschamps, F., Lamartina, L., Lacroix, L., Dupuy, C., Baudin, E., Do Cao, C., & Hadoux, J. (2022). Anaplastic Thyroid Carcinoma: An Update. *Cancers*, *14*(4), 1061. https://doi.org/10.3390/cancers14041061

Jia, L., Li, B., & Yu, H. (2016). The Bub1–Plk1 kinase complex promotes spindle checkpoint signalling through Cdc20 phosphorylation. *Nature Communications*, *7*(1), 10818. https://doi.org/10.1038/ncomms10818

Jiang, S., Huang, Y., Li, Y., Gu, Q., Jiang, C., Tao, X., & Sun, J. (2023). Silencing FOXP2 reverses vemurafenib resistance in $BRAF^{V600E}$ mutant papillary thyroid cancer and melanoma cells. *Endocrine*, *79*(1), 86-97. https://doi.org/10.1007/s12020-022-03180-y

Juhlin, C. C., Mete, O., & Baloch, Z. W. (2022). The 2022 WHO classification of thyroid tumors: novel concepts in nomenclature and grading. *Endocrine-Related Cancer*, *30*(2), e220293. https://doi.org/10.1530/ERC-22-0293

Jung, C. K., Bychkov, A., & Kakudo, K. (2022). Update from the 2022 World Health Organization Classification of Thyroid Tumors: A Standardized Diagnostic Approach. *Endocrinology and Metabolism*, *37*(5), 703-718. https://doi.org/10.3803/EnM.2022.1553

Junqueira, L. C., & Carneiro, J. (2013). *Histologia Básica* (12th ed.). Guanabara Koogan.

Karapanou, O., Simeakis, G., Vlassopoulou, B., Alevizaki, M., & Saltiki, K. (2022). Advanced RAI-refractory thyroid cancer: an update on treatment perspectives. *Endocrine-Related Cancer*, *29*(5), R57-R66. https://doi.org/10.1530/ERC-22-0006

Khonrak, T., Watcharadetwittaya, S., Chamgramol, Y., Intarawichian, P., & Deenonpoe, R. (2023). *RET* rearrangements are relevant to histopathologic subtypes and clinicopathological features in Thai papillary thyroid carcinoma patients. *Pathology and Oncology Research*, *29*, 1611138. https://doi.org/10.3389/pore.2023.1611138

Kim, J., Gosnell, J. E., & Roman, S. A. (2020). Geographic influences in the global rise of thyroid cancer. *Nature Reviews Endocrinology*, *16*(1), 17-29. https://doi.org/10.1038/s41574-019-0263-x

Kim, M. J., Moon, J. H., Lee, E. K., Song, Y. S., Jung, K. Y., Lee, J. Y., Kim, J. H., Kim, K., Park, S. K., & Park, Y. J. (2024). Active Surveillance for Low-Risk Thyroid Cancers: A Review of Current Practice Guidelines. *Endocrinology and Metabolism*, *39*(1), 47-60. https://doi.org/10.3803/EnM.2024.1937

Lacka, K., Maciejewski, A., Tyburski, P., Manuszewska-Jopek, E., Majewski, P., & Więckowska, B. (2025). Rationale for Testing TP53 Mutations in Thyroid Cancer-Original Data and Meta-Analysis. *International Journal of Molecular Sciences*, *26*(3), 1035. https://doi.org/10.3390/ijms26031035

Lamartina, L., Grani, G., Arvat, E., Nervo, A., Zatelli, M. C., Rossi, R., Puxeddu, E., Morelli, S., Torlontano, M., Massa, M., Bellantone, R., Pontecorvi, A., Montesano, T., Pagano, L., Daniele, L., Fugazzola, L., Ceresini, G., Bruno, R., Rossetto, R.,…Durante, C. (2018). 8th edition of the AJCC/TNM staging system of thyroid cancer: what to expect (ITCO#2). *Endocrine-Related Cancer*, *25*(3), L7-L11. https://doi.org/10.1530/ERC-17-0453

Landa, I. (2023). InTERTwined: How TERT promoter mutations impact BRAFV600E-driven thyroid cancers. *Current Opinion in Endocrine and Metabolic Research*, *30*, 100460. https://doi.org/10.1016/j.coemr.2023.100460

Landa, I., & Cabanillas, M. E. (2024). Genomic alterations in thyroid cancer: biological and clinical insights. *Nature Reviews Endocrinology*, *20*(2), 93-110. https://doi.org/10.1038/s41574-023-00920-6

Landa, I., Thornton, C. E. M., Xu, B., Haase, J., Krishnamoorthy, G. P., Hao, J., Knauf, J. A., Herbert, Z. T., Martínez, P., Blasco, M. A., Ghossein, R., & Fagin, J. A. (2023). Telomerase Upregulation Induces Progression of Mouse $Braf^{V600E}$-Driven Thyroid

Cancers and Triggers Nontelomeric Effects. *Molecular Cancer Research*, *21*(11), 1163-1175. https://doi.org/10.1158/1541-7786.MCR-23-0144

Leandro-García, L. J., & Landa, I. (2023). Mechanistic Insights of Thyroid Cancer Progression. *Endocrinology*, *164*(9), bqad118. https://doi.org/10.1210/endocr/bqad118

Li, Y. D., Ye, Q. Y., Chen, Y. X., & Hu, X. R. (2025). Thyroid Cancer: Pathogenesis, Clinicopathology, Diagnosis, and Management. *MedComm*, *6*(11), e70449. https://doi.org/10.1002/mco2.70449

Liu, Q., Jiang, X., Tu, W., Liu, L., Huang, Y., Xia, Y., Xia, X., & Shi, Y. (2024). Comparative efficiency of differential diagnostic methods for the identification of BRAF V600E gene mutation in papillary thyroid cancer (Review). *Experimental and Therapeutic Medicine*, *27*(4), 149. https://doi.org/10.3892/etm.2024.12437

Liu, R., Zhang, T., Zhu, G., & Xing, M. (2018). Regulation of mutant *TERT* by BRAF V600E/MAP kinase pathway through FOS/*GABP* in human cancer. *Nature Communications*, *9*, 579. https://doi.org/10.1038/s41467-018-03033-1

Liu, X., Qu, S., Liu, R., Sheng, C., Shi, X., Zhu, G., Murugan, A. K., Guan, H., Yu, H., Wang, Y., Sun, H., Shan, Z., Teng, W., & Xing, M. (2014). *TERT* Promoter Mutations and Their Association with *BRAF* V600E Mutation and Aggressive Clinicopathological Characteristics of Thyroid Cancer. *The Journal of Clinical Endocrinology & Metabolism*, *99*(6), E1130–E1136. https://doi.org/10.1210/jc.2013-4048

Lorenz, E., Scholz-Kreisel, P., Baaken, D., Pokora, R., & Blettner, M. (2018). Radiotherapy for childhood cancer and subsequent thyroid cancer risk: a systematic review. *European Journal of Epidemiology*, *33*(12), 1139-1162. https://doi.org/10.1007/s10654-018-0467-8

Luzón-Toro, B., Fernández, R. M., Villalba-Benito, L., Torroglosa, A., Antiñolo, G., & Borrego, S. (2019). Influencers on Thyroid Cancer Onset: Molecular Genetic Basis. *Genes*, *10*(11), 913. https://doi.org/10.3390/genes10110913

Ma, W., Tian, M., Hu, L., Ruan, X., Zhang, W., Zheng, X., & Gao, M. (2023). Early Combined SHP2 Targeting Reverses the Therapeutic Resistance of Vemurafenib in Thyroid Cancer. *Journal of Cancer*, *14*(9), 1592-1604. https://doi.org/10.7150/jca.83853

Mady, L. J., Grimes, M. C., Khan, N. I., Rao, R. H., Chiosea, S. I., Yip, L., Ferris, R. L., Nikiforov, Y. E., Carty, S. E., & Duvvuri, U. (2020). Molecular Profile of Locally Aggressive Well Differentiated Thyroid Cancers. *Scientific Reports*, *10*(1), 8031. https://doi.org/10.1038/s41598-020-64635-8

Maji, L., Teli, G., Raghavendra, N. M., Sengupta, S., Pal, R., Ghara, A., & Matada, G. S. P. (2024). An updated literature on BRAF inhibitors (2018–2023). *Molecular Diversity*, *28*(4), 2689-2730. https://doi.org/10.1007/s11030-023-10699-3

Matsuse, M., & Mitsutake, N. (2023). *TERT* promoter mutations in thyroid cancer. *Endocrine Journal*, *70*(11), 1035-1049. https://doi.org/10.1507/endocrj/EJ23-0136

Melo, M., da Rocha, A. G., Vinagre, J., Batista, R., Peixoto, J., Tavares, C., Celestino, R., Almeida, A., Salgado, C., Eloy, C., Castro, P., Prazeres, H., Lima, J., Amaro, T., Lobo, C., Martins, M. J., Moura, M., Cavaco, B., Leite, V.,…Soares, P. (2014). TERT Promoter Mutations Are a Major Indicator of Poor Outcome in Differentiated Thyroid Carcinomas. *The Journal of Clinical Endocrinology & Metabolism*, *99*(5), E754-E765. https://doi.org/10.1210/jc.2013-3734

Montalto, F. I., & De Amicis, F. (2020). Cyclin D1 in Cancer: A Molecular Connection for Cell Cycle Control, Adhesion and Invasion in Tumor and Stroma. *Cells*, *9*(12), 2648. https://doi.org/10.3390/cells9122648

Montero-Conde, C., Ruiz-Llorente, S., Dominguez, J. M., Knauf, J. A., Viale, A., Sherman, E. J., Ryder, M., Ghossein, R. A., Rosen, N., & Fagin, J. A. (2013). Relief of Feedback Inhibition of *HER3* Transcription by RAF and MEK Inhibitors Attenuates Their Antitumor Effects in *BRAF*-Mutant Thyroid Carcinomas. *Cancer Discovery*, *3*(5), 520-533. https://doi.org/10.1158/2159-8290.CD-12-0531

Nguyen, N. C., Anigati, E. M., Desai, N. B., & Öz, O. K. (2024). Radioactive Iodine Therapy in Differentiated Thyroid Cancer: An Update on Dose Recommendations and Risk of Secondary Primary Malignancies. *Seminars in Nuclear Medicine*, *54*(4), 488-496. https://doi.org/10.1053/j.semnuclmed.2024.05.002

Notarangelo, T., Sisinni, L., Condelli, V., & Landriscina, M. (2017). Dual EGFR and BRAF blockade overcomes resistance to vemurafenib in BRAF mutated thyroid carcinoma cells. *Cancer Cell International*, *17*, 86. https://doi.org/10.1186/s12935-017-0457-z

Park, H., Shin, H. C., Yang, H., Heo, J., Ki, C.-S., Kim, H. S., Kim, J.-H., Hahn, S. Y., Chung, Y. J., Kim, S. W., Chung, J. H., Oh, Y. L., & Kim, T. H. (2022). Molecular classification of follicular thyroid carcinoma based on *TERT* promoter mutations. *Modern Pathology*, *35*(2), 186-192. https://doi.org/10.1038/s41379-021-00907-6

Park, K. S., Saindane, M., Yang, E. Y., Jin, T., Rallabandi, H. R., Heil, A., Nam, S. E., Yoo, Y. B., Yang, J.-H., Kim, J. B., Park, S.-Y., Park, W. S., & Youn, Y.-K. (2021). Selective inhibition of V600E-mutant BRAF gene induces apoptosis in thyroid carcinoma cell

lines. *Annals of Surgical Treatment and Research*, *100*(3), 127-136. https://doi.org/10.4174/astr.2021.100.3.127

Pizzato, M., Li, M., Vignat, J., Laversanne, M., Singh, D., La Vecchia, C., & Vaccarella, S. (2022). The epidemiological landscape of thyroid cancer worldwide: GLOBOCAN estimates for incidence and mortality rates in 2020. *The Lancet Diabetes & Endocrinology*, *10*(4), 264-272. https://doi.org/10.1016/S2213-8587(22)00035-3

Prete, A., Borges de Souza, P., Censi, S., Muzza, M., Nucci, N., & Sponziello, M. (2020). Update on Fundamental Mechanisms of Thyroid Cancer. *Frontiers in Endocrinology*, *11*, 102. https://doi.org/10.3389/fendo.2020.00102

Prete, A., Matrone, A., Gambale, C., Torregrossa, L., Minaldi, E., Romei, C., Ciampi, R., Molinaro, E., & Elisei, R. (2021). Poorly Differentiated and Anaplastic Thyroid Cancer: Insights into Genomics, Microenvironment and New Drugs. *Cancers*, *13*(13), 3200. https://doi.org/10.3390/cancers13133200

Qian, C., Li, D., & Chen, Y. (2022). ETS factors in prostate cancer. *Cancer Letters*, *530*, 181-189. https://doi.org/10.1016/j.canlet.2022.01.009

Rao, S. N., & Bernet, V. (2020). Indeterminate thyroid nodules in the era of molecular genomics. *Molecular Genetics & Genomic Medicine*, *8*(9), e1288. https://doi.org/10.1002/mgg3.1288

Registo Oncológico Nacional. (2025). *Registo Oncológico Nacional de Todos os Tumores na População Residente em Portugal, em 2022*. Instituto Português de Oncologia do Porto Francisco Gentil – EPE. https://ron.min-saude.pt/pt/biblioteca/publicacoes-ron/publica%C3%A7%C3%A3o-2022/

Riesco-Eizaguirre, G. (2025). BRAF V600E in thyroid cancer: navigating prognostic uncertainty and therapeutic opportunity. *European Thyroid Journal*, *14*(6), e250225. https://doi.org/10.1530/ETJ-25-0225

Ringel, M. D., Sosa, J. A., Baloch, Z., Bischoff, L., Bloom, G., Brent, G. A., Brock, P. L., Chou, R., Flavell, R. R., Goldner, W., Grubbs, E. G., Haymart, M., Larson, S. M., Leung, A. M., Osborne, J. R., Ridge, J. A., Robinson, B., Steward, D. L., Tufano, R. P., & Wirth, L. J. (2025). 2025 American Thyroid Association Management Guidelines for Adult Patients with Differentiated Thyroid Cancer. *Thyroid®*, *35*(8), 841-985. https://doi.org/10.1177/10507256251363120

Robb, R., Yang, L., Shen, C., Wolfe, A. R., Webb, A., Zhang, X., Vedaie, M., Saji, M., Jhiang, S., Ringel, M. D., & Williams, T. M. (2019). Inhibiting BRAF Oncogene–Mediated Radioresistance Effectively Radiosensitizes $BRAF^{V600E}$-Mutant Thyroid Cancer Cells

by Constraining DNA Double-Strand Break Repair. *Clinical Cancer Research*, *25*(15), 4749-4760. https://doi.org/10.1158/1078-0432.CCR-18-3625

Romei, C., & Elisei, R. (2021). A Narrative Review of Genetic Alterations in Primary Thyroid Epithelial Cancer. *International Journal of Molecular Sciences*, *22*(4), 1726. https://doi.org/10.3390/ijms22041726

Roskoski, R. J. (2010). RAF protein-serine/threonine kinases: Structure and regulation. *Biochemical and Biophysical Research Communications*, *399*(3), 313-317. https://doi.org/10.1016/j.bbrc.2010.07.092

Roy, A. (2024). Crosstalk Between MAPK and PI3K/AKT Signaling Pathways in Cellular Responses: Implications for Cancer Therapy. *Universal Research Reports*, *11*(4), 30-45. https://doi.org/10.36676/urr.v11.i4.1304

Run, L., Wang, L., Nong, X., Li, N., Huang, X., & Xiao, Y. (2021). Involvement of HMGB1 in vemurafenib resistance in thyroid cancer cells harboring BRAF (V600E) mutation by regulating excessive autophagy. *Endocrine*, *71*(2), 418-426. https://doi.org/10.1007/s12020-020-02417-y

Scheffel, R. S., Dora, J. M., & Maia, A. L. (2022). BRAF mutations in thyroid cancer. *Current Opinion in Oncology*, *34*(1), 9-18. https://doi.org/10.1097/CCO.0000000000000797

Schlumberger, M., & Leboulleux, S. (2021). Current practice in patients with differentiated thyroid cancer. *Nature Reviews Endocrinology*, *17*(3), 176-188. https://doi.org/10.1038/s41574-020-00448-z

Schrumpfová, P. P., & Fajkus, J. (2020). Composition and Function of Telomerase-A Polymerase Associated with the Origin of Eukaryotes. *Biomolecules*, *10*(10), 1425. https://doi.org/10.3390/biom10101425

Shahid, M. A., Ashraf, M. A., & Sharma, S. (2023). Physiology, Thyroid Hormone. In *StatPearls*. StatPearls Publishing. https://www.ncbi.nlm.nih.gov/books/NBK500006/

Shou, S., Maolan, A., Zhang, D., Jiang, X., Liu, F., Li, Y., Zhang, X., Geer, E., Pu, Z., Hua, B., Guo, Q., Zhang, X., & Pang, B. (2025). Telomeres, telomerase, and cancer: mechanisms, biomarkers, and therapeutics. *Experimental Hematology & Oncology*, *14*(1), 8. https://doi.org/10.1186/s40164-025-00597-9

Smith, E. M., Pendlebury, D. F., & Nandakumar, J. (2020). Structural biology of telomeres and telomerase. *Cellular and Molecular Life Sciences*, *77*(1), 61-79. https://doi.org/10.1007/s00018-019-03369-x

Soares, P., Póvoa, A. A., Melo, M., Vinagre, J., Máximo, V., Eloy, C., Cameselle-Teijeiro, J. M., & Sobrinho-Simões, M. (2021). Molecular Pathology of Non-familial Follicular Epithelial–Derived Thyroid Cancer in Adults: From *RAS/BRAF*-like Tumor Designations to Molecular Risk Stratification. *Endocrine Pathology*, *32*(1), 44-62. https://doi.org/10.1007/s12022-021-09666-1

Song, Y. S., & Park, Y. J. (2020). Mechanisms of *TERT* Reactivation and Its Interaction with $BRAF^{V600E}$. *Endocrinology and Metabolism*, *35*(3), 515-525. https://doi.org/10.3803/EnM.2020.304

Song, Y. S., Yoo, S.-K., Kim, H. H., Jung, G., Oh, A.-R., Cha, J.-Y., Kim, S.-j., Cho, S. W., Lee, K. E., Seo, J.-S., & Park, Y. J. (2019). Interaction of *BRAF*-induced ETS factors with mutant *TERT* promoter in papillary thyroid cancer. *Endocrine-Related Cancer*, *26*(6), 629-641. https://doi.org/10.1530/ERC-17-0562

Standring, S. (2011). *Gray's Anatomia: A Base Anatômica da Prática Clínica* (40th ed.). Elsevier Editora Ltda.

Stathatos, N. (2019). Anatomy and Physiology of the Thyroid Gland. In M. Luster, L. H. Duntas, & L. Wartofsky (Eds.), *The Thyroid and Its Diseases: A Comprehensive Guide for the Clinician* (pp. 3-12). Springer International Publishing. https://doi.org/10.1007/978-3-319-72102-6_1

Subbiah, V., Kreitman, R. J., Wainberg, Z. A., Cho, J. Y., Schellens, J. H. M., Soria, J. C., Wen, P. Y., Zielinski, C. C., Cabanillas, M. E., Boran, A., Ilankumaran, P., Burgess, P., Romero Salas, T., & Keam, B. (2022). Dabrafenib plus trametinib in patients with *BRAF* V600E-mutant anaplastic thyroid cancer: updated analysis from the phase II ROAR basket study. *Annals of Oncology*, *33*(4), 406-415. https://doi.org/10.1016/j.annonc.2021.12.014

Sung, H., Filho, A. M., Laversanne, M., Ferlay, J., Siegel, R. L., Soerjomataram, I., Jemal, A., & Bray, F. (2026). Global cancer statistics 2024: GLOBOCAN estimates of incidence and mortality worldwide for 34 cancers in 186 countries. *CA: A Cancer Journal for Clinicians*, *76*(4), e70090. https://doi.org/10.3322/caac.70090

Thermo Fisher Scientific. (2014, January 6). *Click-iT® Plus EdU Imaging Kits*. Retrieved June 5, 2026, from https://documents.thermofisher.com/TFS-Assets/LSG/manuals/mp10637.pdf

Thermo Fisher Scientific. (2019, January 7). *PrestoBlue™ Cell Viability Reagent Product Information Sheet*. Retrieved June 5, 2026, from

https://documents.thermofisher.com/TFS-Assets/LSG/manuals/MAN0018370-PrestoBlueCellViabilityReagent-PI.pdf

Tirrò, E., Martorana, F., Romano, C., Vitale, S. R., Motta, G., Di Gregorio, S., Massimino, M., Pennisi, M. S., Stella, S., Puma, A., Gianì, F., Russo, M., Manzella, L., & Vigneri, P. (2019). Molecular Alterations in Thyroid Cancer: From Bench to Clinical Practice. *Genes*, *10*(9), 709. https://www.mdpi.com/2073-4425/10/9/709

Tuttle, R. M., & Alzahrani, A. S. (2019). Risk Stratification in Differentiated Thyroid Cancer: From Detection to Final Follow-Up. *The Journal of Clinical Endocrinology & Metabolism*, *104*(9), 4087-4100. https://doi.org/10.1210/jc.2019-00177

Vinagre, J., Almeida, A., Pópulo, H., Batista, R., Lyra, J., Pinto, V., Coelho, R., Celestino, R., Prazeres, H., Lima, L., Melo, M., Rocha, A. G. d., Preto, A., Castro, P., Castro, L., Pardal, F., Lopes, J. M., Santos, L. L., Reis, R. M.,…Soares, P. (2013). Frequency of *TERT* promoter mutations in human cancers. *Nature Communications*, *4*(1), 2185. https://doi.org/10.1038/ncomms3185

Vodopivec, D. M., & Hu, M. I. (2022). RET kinase inhibitors for *RET*-altered thyroid cancers. *Therapeutic Advances in Medical Oncology*, *14*. https://doi.org/10.1177/17588359221101691

Wang, W., Kang, H., Zhao, Y., Min, I., Wyrwas, B., Moore, M., Teng, L., Zarnegar, R., Jiang, X., & Fahey, T. J., III. (2017). Targeting Autophagy Sensitizes BRAF-Mutant Thyroid Cancer to Vemurafenib. *The Journal of Clinical Endocrinology & Metabolism*, *102*(2), 634-643. https://doi.org/10.1210/jc.2016-1999

Xing, M. (2010). Genetic Alterations in the Phosphatidylinositol-3 Kinase/Akt Pathway in Thyroid Cancer. *Thyroid®*, *20*(7), 697-706. https://doi.org/10.1089/thy.2010.1646

Xing, M. (2013). Molecular pathogenesis and mechanisms of thyroid cancer. *Nature Reviews Cancer*, *13*(3), 184-199. https://doi.org/10.1038/nrc3431

Xing, M., Liu, R., Liu, X., Murugan, A. K., Zhu, G., Zeiger, M. A., Pai, S., & Bishop, J. (2014). *BRAF* V600E and *TERT* Promoter Mutations Cooperatively Identify the Most Aggressive Papillary Thyroid Cancer With Highest Recurrence. *Journal of Clinical Oncology*, *32*(25), 2718-2726. https://doi.org/10.1200/jco.2014.55.5094

Xu, S., Peng, Y., Li, X., Li, H., Liu, T., Li, X., & Du, Y. (2025). TSHR in thyroid cancer: bridging biological insights to targeted strategies. *European Thyroid Journal*, *14*(4), e240369. https://doi.org/10.1530/ETJ-24-0369

Xu, Y., Gao, J., Wang, N., Zedenius, J., Nilsson, I.-L., Lui, W.-O., Xu, D., Juhlin, C. C., Larsson, C., & Mu, N. (2025). BRAF-induced *EHF* Expression Affects *TERT* in

Aggressive Papillary Thyroid Cancer. *The Journal of Clinical Endocrinology & Metabolism*, *110*(3), 693-705. https://doi.org/10.1210/clinem/dgae589

Yang, Y., Zhang, Y., Xu, Y., Gu, X., Lou , N., & Ye, G. (2026). Targeted therapy in thyroid cancer: molecular alterations and clinical management. *Frontiers in Endocrinology*, *17*, 1810813. https://doi.org/10.3389/fendo.2026.1810813

Zhang, J., & Xu, S. (2024). High aggressiveness of papillary thyroid cancer: from clinical evidence to regulatory cellular networks. *Cell Death Discovery*, *10*(1), 378. https://doi.org/10.1038/s41420-024-02157-2

Zhang, L., Feng, Q., Wang, J., Tan, Z., Li, Q., & Ge, M. (2023). Molecular basis and targeted therapy in thyroid cancer: Progress and opportunities. *Biochimica et Biophysica Acta (BBA) - Reviews on Cancer*, *1878*(4), 188928. https://doi.org/10.1016/j.bbcan.2023.188928

Zhang, X., Yang, Y., Wang, Y., & Fan, Q. (2019). Detection of the BRAF V600E Mutation in Colorectal Cancer by NIR Spectroscopy in Conjunction with Counter Propagation Artificial Neural Network. *Molecules*, *24*(12), 2238. https://doi.org/10.3390/molecules24122238

8. Appendix

Supplementary Table 1: *Cell viability (%), expressed as mean ± SD, of Nthy-Ori 3-1 cells at each Vemurafenib concentration (0, 2.5, 5, 10, 25, and 50 μM) at 48 and 72 h post-treatment.*

Vemurafenib concentration (μM)	Cell viability (%), mean ± SD		*p-value*[a]
	48 h	72 h	
0 (DMSO control)	100.00 (0.00)	100.00 (0.00)	> 0.9999
2.5	92.42 (21.51)	97.34 (10.68)	0.9749
5	105.56 (14.01)	105.75 (11.37)	> 0.9999
10	116.69 (15.12)	106.98 (9.34)	0.6236
25	81.82 (9.82)	76.17 (8.82)	0.9516
50	73.68 (7.73)	61.28 (5.50)	0.3522

[a] *p-values* correspond to Sidak's multiple comparisons between the 48 h and 72 h timepoints at each Vemurafenib concentration.

Supplementary Table 2: *Cell viability (%), expressed as mean ± SD, of B-CPAP cells at each Vemurafenib concentration (0, 2.5, 5, 10, 25, and 50 μM) at 48 and 72 h post-treatment.*

Vemurafenib concentration (μM)	Cell viability (%), mean ± SD		*p-value*[a]
	48 h	72 h	
0 (DMSO control)	100.00 (0.00)	100.00 (0.00)	> 0.9999
2.5	67.52 (6.68)	51.93 (4.49)	0.0015
5	64.94 (7.65)	51.21 (6.22)	0.0055
10	62.49 (5.77)	44.99 (5.37)	0.0004
25	43.35 (7.67)	33.31 (2.72)	0.0631
50	29.95 (8.90)	19.74 (1.78)	0.0568

[a] *p-values* correspond to Sidak's multiple comparisons between the 48 h and 72 h timepoints at each Vemurafenib concentration.

Supplementary Table 3: *Cell viability (%), expressed as mean ± SD, of TPC-1 cells at each Vemurafenib concentration (0, 2.5, 5, 10, 25, and 50 μM) at 48 and 72 h post-treatment.*

Vemurafenib concentration (μM)	Cell viability (%), mean ± SD		*p-value*[a]
	48 h	72 h	
0 (DMSO control)	100.00 (0.00)	100.00 (0.00)	> 0.9999
2.5	129.57 (15.72)	111.19 (8.46)	0.0485
5	124.74 (13.51)	111.85 (8.65)	0.2862
10	125.81 (17.68)	110.59 (13.73)	0.1430
25	107.06 (12.46)	94.86 (10.93)	0.3443
50	82.00 (8.18)	72.64 (8.48)	0.6364

[a] *p-values* correspond to Sidak's multiple comparisons between the 48 h and 72 h timepoints at each Vemurafenib concentration.

Supplementary Table 4: *Percentage of EdU-positive cells, expressed as mean ± SD, in Nthy-Ori 3-1, B-CPAP, and TPC-1 cells under each experimental condition (Media control, DMSO control, and 15 µM Vemurafenib) at 48 and 72 h post-treatment.*

Cell line	Timepoint	EdU-positive cells (%), mean ± SD		
		Media control	DMSO control	15 µM Vemurafenib
Nthy-Ori 3-1				
	48 h	44.38 (2.64)	44.46 (0.14)	41.29 (3.18)
	72 h	44.18 (1.08)	42.93 (0.49)	38.12 (0.54)
B-CPAP				
	48 h	33.97 (0.59)	33.21 (0.21)	16.94 (0.61)
	72 h	27.93 (0.74)	27.35 (2.80)	17.52 (1.07)
TPC-1				
	48 h	54.45 (1.42)	53.51 (2.94)	46.70 (1.94)
	72 h	49.26 (0.79)	50.11 (3.42)	45.03 (1.72)